A Progress Report
Grant No. NAG-1-745-2
April 1, 1987 - April 30, 1989

ENVIRONMENT ASSISTED DEGRADATION MECHANISMS IN ADVANCED LIGHT METALS

Submitted to:

Mr. Dennis Dicus
M/S 188A, Metallic Materials Branch
National Aeronautics and Space Administration
Langley Research Center
Hampton, VA 23665

Submitted by:

Richard P. Gangloff
Associate Professor

Glenn E. Stoner
Professor
Department of Materials Science
University of Virginia

Robert E. Swanson
Assistant Professor
Department of Materials Engineering
Virginia Polytechnic Institute and State University

Report No. UVA/528266/MS88/102

June 1988

SCHOOL OF ENGINEERING AND APPLIED SCIENCE

DEPARTMENT OF MATERIALS SCIENCE

UNIVERSITY OF VIRGINIA
CHARLOTTESVILLE, VIRGINIA 22901

A Progress Report
Grant No. NAG-1-745-2
April 1, 1987 - April 30, 1989

ENVIRONMENT ASSISTED DEGRADATION MECHANISMS IN ADVANCED LIGHT METALS

Submitted to:

Mr. Dennis Dicus
M/S 188A, Metallic Materials Branch
National Aeronautics and Space Administration
Langley Research Center
Hampton, VA 23665

Submitted by:

Richard P. Gangloff
Associate Professor

Glenn E. Stoner
Professor
Department of Materials Science
University of Virginia

Robert E. Swanson
Assistant Professor
Department of Materials Engineering
Virginia Polytechnic Institute and State University

Department of Materials Science
SCHOOL OF ENGINEERING AND APPLIED SCIENCE
UNIVERSITY OF VIRGINIA
CHARLOTTESVILLE, VIRGINIA

Report No. UVA/528266/MS88/102
June 1988

Copy No. 24

ENVIRONMENT ASSISTED DEGRADATION MECHANISMS IN ADVANCED LIGHT METALS

INTRODUCTION

This report summarizes the research progress which has been achieved on NASA-LaRC Grant NAG-1-745 during the period from December 1, 1987 to May 31, 1988.

A multifaceted research program on environmental failure mechanisms in advanced light metallic alloys was initiated in April of 1987 [1]. The current participants in this NASA-sponsored work include two faculty and three PhD level graduate students in the Department of Materials Science at the University of Virginia, one faculty and an MS graduate student in the Department of Materials Engineering at the Virginia Polytechnic Institute and State University, and a NASA/LaRC based employee enrolled in the PhD program at UVa. The NASA grant monitor for this program is D.L. Dicus of the Metallic Materials Branch at the Langley Research Center.

This program has been recently expanded to include two additional faculty and two graduate students in Materials Science at UVa [2]. This new work on the NASA-UVa Light Alloy Technology Program is about to initiate and will not be reported here.

Problem

Problems of long-term environmental degradation and failure could impede reliable applications of advanced light metallic alloys and composites in aerospace structures. Materials of particular interest include wrought Al-Li-X alloys, powder metallurgy Al-Fe ternary and quaternary alloys, and titanium aluminides. Environments include terrestrial aqueous electrolytes, cryogenic and elevated temperatures, and gaseous hydrogen. The challenge at hand is to examine alloys; which have been developed based on short term, benign environment strength and ductility; in terms of resistance to localized corrosion, hydrogen embrittlement, stress corrosion cracking and corrosion fatigue during prolonged environmental exposures.

Several deficiencies are generically relevant to the performance of advanced light metallics.

+ Predictions of long term durability and reliability, based on short term laboratory data, are hindered by a lack of experimental observations, fundamental understanding, and predictive models of time dependencies.

+ Laboratory measurements have not separated and characterized the localized processes which are relevant to complex failure modes. Data are not scalable to predict performance.

+ Hydrogen contributions to localized corrosion, deformation and brittle fracture have not been studied systematically.

+ Fatigue-environment interactions have not been studied, particularly with regard to transgranular crack propagation relevant to thin sheet.

+ The effects of defects common to advanced PM alloys and service have not been characterized.

Program Objectives and Output

The general goals of the research program are to characterize alloy behavior quantitatively and to develop predictive mechanisms for environmental failure modes. Successes in this regard will provide the basis for metallurgical optimization of alloy performance, for chemical control of aggressive environments and for engineering life prediction with damage tolerance and long term reliability.

Current Projects and Personnel

1. DAMAGE LOCALIZATION MECHANISMS IN AQUEOUS CHLORIDE CORROSION FATIGUE OF ALUMINUM-LITHIUM ALLOYS
   R.P. Gangloff and Robert S. Piascik, PhD candidate

2. MEASUREMENTS AND MECHANISMS OF LOCALIZED AQUEOUS CORROSION IN ALUMINUM-LITHIUM ALLOYS
   G.E. Stoner and Rudolph G. Buchheit, Jr., PhD candidate

3. DEFORMATION AND FRACTURE OF ALUMINUM-LITHIUM ALLOYS:THE EFFECT OF DISSOLVED HYDROGEN
   R.E. Swanson and graduate student to be recruited

4. DEFORMATION AND FRACTURE OF ALUMINUM LITHIUM ALLOYS: THE EFFECT OF CRYOGENIC TEMPERATURES
   Richard P. Gangloff and John A. Wagner, PhD candidate

5. ELEVATED TEMPERATURE CRACK GROWTH IN ADVANCED PM ALUMINUM ALLOYS
   Richard P. Gangloff and William C. Porr, Jr., a PhD candidate

Research Status

Research progress for the period from April 1, 1987 to November 31, 1987 was reported previously [3]. Work conducted during the past six months is summarized below.

Appendix I contains publications which were issued under grant sponsorship. Appendix II summarizes grant travel and conference participation.

References

1. R.P. Gangloff, G.E. Stoner and M.R. Louthan, Jr., "Environment Assisted Degradation Mechanisms in Al-Li Alloys", University of Virginia, Proposal No. MS-NASA/LaRC-3545-87, October, 1986.

2. T.H. Courtney, R.P. Gangloff, G.E. Stoner and H.G.F. Wilsdorf, "The NASA-UVA Light Alloy Technology Program", University of Virginia, Proposal No. MS_NASA/LaRC-3937-88, March, 1988.

3. R.P. Gangloff, G.E. Stoner and R.E. Swanson, "Environment Assisted Degradation Mechanisms in Al-Li Alloys", University of Virginia, Report No. UVA/528266/MS88/101, January, 1988.

SUMMARY OF RESEARCH (December 1, 1987 to May 31, 1988) and PLANS

Program 1 DAMAGE LOCALIZATION MECHANISMS IN AQUEOUS CHLORIDE CORROSION FATIGUE OF ALUMINUM-LITHIUM ALLOYS

Robert S. Piascik and R.P. Gangloff

Objective. The objective of this PhD study is to characterize and understand intrinsic fatigue crack propagation in the class of new Al-Li-X alloys, with emphasis on the damage mechanisms for transgranular environmentally assisted cracking.

Approach. Experimental design and analysis were presented in the last progress report [1]. Work on corrosion fatigue in aluminum-lithium-copper alloy 2090 is progressing on three fronts; specifically: 1) intrinsic fatigue crack propagation kinetics, 2) gaseous environmental effects and 3) aqueous electrolyte environmental effects.

Results. Generally, the data presented previously have been confirmed and expanded during this reporting period. Results summarized in Figs. 1 through 5 are, perhaps, the most complete and rigorous set of Al-Li corrosion fatigue crack propagation kinetics available worldwide. Results are, as yet, insufficient to quantitatively define the contributions of hydrogen, dissolution/film rupture and film-plastic deformation mechanisms to corrosion fatigue crack propagation. Progress has, however, been recorded in developing qualitative understanding of these complex mechanisms. This work is presented in an appendixed paper [2] and extended abstract, and is summarized here.

Intrinsic Fatigue Crack Propagation Kinetics. Two significant findings have been recorded during the past six months. Firstly, constant stress intensity experiments prove that stress intensity range (ΔK) can be decreased substantially without delay retardation, if the maximum stress intensity is maintained constant. This result supports the use of the step-decreased ΔK/increased R/constant K_{max} technique, which is the basis for the current work.

Secondly, we have found that near threshold fatigue crack growth rates are increased significantly and the threshold stress intensity range is decreased when the single edge cracked specimen is rigidly gripped to prevent free, in plane rotation. This result is illustrated in Fig. 1. The two dashed lines and the data points represent the intrinsic FCP behavior for two orientations of alloy 2090 as freely rotating SEN specimens and for the increasing stress ratio methods described previously [1]. These data were recently confirmed by a standardized compact tension experiment which included measurement of crack closure.

The shaded band represents the behavior of the same material under fixed grip conditions. Enhanced fatigue crack growth is observed for each orientation, LT (upper line) and ST (lower line). These new data approximate the very high fatigue crack growth rates reported by Ritchie and coworkers for small surface cracks.

There are currently two explanations for the effect shown in Fig. 1. While we employed a fixed grip stress intensity solution which has been confirmed by extensive 3-dimensional finite element analyses (by the mechanics group at the General Electric Aircraft Engine laboratories), the gripping system may not have been sufficiently rigid to eliminate rotation. The actual stress intensity could therefore be higher than that plotted in Fig.1 and perhaps in agreement with the rotating specimen case. Alternately, the effect in Fig. 1 may be real and due to fixed grip suppression of Mode II crack opening displacements. The effect of pure Mode I opening versus a mixed Mode I/II opening on fatigue crack tip damage is not known, particularly for the case where crack closure is unimportant.

If real, the result in Fig. 1 is important to interpretations of small surface crack fatigue data which have here-to-fore been ascribed to microstructural effects on Mode I opening strain. Understanding in this regard is basic to life prediction models of surface fatigue and corrosion fatigue crack growth, and to relevant laboratory experiments for evaluations of environmental and metallurgical effects. Additional experiments are in progress to determine the importance of the two possible explanations and the generality of the effect.

Aqueous Electrolyte Environmental Effects. The aqueous environment effects introduced in the previous progress report [1], have been confirmed by additional corrosion fatigue experimentation and fractographic analyses. The data are compiled in Fig. 2 and several conclusions are supported.

Firstly, Alloy 2090 (peak aged) is susceptible to corrosion fatigue crack propagation in aqueous 1% NaCl (full immersion) under constant anodic polarization at -760 mV (SCE). At low ΔK/high R, near threshold rates are significantly increased relative to cracking in moist air, with growth occurring by a cleavage process. High ΔK/low R growth rates are increased by about a factor of 3, with highly deflected slip band cracking the dominant microscopic mode.

Cathodic polarization and loading frequency effects are not indicative of hydrogen embrittlement, at least based on classical arguments. As shown in Fig. 2, corrosion fatigue crack growth in NaCl is decreased by an applied cathodic potential of -1160 mV (SCE), with resulting rates about equal to those observed for moist air. Constant stress intensity experiments show that

crack propagation at the anodic potential is arrested by cathodic polarization.

Results in Fig. 2 were obtained at constant frequency, 5 Hz. As shown in Fig. 3, corrosion fatigue crack growth (1% NaCl, anodic potential) is reduced by decreased loading frequency for high ΔK/low R, and is insensitive to frequency for near threshold cracking. The scatter bands represent the maximum variation in point by point, secant-based growth rates observed during constant ΔK experimentation at each frequency. The classical frequency effect reported for high strength aluminum alloys and characteristic of hydrogen environment embrittlement is not observed. Rather, the trends in Fig. 3 suggest that time dependent chemical reactions and mass transport, a requisite for hydrogen environment embrittlement, do not rate limit corrosion fatigue. Considering fractographic evidence and the effect of cathodic polarization, it is unlikely that the beneficial effect of low loading frequency is due to crack tip blunting by long term corrosion.

We currently believe that the aqueous environment corrosion fatigue response of alloy 2090 is rationalized based on surface film effects on crack tip damage. Those environmental conditions which favor the presence of a protective film; namely low strain rate (frequency), cathodic polarization, and passivating ions such as lithium (see the Li_2CO_3 experiment, Fig. 2); mitigate corrosion fatigue crack propagation. Corrosion product induced closure is not an important factor here, given the high stress ratios examined. Surface films may alter crack tip dislocation processes or affect the kinetics of hydrogen production and subsequent uptake into the metal. These arguments are highly speculative; experiments are being devised to further our understanding in this regard.

Gaseous Environmental Effects. All corrosion fatigue crack growth rate data for the LT orientation of alloy 2090, stressed in highly purified gaseous environments, are presented in Fig. 4. These results were reported previously; no new experiments have been conducted in the past six months.

The data in Fig. 4 support the hypothesis that surface films mitigate environmental fatigue crack propagation rates, apart form crack closure effects. The data for water vapor also suggest that hydrogen may embrittle aluminum-lithium based alloys, at least at high stress intensities.

The helium and oxygen environmental data shown in Fig. 4 are particularly important from both the aerospace design and damage mechanism perspectives. During this reporting period, we have considered the possibility that these data are influenced by trace impurities, particularly water and hydrocarbons, in the

ultra-high vacuum system described previously [1]. We are particularly concerned about the purity of nitrogen cold trapped, high purity (99.998%) He, and about contamination during very long term fatigue experimentation in the static gas environment. The question at hand is whether very low levels of water vapor can exacerbate environmental cracking. As described for Program 5, we have assembled a gas purification system to examine these concerns. The data contained in Fig. 4 will be confirmed by experiments during the next reporting period.

General Trends. Environment affects fatigue crack propagation in peak aged alloy 2090. At high stress intensity, the order of growth rate ranking from fastest to slowest is aqueous chloride (anodic), aqueous chloride (cathodic), water vapor, purified helium, moist air and oxygen. Oxygen particularly retards crack growth, while unexpectedly high rates are observed for pure helium. At near-threshold stress intensities, chloride and helium environments promote fatigue, with water vapor, moist air, cathodic polarization and pure oxygen progressively decreasing environmental crack growth rates.

We have also characterized the intrinsic corrosion fatigue crack propagation of peak aged alloy 7075. The data compiled in Fig. 5 show that the resistance of the advanced aluminum-lithium alloy to transgranular environmental cracking is better than that of the current aerospace alloy 7075. The high chemical reactivity associated with lithium does not result in abnormally high rates of corrosion fatigue for the conditions examined.

Conclusions.

1. The constant K_{max}/step increased constant ΔK and R method accurately characterizes the intrinsic fatigue crack growth behavior of Al-Li alloys.

2. Near threshold, intrinsic fatigue crack growth rates may be enhanced substantially by fixed grip loading, due to suppressed Mode II crack opening displacements.

3. Alloy 2090 is susceptible to corrosion fatigue crack propagation in aqueous NaCl under anodic polarization, with the effect particularly significant near threshold.

4. Classical hydrogen environment embrittlement is not supported by experimental observations. Rather, crack tip films play a role in corrosion fatigue damage as evidenced by 1) increased da/dN with increasing frequency, 2) reduced da/dN upon cathodic polarization and 3) reduced da/dN due to Li_2CO_3 additions.

5. Fatigue crack growth rates in gaseous environments support

the concept that surface films are critical to environmental fatigue damage.

6. Alloy 2090 is intrinsically more resistant to corrosion fatigue crack propagation compared to conventional alloy 7075.

Future Work.

1. Prove conclusion #2.

2. Devise experiments to substantiate conclusion #4.

3. Establish the effect of trace environment impurities on fatigue crack propagation in high purity gaseous environments.

4. Develop correlations between environmental crack growth rates and high resolution fractographic observations.

It is anticipated that Mr. Piascik's research project will be completed by the end of year 2 in April, 1989.

References

1. R.P. Gangloff, G.E. Stoner and R.E. Swanson, "Environment Assisted Degradation Mechanisms in Al-Li Alloys", University of Virginia, Report No. UVA/528266/MS88/101, January, 1988.

2. R.S. Piascik and R.P. Gangloff, "Aqueous Environment Effects on Intrinsic Corrosion Fatigue Crack Propagation in an Al-Li-Cu Alloy", submitted, Environmental Cracking of Metals, M.B. Ives and R.P. Gangloff, eds., NACE, Houston, TX in review.

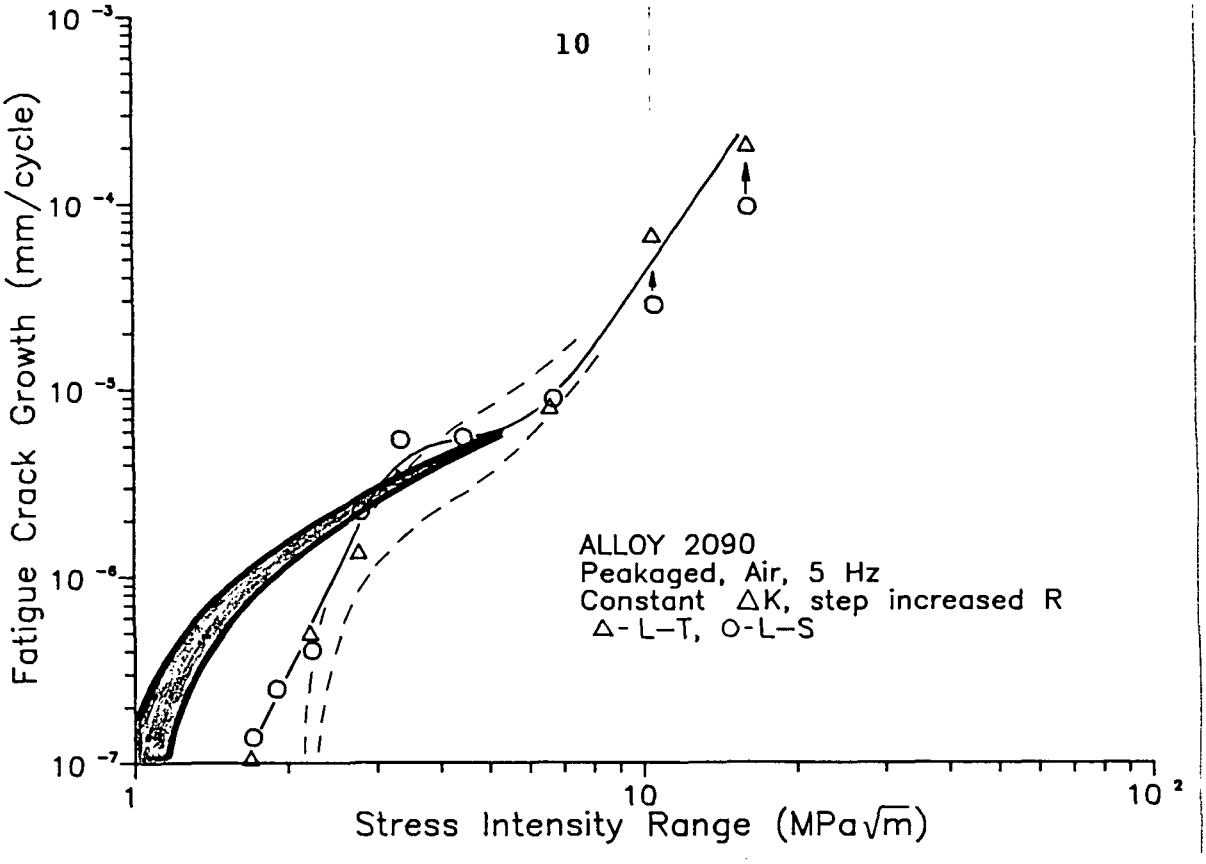

Figure 1 - The effect of gripping mode on near-threshold, intrinsic fatigue crack growth rates in alloy 2090 in moist air. The shaded band represents data for fixed grip, rotation free loading, while the data and dashed lines relate to freely rotating SEN and CT specimens.

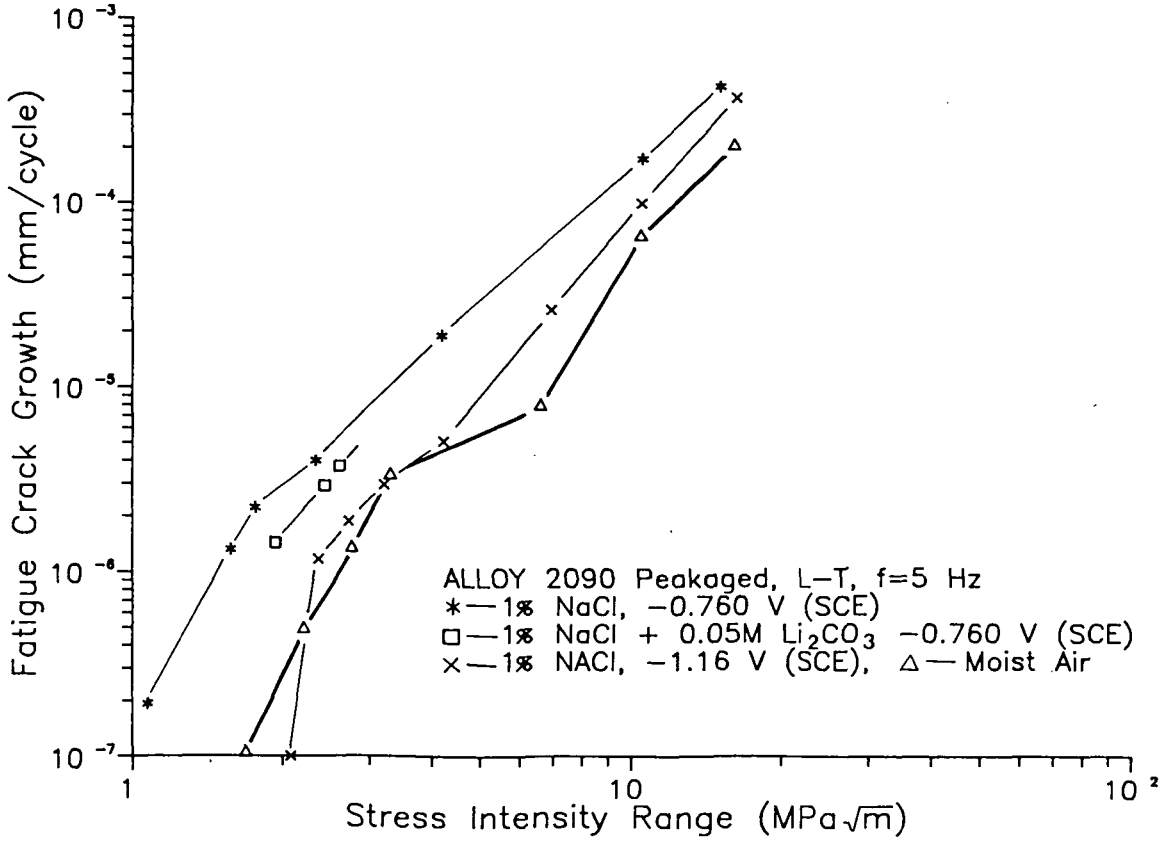

Figure 2 - Intrinsic corrosion fatigue crack growth in alloy 2090 (peak aged, LT) in aqueous 1% NaCl at constant anodic and cathodic potentials, and in 1% NaCl+0.05M Li_2CO_3. Air data are from Fig. 1.

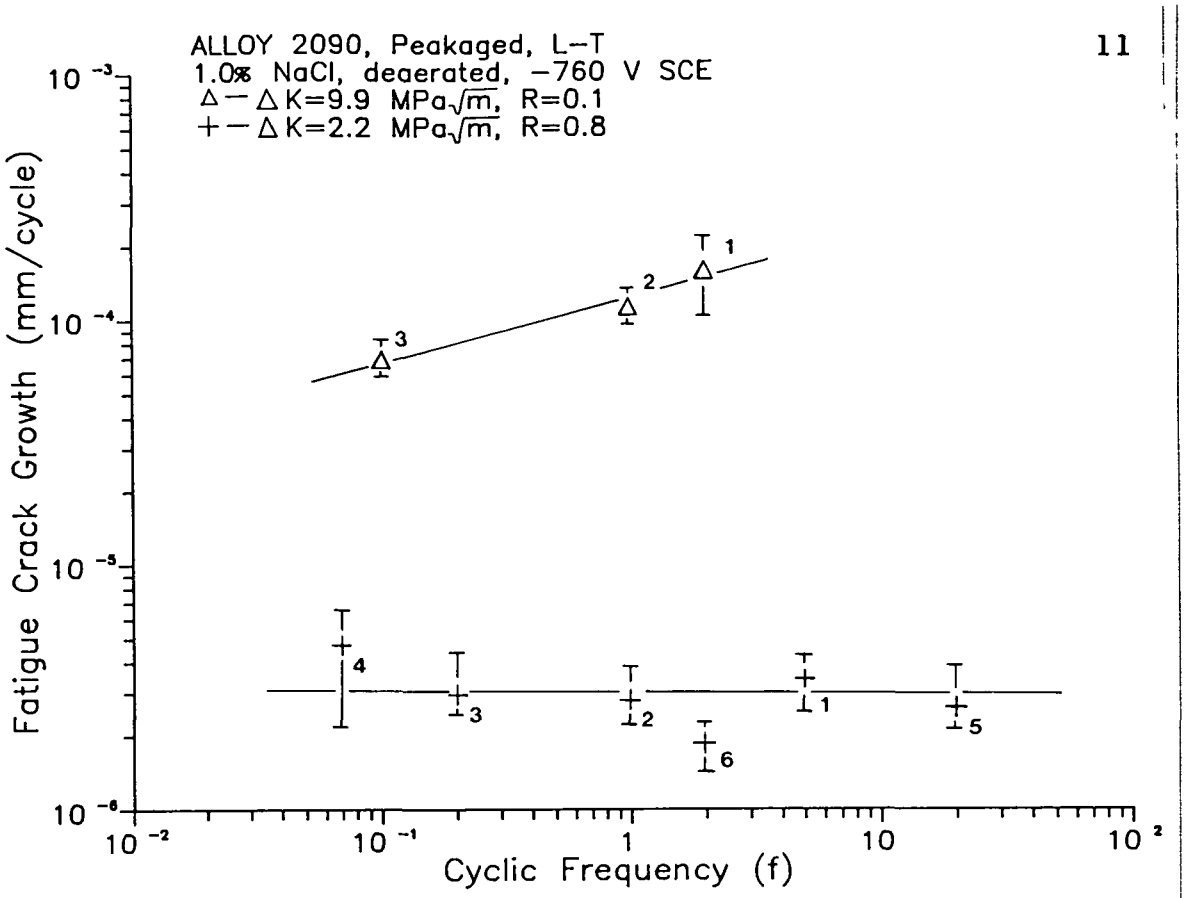

Figure 3 - The effect of cyclic load frequency on corrosion fatigue crack growth in alloy 2090 exposed to 1% NaCl at constant anodic potential for two stress intensity/stress ratio regimes.

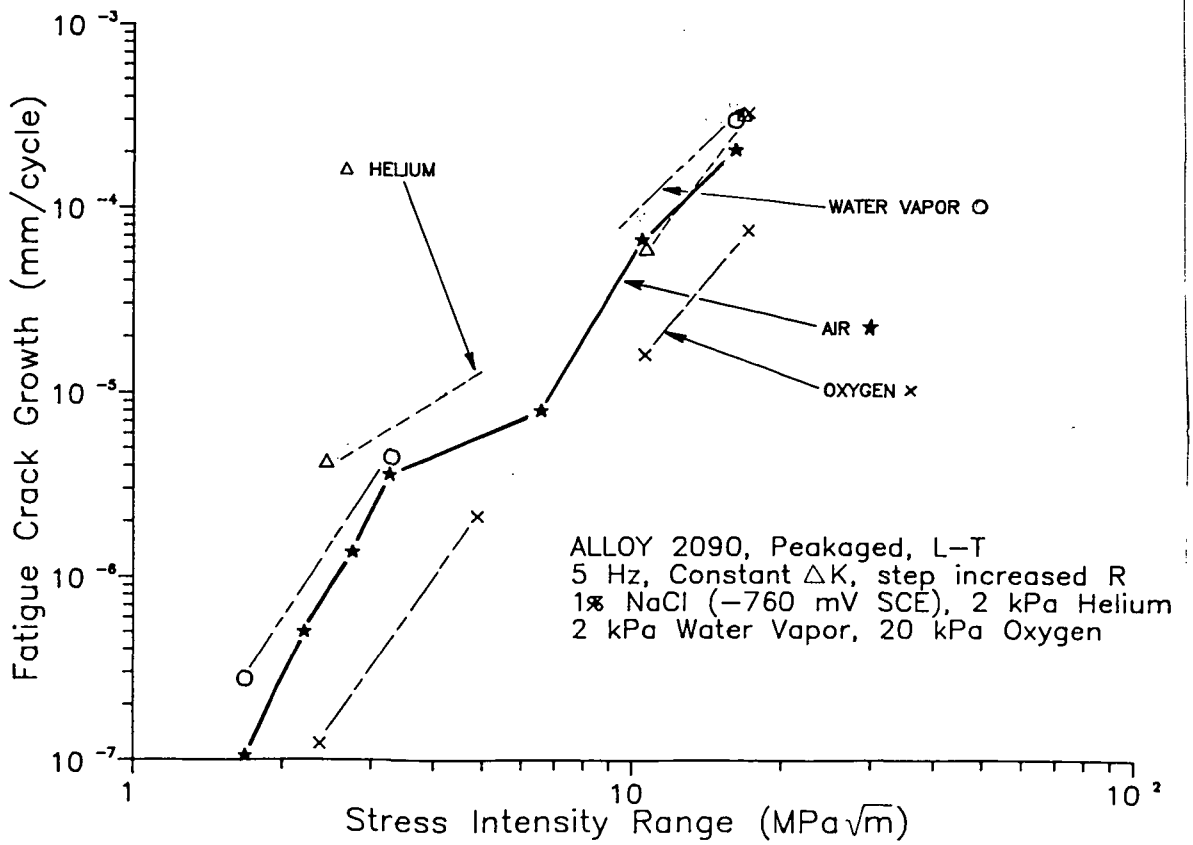

Figure 4 - Intrinsic corrosion fatigue crack growth in alloy 2090 (peak aged, LT) in highly purified gaseous environments including oxygen, helium and water vapor. Moist air data are from Fig. 1.

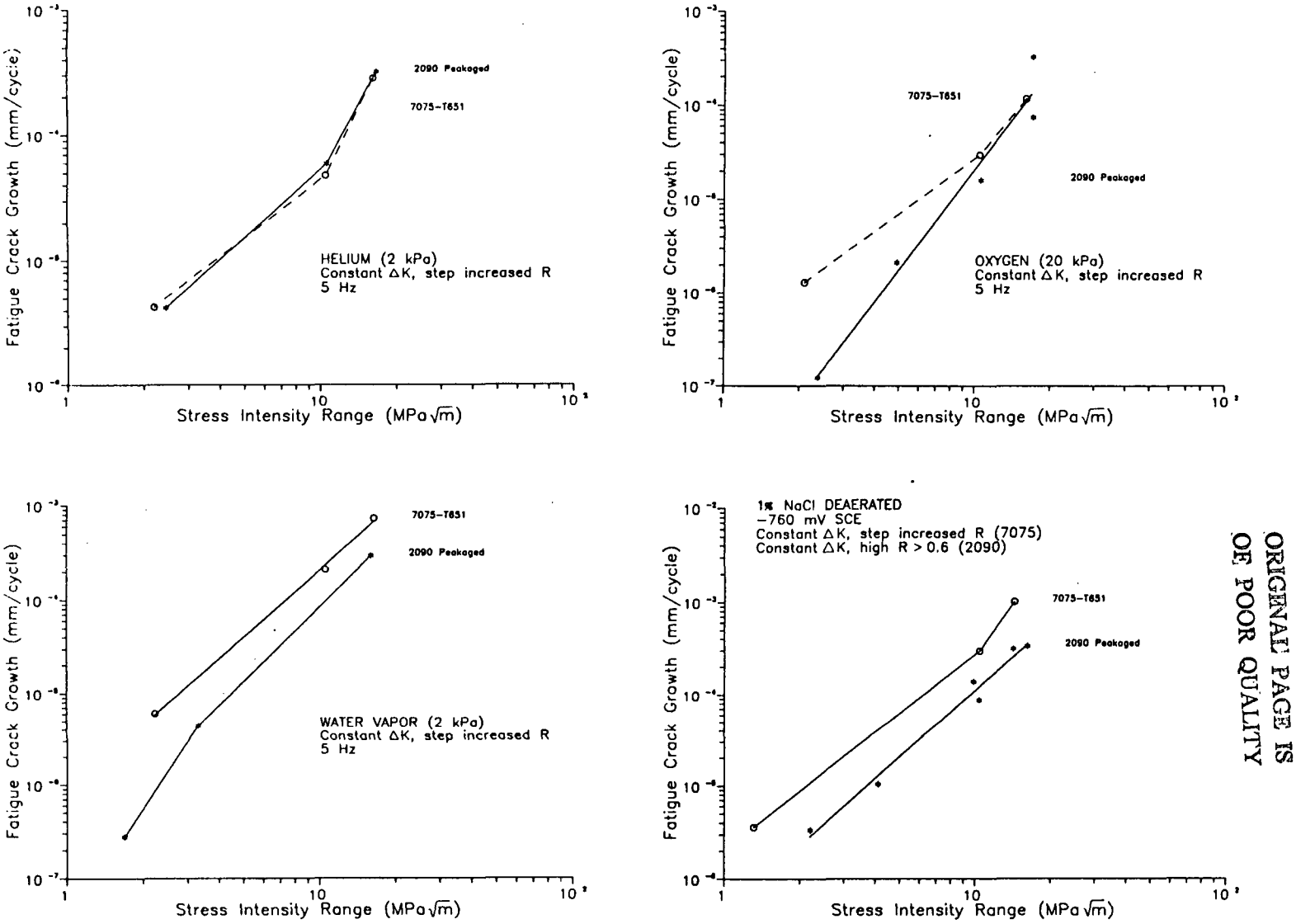

Figure 5 - Intrinsic fatigue crack propagation kinetics for peak aged 2090 and 7075 in various aqueous and gaseous environments.

Program 2. MEASUREMENTS AND MECHANISMS OF LOCALIZED AQUEOUS CORROSION IN ALUMINUM-LITHIUM ALLOYS

Rudolph G. Buchheit, Jr. and Glenn E. Stoner

Summary of Project Results:
December 1, 1987 through June 1, 1988

Objectives

The objectives of this work are:

1.) the development of experimental techniques which surmount the difficulties associated with monitoring solution chemistries that develop in occluded environments;

2.) the use of these experimental techniques to monitor the processes that contribute to the local corrosion and embrittlement of aluminum-lithium alloys.

Introduction

The crevice corrosion behavior of 2090 in 3.5 w/o NaCl solution has been examined using artificial crevice experiments. The results of artificial crevice experiments using 2090 have been compared to results obtained from similar experiments performed with 2024 and 7075. The technique used for artificially inducing crevice corrosion has been described in a previous report [1].

Crevice corrosion behavior has been monitored by measuring the pH and free corrosion potential inside and outside the crevice as a function of time. When the environmental conditions outside the crevice are varied, the crevice corrosion behavior is observed to change. The conditions varied were degree of bulk solution aeration and the degree of bulk solution agitation. The behavior of an isolated crevice has also been compared to that of a crevice coupled to an external surface cathode.

Scanning electron microscopy and X-ray energy analyses have been used to characterize the morphology and composition of the surfaces of specimens used in artificial crevice experiments.

Experimental Results

pH vs. Time Experiments. Two methods for simulating a crevice environment have been used to monitor pH vs. time response. In the first technique a hole slightly larger than the

measuring pH electrode is bored in a specimen [2,3]. The electrode is inserted into the bore. The small gap between the electrode and the specimen simulates the geometry of the crevice and allows pH measurements to be made. In the second technique, machine shavings of the test alloy are immersed in a small volume of test solution [4,5]. This simulates a high metal surface area to solution volume ratio characteristic of crevice corrosion situations. The pH of the solution is measured with a combination pH electrode. The two situations are not completely equivalent as evidenced by the fact that the pH response is different in each case. The pH that develops in 2090 shavings experiments is 2 to 3 pH units more alkaline than that developed in artificial crevice experiments. The differences in the responses of the two experiments is attributed to the higher metal surface area to solution volume ratio that exists in the shavings experiments.

Results of the pH vs. time experiments indicate several trends. Isolated crevices (crevices which are holes filled with solution, contain a pH electrode and are sealed) in conventional high strength aluminum alloys develop acidic crevices [6]. In contrast, isolated crevices in solution heat treated (SHT) and peak aged 2090 become mildly alkaline. This trend is commonly observed in lithium bearing aluminum alloys [6]. Experiments performed in this study have confirmed results reported in the literature. Alloy 2024-T3 quickly achieved a pH of 4.5 while peak aged 2090 developed a pH of 8.5 (Fig. 1). However, when the crevice in 2090 is coupled to an external surface cathode (achieved by immersing the specimen in bulk solution) the crevice will become acidic reaching a pH of 4.5.

The pH of isolated crevices in 2090 depends on alloy temper. Isolated crevices in peak aged alloys become more alkaline than those in under aged or SHT alloys. The solution in artificial crevices in peak aged 2090 specimens achieve a maximum pH of 8.5 to 9 compared to a pH of 7.5 to 8 for crevice solutions in the SHT alloy. A temper dependence in pH versus time response also exists in the shavings experiments. Solution containing peak aged shavings develop pH values between 10 and 11, while the pH of solutions containing SHT shavings generally ranges between 9 and 10.

Experiments monitoring the effects of aeration and agitation of the bulk solution on the crevice pH in 2090, 2024 and 7075 are currently in progress.

Potential vs. Time Experiments. Potential versus time measurements in shavings experiments are not practical since the measurement requires that the specimen be connected to the measuring circuit. In these experiments the specimen is finely divided metallic shavings. Therefore potential versus time

experiments can be made for artificial crevices only.

In these experiments two free corrosion potentials are measured. The first potential is the crevice corrosion potential measured between a Ag‖AgCl reference electrode inserted into a crevice and the metal specimen. The second potential is the free corrosion potential measured between a calomel reference electrode in the bulk solution and the metal specimen external surface.

Potential versus time response depends strongly on alloy composition, degree of bulk solution agitation and degree of solution aeration. Experiments are being performed to determine the effect of alloy temper on crevice potential versus time response.

Normally, free corrosion potentials for peak aged 2090 in aerated 3.5 w/o NaCl solutions achieve a steady state value of approximately -710 mV_{SCE} after 100 minutes of immersion in solution. However, in artificial crevice experiments with peak aged 2090, steady state crevice and bulk potentials were achieved only after 300 minutes. Further, in the first 300 minutes of these experiments, a potential spike of as much as 150 mV in the negative direction is observed in quiescent bulk solutions (Fig. 2). After the potential transient, a steady state bulk potential of about -710 mV is then recovered. Corresponding crevice potentials are generally 20 to 50 mV more negative than the bulk potentials after this potential transient.

Degree of aeration and agitation of the bulk solution altered the transient potential response in 2090. Deaerating the bulk solution before and during immersion of the specimen eliminated the transient response; that is , the more noble potential was never recovered (Fig. 3). Both the crevice and bulk potentials achieved a steady state value of -950 mV_{SCE}. The crevice potential was no more negative than the bulk potential suggesting that artificially stimulated crevice corrosion was suppressed due to the reduction in the dissolved oxygen content in solution.

Active aeration was accomplished by bubbling air through the bulk solution. Aeration reduced the magnitude of the potential transient to 50 mV in the negative direction (Fig. 4). The steady state bulk potential recovered to -730 mV after 400 minutes. The crevice potential was 15 mV more negative than the bulk corrosion potential in the steady state regime.

The reduction in the size of the potential transient when the bulk solution was actively aerated appeared to be caused by the agitation introduced by the bubbling action. When the bulk solution was agitated (but not actively aerated) by stirring with a magnetic stirring bar, transient response was eliminated

entirely (Fig. 5). Steady state potentials were achieved after 1000 minutes. In this case, the crevice potential was 75 mV more negative than the bulk potential in the steady state regime.

Potential versus time experiments have been performed on 2024-T3 and 7075-T651 in quiescent bulk solutions. The crevice and bulk potential response of 2024 were similar to those of peak aged 2090 in that a 150 mV potential transient in the negative direction before 300 minutes had elapsed (Fig. 6). However, the bulk corrosion potential eventually became more negative than the crevice potential. This behavior was attributed to severe crevice corrosion which occurred under the stop lacquer applied to the exterior of the specimen over an electrical connection.

In 7075, no potential transient was observed (Fig. 7). Initially, the crevice potential was 100 mV more negative than the bulk potential, but the difference decreased with time until the potentials were nearly equal after 4000 minutes.

Scanning Electron Microscopy and X-Ray Analysis. Alloy 2090 specimens used in artificial crevice experiments exhibited corrosion morphologies with several common characteristics. Corrosion was not homogeneous over the wall of the crevice. In crevices with longer aspect ratios the regions of most aggressive corrosion were concentrated near the crevice mouth.

Surrounding the mouth of the crevice on the specimen surface was a region where corrosion product build up was greater than at other points on the specimen surface. X-ray mapping showed a dramatic increase in copper at the lip of the crevice. Further away from the mouth of the crevice, small amounts of copper were deposited on surfaces in between larger areas of corrosion product build up. Under an optical microscope the deposits appeared to be pure, metallic copper. Copper deposits have also been observed at the mouths of crevices in 2024 specimens used in artificial crevice experiments.

X-ray analyses performed on corroded surfaces were done using a energy dispersive spectrometer attached to a scanning electron microscope. The solid state detector on the spectrometer is not capable of detecting elements below oxygen. As a result, detection of lithium was not feasible using this technique.

Conclusions

1. An alkaline pH (8.5 to 9) develops in isolated solutions in 2090 crevices while an acidic pH (4.5) develops in isolated solutions contained in 2024 crevices.

2. Coupling the crevice in a 2090 specimen to an external surface cathode causes the pH in the crevice solution to become acidic (pH = 4.5).

3. Crevice potential response in 2090 can be affected by changing the degree of aeration and agitation of the bulk solution in artificial crevice experiments.

4. Copper dissolution and reduction results in the formation of copper deposits at the mouths of artificial crevices.

Future Work

Planned research activities for 6/1/88 through 1/1/89 are aimed at understanding the following:

1.) Are the potential transients observed in artificial crevice experiments related to the phenomenon of copper dissolution and reduction observed in Al-Cu-X ternary alloys?

2.) Does copper dissolution and reduction control localized corrosion in Al-Li alloys?

3.) Does the crevice chemistry (e.g. potential, pH, $[Cl^-]$, dissolved oxygen) change with depth, and if so can these changes be monitored and used to understand the stress corrosion behavior of Al-Li alloys?

Specific experiments to be performed will include:

1.) An attempt to determine if the potential transient observed in copper bearing aluminum is related to the phenomenon of metallic copper deposition. Efforts will focus on corrosion activity which occurs in the first 300 to 400 minutes of an artificial crevice immersion experiment. Initial attempts will include:

a.) measurement of Cu^{2+} ion with an ion selective electrode as a function of time in solution periodically decanted from shavings experiments.

b.) interrupting artificial crevice experiments to analyze copper redistribution using scanning electron microscopy and X-ray analysis.

2.) Artificial crevice experiments will be performed on Al-Cu binary systems to determine if the copper deposition phenomenon is limited to ternary (or multicomponent) aluminum alloy systems.

4. J.G. Craig, R.C. Newman, M.R. Jarrett and N.J.H. Holroyd, "Local Chemistry of Stress Corrosion Cracking in Al-Li-Cu-Mg Alloys," Conf. Proc. 4th International Conference on Aluminum-Lithium Alloys, to be published (1987).

5. N.J.H. Holroyd, A. Gray, G.M. Scamans and R. Hermann, "Environment Sensitive Fracture of Al-Li-Cu-Mg Alloys," Aluminum-Lithium Alloys III, C. Baker, P.J. Gregson, S.J. Harris and C.J. Peel, eds., Institute of Metals, Oxford, UK, pp. 273-281 (1986).

6. N.J.H. Holroyd, G.M. Scamans and R. Hermann, "Environmental Interaction with the Crack Tip Region During Environment Sensitive Fracture of Aluminum Alloys," Embrittlement by the Localized Crack Environment, R.P. Gangloff, ed., TMS, Warrendale, PA, pp. 327-347 (1984).

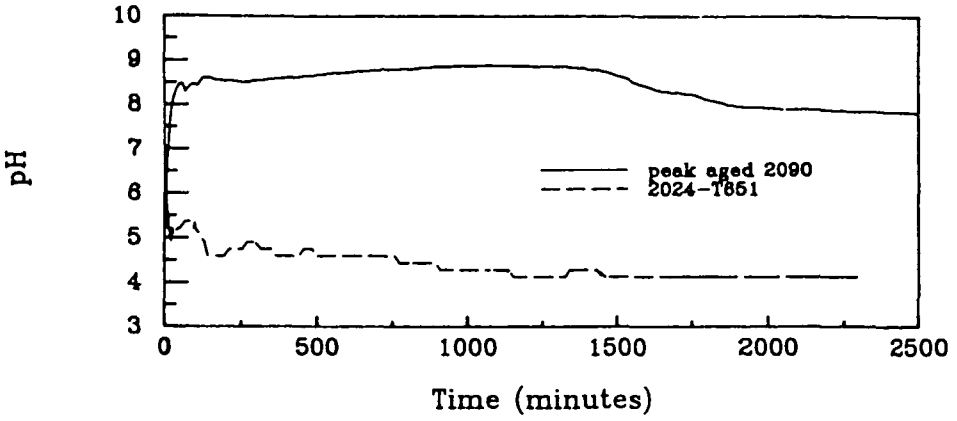

Figure 1. Plot of crevice solution pH versus time for peak aged 2090 and 2024-T651 in an isolated crevice experiment.

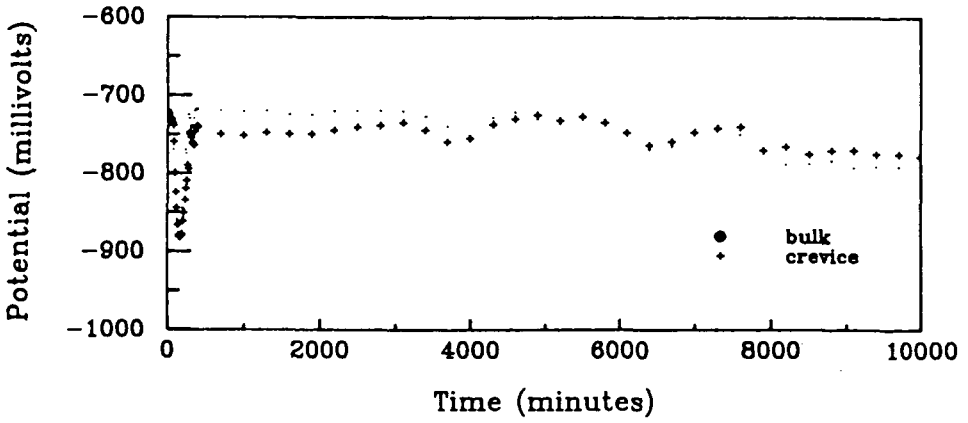

Figure 2. Plot of bulk and crevice corrosion potentials versus time for peak aged 2090 immersed in quiescent 3.5 w/o NaCl solution.

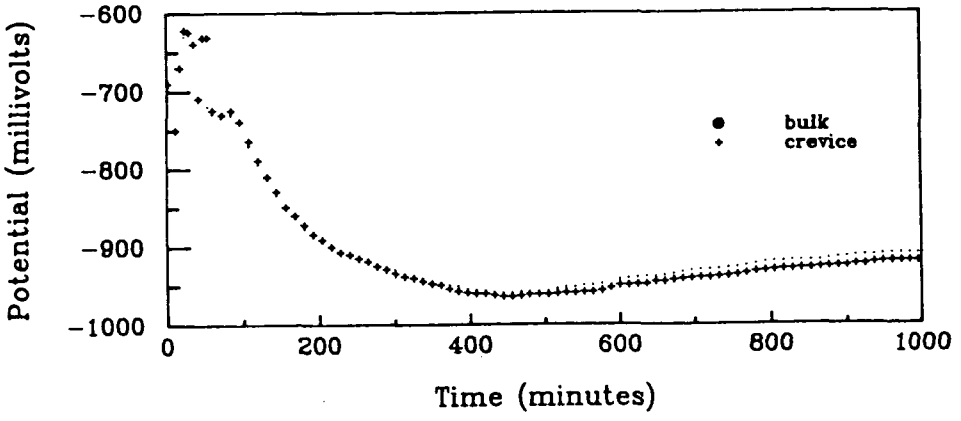

Figure 3. Plot of bulk and crevice corrosion potentials versus time for peak aged 2090 immersed in deaerated 3.5 w/o NaCl solution.

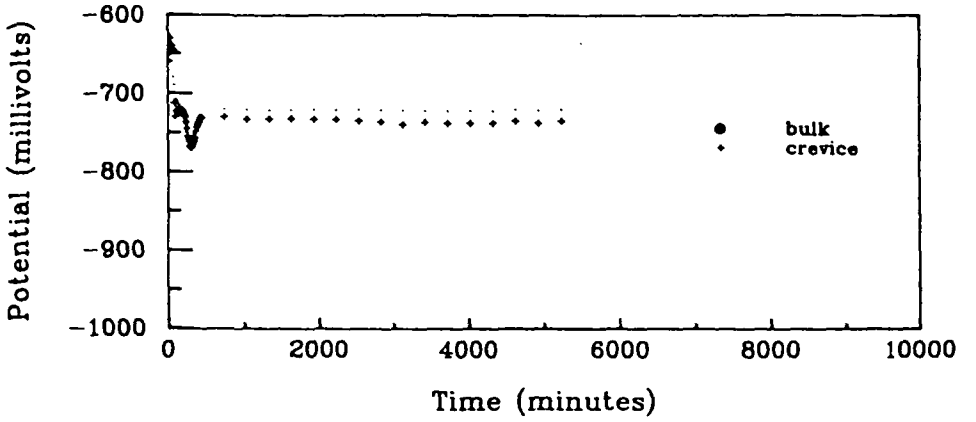

Figure 4. Plot of bulk and crevice corrosion potential versus time for peak aged 2090 immersed in actively aerated 3.5 w/o NaCl solution.

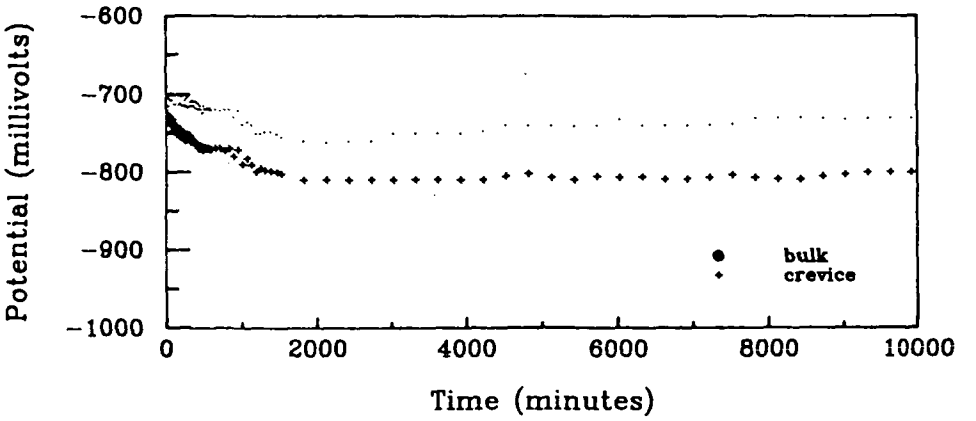

Figure 5. Plot of bulk and crevice corrosion potential versus time for peak aged 2090 immersed in agitated 3.5 w/o NaCl solution.

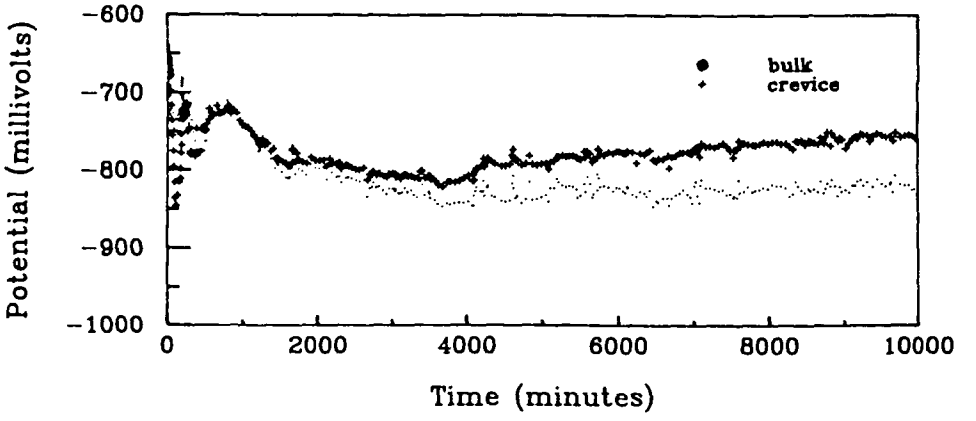

Figure 6. Plot of bulk and crevice corrosion potential versus time for 2024-T3 immersed in quiescent 3.5 w/o NaCl solution.

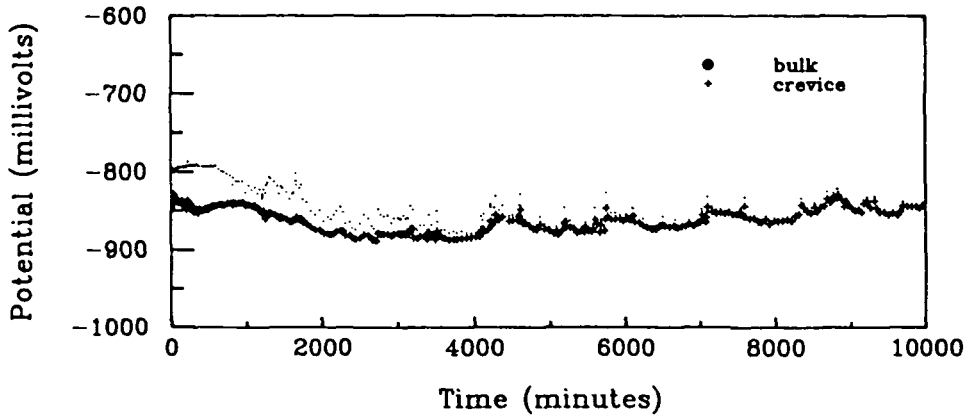

Figure 7. Plot of bulk and crevice potential versus time for 7075-T651 immersed in quiescent 3.5 w/o NaCl solution.

Program 3. DEFORMATION AND FRACTURE OF ALUMINUM-LITHIUM ALLOYS: THE EFFECT OF DISSOLVED HYDROGEN

R.E. Swanson

Background

A new program on "Environmental Degradation of Al-Li Alloys: The Effect of Hydrogen" has been approved by NASA for startup in year 2. The detailed proposal is presented elsewhere and describes a 24-month study to characterize the effects of hydrogen on the mechanical behavior and microstructure of Alloy 2090 [1].

The goal of this work is to increase our understanding of the role of microstructure and stress state on the susceptibility to hydrogen damage in Al-Li alloys. Microstructural characterizations will include: optical microscopy, scanning electron microscopy, transmission electron microscopy and differential thermal analysis or scanning calorimetry. Mechanical property characterizations will include uniaxial tension tests, biaxial loading tests, Charpy impact tests, and microhardness indention tests.

Progress has been achieved in anticipation of the program start and with the preliminary funding provided to VPI under the year 1 proposal. Specifically, a pressurized disk biaxial stressing apparatus has been modified for hydrogen embrittlement testing of alloy 2090. A significant portion of the year 1 (1987-88) funding was not spent due to Louthan's departure, and has been carried over to support the newly proposed program. A masters degree graduate student has been recruited and should begin work in July of 1988.

References

1. R.P. Gangloff, G.E. Stoner and R.E. Swanson, "Environment Assisted Degradation Mechanisms in Al-Li Alloys", University of Virginia, Report No. UVA/528266/MS88/101, January, 1988.

Program 4. DEFORMATION AND FRACTURE OF ALUMINUM LITHIUM ALLOYS: THE EFFECT OF CRYOGENIC TEMPERATURES

John A. Wagner and Richard P. Gangloff

Background

Cryogenic tanks are responsible for a large portion of the weight of current launch vehicles. It is envisioned that, by employing advanced alloy systems and advanced processing techniques, a significant savings can be realized. Superplastic forming (SPF) of Al-Li alloys offers the potential of such savings over current tanks fabricated from 2219 aluminum alloy. Al-Li alloy 2090 not only offers lower density and higher elastic modulus, but also the potentially desirable characteristic of increasing strength and toughness with decreasing temperature.

Currently 2090 + In is being investigated for application in cryogenic tanks. Indium is added to the alloy in an attempt to increase post-SPF properties without stretching. A program at NASA-LaRC has shown that by adding In to a basic 2090 alloy chemistry, strength levels could be achieved which approach the T8 condition without stretching. This approach is attractive for SPF operations since formed parts are not likely to be stretched to achieve high strength levels.

Northrop has recently demonstrated the superplastic formability of alloys based on the 2090, 8090 and 2090 + In compositions. Northrop was, however, unable to achieve high strength levels in post-SPF parts of indium modified 2090.

Objective and Approach

The goal of this research is to understand and optimize the fracture resistance of aluminum-lithium-copper alloys processed for thin sheet, cryogenic tankage applications. Both novel alloy compositions developed under NASA programs, and conventionally stretched or superplastically formed, precipitation hardened microstructures will be investigated, with materials purchased from Reynolds Metals.

Four issues will be emphasized:

(1) Examination of the deformation and fracture resistance of new Al-Li-Cu-In alloys and of superplastically formed microstructures.

(2) Development of quantitative fracture mechanics methods for characterizing the fracture initiation and stable growth resistance of thin sheet. Experiments will be designed to discriminate the behavior of different microstructures in a way which is both mechanistically interpretable and relevant to damage tolerant designs of cryotankage structures.

(3) Determination of the micromechanical mechanism(s) for the significant improvements in fracture (initiation) toughness observed for thick section Al-Li based alloys stressed at cryogenic temperatures.

(4) Definition of the role of dissolved hydrogen in the fracture process at both cryogenic and ambient temperatures.

Results

The initial phase of this study is concerned with determining if indium additions to 2090 do indeed promote increased strength levels in the T6 condition. Differential scanning calorimetry studies revealed a fairly narrow window for solution heat treatment (SHT) of the alloy. In early work at LaRC, an SHT of 560 C was employed and resulted in superior hardenability of the In bearing alloy, particularly for aging at 160 C. This effect was attributed to increased number density and homogeneous distribution of T1 precipitates. An SHT of 535 C was used in the Northrop study and the beneficial effect of adding In to the alloy was not realized. It was hypothesized that an SHT temperature of 535 C did not permit complete dissolution of T2 for subsequent optimal age hardening by T1.

Specimens of the Northrop material were obtained, solution treated at 560 C and aged for 72 hours at 160 C For the 2090 + In composition, the higher solution treatment temperature resulted in higher hardenability.

Because of the reasonable strain to fracture of the 2090 + In alloy and the potential to obtain T8 strength levels in SPF components given T6 aging treatments, this alloy and a 2090 baseline were scaled from 30 pound permanent mold castings to 400 pound DC castings by Reynolds. The following specific materials have been delivered to NASA-LaRC;

Plates:	1/2"x47"x34"
	1/8"x17"x34"
Compositions:	Al-2.65Cu-2.17Li-0.13Zr-0.05Si-0.05Fe
	Al-2.60Cu-2.34Li-0.16Zr-0.04Si-0.05Fe-0.17In

Processing: Solution heat treat at 556 C
Ice water quench
3% stretch or 0% stretch for In alloy

Solution heat treat at 537 C
Ice water quench
Age 413 C for 16 hours
Hot roll at 288 C to 1/8 thickness
(This is the so-called TMT C process)

The isothermal aging response of the following combinations of these alloy and process conditions are being defined for 160 and 190 C:

2090; 1/8" plate; SHT 556 C; stretch 3%
2090; 1/8" plate; TMT C; SHT 556 C
2090; 1/2" plate; SHT 556 C; stretch 3%

2090+In; 1/8" plate; SHT 556 C; stretch 3%
2090+In; 1/8" plate; TMT C; SHT 556 C
2090+In; 1/2" plate; SHT 556 C; stretch 3%
2090+In; 1/2" plate; SHT 556 C

Additionally, 2090 and 2090+In specimens obtained from Northrop will be examined in terms of aging behavior. Solution heat treatment temperatures of 537 and 556 C will be evaluated.

This hardness study will enable us to establish the influence of casting practice, SHT temperature, alloy addition, product form and stretching on the hardenability of 2090 based alloys. From this initial evaluation, alloy compositions and processing conditions will emerge for subsequent evaluations of the effects of crack/sheet geometry, cryogenic temperatures and dissolved hydrogen on deformation and fracture resistance.

We have also received six square feet of 0.081" thick, 2090 sheet from the Alcoa Technical Center. This material is provided in the T8E53 temper, an experimental condition, after 1 to 3% stretch. While not firmly established, it is likely that this temper involved 10 hours at between 150 and 163 C. The yield strength is specified as 467 MPa (longitudinal) and 459 MPa (long transverse). The plane stress fracture toughness is 73 $MPa \cdot m^{1/2}$ for the LT orientation and 77 $MPa \cdot m^{1/2}$ for the TL orientation, with each value obtained for 16" wide and 44" high test panels. Apparently, this material was processed for optimal strength and toughness, with the lower temperature underaging critical in this regard.

Program 5. ELEVATED TEMPERATURE CRACK GROWTH IN ADVANCED PM ALUMINUM ALLOYS

William C. Porr, Jr. and Richard P. Gangloff

Background

Advanced light metallic materials are typically evaluated in terms of simple microstructural, tensile, toughness and corrosion behavior. As a second stage in this development, it is critical to assess environmental fatigue and fracture resistance in terms of modern fracture mechanics concepts, and to enable defect tolerant design for component durability in a variety of aggressive aerospace environments.

A new program was initiated in April of 1988 to examine the elevated temperature subcritical crack growth and fracture resistance of advanced, powder metallurgy Al-Fe based ternary and quaternary alloys. Over the next few months, the student will review the literatures of elevated temperature ductility and "creep crack growth" in aluminum alloys, and of time dependent elastic-plastic fracture mechanics crack tip fields and experimental techniques. In conjunction with NASA-LaRC researchers in metals and fatigue/fracture, Mr. Porr will develop a research plan involving alloy selection and experimental design.

Mr. Porr has worked on NASA program areas since the Fall of 1987. This effort was enabled by the fact that Mr. Piascik was appointed and funded as a Teaching Assistant by the Materials Science Department for the Fall, 1987 term. Mr. Porr filled Mr. Piascik's grant slot and was funded for 6 months by NAG-1-745. Several accomplishments were recorded.

Research

Mr. Porr has designed, specified and participated in the purchase of an environmental system for crack growth and fracture experimentation in controlled pure gas or vacuum environments and as a function of cryogenic to elevated temperature. The funding for this capital equipment was a line item in the year 1 budget.

Specifically, we have taken delivery on an ATS box furnace which is attachable to our servoelectric Instron machine or our servohydraulic MTS machine. This apparatus, in conjunction with a microprocessor based controller, will allow mechanical specimen temperature control from -170 C to +450 C. Porr has designed and is assembling an ultrahigh vacuum chamber to fit within the temperature chamber, and to contain crack growth and tensile fracture specimens. This chamber will be evacuated by the ultra-

high vacuum roughing/oil diffusion pump system which is currently used in the corrosion fatigue experiments reported in Program #1. We anticipate that this system will achieve chamber pressures of better that 4×10^{-7} torr with full specimen instrumentation; including load, displacement, crack growth by electrical potential and temperature. Initial experiments are likely to be simple tensile or creep rupture types with a minimum of complex instrumentation. The system will be made operational during the next reporting period.

Secondly, Mr. Porr has collaborated in the design and construction of an improved system to purify gaseous helium for introduction to the vacuum system employed in corrosion fatigue experimentation, Program #1. This new system purifies He by a room temperature molecular sieve followed by a commercial, hot metal chip gettering furnace. The connections between this ultra-low oxygen and water vapor gas source are of minimal length and were made according to good high vacuum procedures to minimize recontamination of gettered helium. The construction of this purification system was completed during the this reporting period. Corrosion fatigue experiments are planned for the next two months, and the apparatus will also be used in conjunction with the temperature environment chamber described in the previous paragraph.

APPENDIX I. GRANT PUBLICATIONS

Invited paper for the ASTM 20th National Symposium on Fracture Mechanics, Lehigh University, Bethlehem, PA, 23-25 June 1987

ENVIRONMENTALLY ASSISTED CRACK GROWTH IN STRUCTURAL ALLOYS: PERSPECTIVES AND NEW DIRECTIONS

Robert P. Wei[1/] and Richard P. Gangloff[2/]

ABSTRACT

Environmentally assisted crack growth (namely, stress corrosion cracking and corrosion fatigue) in alloys is one of the principal determining factors for durability and reliability of engineering structures. Over the past 20 years, activities in this area have transformed from principally that of screening and of qualitative characterizations of the phenomena, to that of quantitative assessment and scientific understanding. This work has enabled the recent development of life prediction procedures.

In this paper, the contributions of fracture mechanics in this transformation are reviewed. Current mechanistic understanding of environmentally assisted crack growth by hydrogen embrittlement is summarized, and is placed in perspective. Applications to mitigate stress corrosion and corrosion fatigue cracking in marine environments are summarized. Some outstanding issues and new directions for research are discussed.

[1/] Professor, Department of Mechanical Engineering and Mechanics, Lehigh University, Bethlehem, PA 18015

[2/] Associate Professor, Department of Materials Science, University of Virginia, Charlottesville, VA 22901

ENVIRONMENTALLY ASSISTED CRACK GROWTH IN STRUCTURAL ALLOYS: PERSPECTIVES AND NEW DIRECTIONS

Robert P. Wei[1/] and Richard P. Gangloff[2/]

INTRODUCTION

Environmentally assisted cracking of structural alloys (incorporating the well known phenomena of stress corrosion cracking and corrosion fatigue) is well recognized as an important cause for the failure or early retirement of engineering structures. Stress corrosion cracking (SCC) was first recognized as a technological problem in the last half of the 19th century as "season cracking" in cold drawn brass [1], with corrosion fatigue (CF) being recognized in the early 1900's [2,3]. Brown, tracing the historical background through 1972, concluded that "SCC, once thought confined to a few systems (combinations of metals and environments), must now be regarded as a general phenomenon which any alloy family may experience, given the wrong combination of heat treatment and environment" [1].

Bolstered by defense related interests and by safety issues in the energy industry, there was a decade of unusually high research activity from the early 1960's to the early 1970's [1]. Because of these interests and of the impact of the "energy crisis", work continued through the 1970's in support of offshore oil exploration and various alternative energy systems, such as, coal gasification and liquefaction, and solar energy. Coincidental to these activities, fracture mechanics was under-

going considerable development and maturation, and became increasingly accepted as an important tool in structural analysis and materials research.

In this paper a heuristic summary of the key developments in environmentally assisted crack growth in structural alloys is given, and key issues and new directions for research are discussed. The intent of this summary is to highlight the significant milestones and the contributions of fracture mechanics. As such, it does not include a complete chronology of all of the developments and contributions to this field. A complete view of these developments over the past 20 years may be gleaned from several monographs and from the proceedings of a large number of international conferences and symposia [1,4-23].

Chronologically, it is convenient to think of three periods, 1966 to 1972, 1972 to 1978, and 1978 to the present. Much of the groundwork in the United States was established during the first of these periods under two major programs, one sponsored by the Advanced Research Projects Agency of the Department of Defense (ARPA Coupling Program on Stress Corrosion Cracking) and the other by the Air Force Materials Laboratory [1,24]. It was during this period that the fracture mechanics methodology was first introduced.

Activities in the 1972 to 1978 period were devoted principally to phenomenological characterizations of cracking response, and to the development of empirically based design and failure analysis methods. Initial efforts toward quantitative mechanis-

tic understanding were launched, and science based approaches began to be formulated.

The past decade, beginning with 1978, is a period of transition. Scientific understanding of environmentally assisted crack growth and engineering application of this understanding are placed on a quantitative footing. Significant advances have been made, and are possible with the development of more sophisticated analytical instrumentation and experimental techniques. More emphasis is now needed to translate the improved understanding into methods for quantitative design and to improve structural reliability.

INITIATION vs PROPAGATION (Dawn of an Era)

A key turning point in the study of environmentally assisted crack growth and in the approach to design occurred in 1965. Brown and his coworkers [25,26] at the Naval Research Laboratory were encouraged to investigate the stress corrosion cracking susceptibility of titanium alloys by using specimens which were deliberately precracked in fatigue. Due to this initial crack, the alloy was highly susceptible and fractured in a matter of minutes, even though it appeared immune to stress corrosion cracking when stressed in the smooth (uncracked) state in the same electrolyte.

As a result of these findings, a major shift in emphasis was made from testing of smooth and mildly notched specimens to that of cracked bodies. Fracture mechanics was introduced as a basis for analyzing environmentally assisted cracking in a paper by H.

H. Johnson and P. C. Paris [27] in the First National Symposium on Fracture Mechanics in 1967. Experimental support for the use of the crack tip stress intensity factor (K) to describe the mechanical driving force was provided by Smith, Piper and Downey [28] for stress corrosion crack growth (Fig. 1), and by Feeney, McMillan and Wei [29] for corrosion fatigue (Fig. 2). A formal discussion of the use of crack tip stress intensity to describe the mechanical driving force for crack growth was given by Wei [30].

Early users of this emerging technology for environmental cracking investigations include Steigerwald and Troiano [31], Hanna and Steigerwald [32], Johnson and Willner [33], and Hancock and Johnson [34] for stress corrosion cracking (or crack growth under sustained loading), and Bradshaw and Wheeler [35], Hartman [36], and Li, Talda and Wei [37] for corrosion fatigue. Some early work predated the usage of the K concept. The effort associated with the ARPA Coupling Program made extensive use of fracture mechanics, and contributed to the development of fracture mechanics based technology for materials evaluation and for design [1].

PHENOMENOLOGICAL CHARACTERIZATION (1966 to 1972)

Two important approaches emerged from the early activities on stress corrosion cracking using precracked specimens [30,38]; namely the threshold and the kinetics approaches. The choice of a particular approach was determined in part by tradition and design philosophy, and in part by practical considerations of

experimentation and cost.

The simpler and less expensive approach involves the measurement of time-to-failure for precracked specimens under different applied loads, and the determination of a so-called threshold stress intensity factor (designated as K_{Iscc}), below which (presumably) no failure would occur by stress corrosion cracking [25,30,38,39]. The level of K_{Iscc} in relation to K_{Ic}, the plane strain fracture toughness of a material, provided a measure of stress corrosion cracking susceptibility. The use of the threshold approach was favored for material selection and for safe-life design.

The second approach was more complex, and involved the determination of crack growth kinetics [30,38]. It required the measurement of crack growth rate (da/dt) under controlled environmental conditions and as a function of the mechanical crack driving force, which is characterized by the stress intensity factor K. This approach required greater effort and more sophisticated instrumentation, and was favored for mechanistic studies and for fail-safe design. A similar distinction in approach existed for corrosion fatigue [40].

Both of these approaches were widely used. The period from 1966 to 1972 was principally devoted to phenomenological characterizations of materials response and to the development of empirically based design approaches. The final report for the ARPA Coupling Program, published as a monograph [1], reflects the typical efforts during this period.

It was during this period that a number of key studies [30,33-37,41-47] took place which helped to set the stage for the development of quantitative understanding of environmentally assisted crack growth over the next decade. These studies also showed the importance of the kinetics approach, and served to establish its use in subsequent investigations. Some of the important findings are as follows:

- o There was an increasing awareness of the importance of the kinetics approach, and a recognition of the fact that stress corrosion crack growth progresses in three stages (Fig. 3) [31,41]. The particular significance of the K-independent Stage II in terms of mechanistic understanding of crack growth response was also recognized. The approach was used extensively by Speidel [42] to study the influence of halide ions on stress corrosion crack growth in high strength aluminum alloys, and by Wei and his coworkers [43-44] to examine hydrogen embrittlement of high strength steels.
- o The effectiveness of using crack growth rate as a means for understanding the mechanisms for environmental enhancement of crack growth under sustained loading was demonstrated by Johnson and coworkers [33,34], and of fatigue crack growth by Bradshaw and Wheeler [35], Hartman [36], and Wei et al [37]. Through studies of the influences of different environments and of the inhibiting effect of trace amounts of oxygen, these researchers demonstrated the importance of surface reactions as a part of the embrittlement sequence (Fig. 4).

- o Pressure and temperature were recognized as important probes for identifying the processes that control environmentally assisted crack growth under sustained loading [31,33,34,45, 46] and in fatigue [31,35,37,47].
- o Early recognition of the relationship between stress corrosion and corrosion fatigue crack growth, and modeling of corrosion fatigue crack growth as a superposition of fatigue and stress corrosion cracking processes [48].

As an illustration of the phenomenological characterization effort, typical Stage II crack growth rate data for a high strength (AISI 4340) steel, stressed in various environments, are shown as a function of temperature in Fig. 4 [44,49]. These data demonstrated that the crack growth response can vary widely with environmental conditions, and can depend uniquely on temperature. Fractographic evidence suggested that the micromechanism for crack growth in these diverse, hydrogen producing environments was the same. Thus, the different response had to be attributed to one of several chemical processes in the overall chain.

Based on these initial findings, it was recognized that further progress in understanding environmentally assisted crack growth was not possible without integrating, at least, the fracture mechanics based kinetic measurements with independent measurements of the kinetics of participating chemical processes.

DEVELOPMENT OF A SCIENTIFIC APPROACH (1972-1978)

Beginning in 1972, a scientific approach to the study of environmentally assisted crack growth in high strength alloys began to be developed, and evolved over the following years [40,43,44,50,51]. The approach was grounded in linear fracture mechanics and was predicated on the recognition that environmentally assisted crack growth is the result of a sequence of processes and is controlled by the slowest process in the sequence [40,50].

The processes that are involved in the environmental enhancement of crack growth in high-strength alloys by hydrogen and hydrogenous gases (such as H_2O and H_2S) and by aqueous environments are as follows, and are illustrated schematically in Fig. 5 for the case of gaseous environments [40,50]:

1. Transport of the deleterious environment to the crack tip.
2. Reactions of the deleterious environment with newly produced crack surfaces to effect localized dissolution and to produce hydrogen.
3. Hydrogen entry (or absorption).
4. Diffusion of hydrogen to the fracture (or embrittlement) site.
5. Partitioning or distribution of hydrogen among various microstructural sites.
6. Hydrogen-metal interactions leading to embrittlement at the microstructural sites.

The actual processes depend on the mechanism of crack growth enhancement; namely, active path dissolution or hydrogen embrittlement. For a dissolution mechanism (see (6)), only the first two steps in the sequence need to be considered, and the

anodic (dissolution) reactions in the second step are directly responsible for crack growth enhancement. On the other hand, if hydrogen embrittlement is the responsible mechanism, then the reaction step serves only as the source for hydrogen; the remaining processes (3 through 6) must be considered. These steps are identical for aqueous and gaseous environments.

The overall crack growth response is governed by the rate controlling process in conjunction with the mechanical driving force, which is characterized here by either the local stress or the crack tip stress intensity factor, K [27,31,40].

Embrittlement, or the final step in the sequence is a function of microstructure. The extent of embrittlement, or the rate of cracking along each microstructural path, depends on the local hydrogen concentration, which depends in turn upon the external conditions (i.e., pressure, pH, electrode potential, temperature). Cracking along the various microstructural paths can take place concurrently (in parallel) with the overall crack growth rate given as the weighted average of the individual rates.

Clearly, the understanding of crack growth required identification and quantification of the rate controlling process. The evolving scientific approach, therefore, focused upon well defined and coordinated chemical/electrochemical, mechanical and metallurgical experiments.

It was recognized from the outset that the concept of rate controlling processes applied to both stress corrosion (or sustained-load) and corrosion fatigue crack growth, and that considerations of both modes of crack growth would afford a syner-

gism in exploring the fundamental issues. Because of the ready linkage of a K-independent regime (Stage II) of crack growth to the underlying rate controlling process, early efforts were directed at sustained-load crack growth. Detailed studies of the kinetics and mechanisms of reactions of water with iron and steel, and of Stage II crack growth were carried out as a function of temperature [51-55]. These efforts led to an unambiguous identification of the iron-water oxidation reaction as the rate controlling process for crack growth in high-strength steels in 1977, and a realization of the very limited extent of these reactions [6-10] (see Fig. 6).

With additional work on surface reactions and on crack growth, a broader based understanding of rate controlling processes emerged during the remainder of the 1970's, and modeling of sustained-load crack growth was begun. In 1977, this approach was used to examine the role of water vapor in enhancing fatigue crack growth in high-strength aluminum alloys [56], and the role of hydrogen sulfide in enhancing fatigue crack growth in steels [57]. These efforts led to the modeling of corrosion fatigue crack growth [58,59], which led in turn to the recognition and modeling of transport-controlled crack growth under sustained loading [60].

CHEMICAL AND MICROSTRUCTURAL MODELING

The modeling effort, which began in the late 1970's, emerged as an important adjunct of the scientific approach over the past 10 years. It has provided guidance and a formalized framework

for examining the fundamental issues, and has served as a basis for the utilization of data in design. Chemical and microstructural modeling of stress corrosion and corrosion fatigue crack growth are briefly summarized to provide perspective and to serve as a basis for discussing directions for future research.

Modeling of crack growth may be sub-divided in terms of loading conditions, and additionally according to the various processes that affect crack growth (see Fig. 5). Assuming hydrogen embrittlement as the responsible mechanism, modeling may then be grouped in terms of hydrogen supply (transport, reactions and diffusion), hydrogen distribution within the material (partition), and embrittlement reactions (which determine the rates of cracking along the various microstructural paths), and incorporates suitable methods for obtaining an average or macroscopic crack growth rate. Most of the effort during this period has concentrated on chemical modeling, and reflects developments in understanding the chemical and fracture mechanics aspects of environmentally assisted crack growth. More recently, this effort has been extended to include the influence of microstructure.

Sustained-Load Crack Growth

Initial modeling of sustained-load crack growth was largely phenomenological and was limited to the case of hydrogen-supply controlled Stage II crack growth in the lower temperature region (Region A in Fig. 6). The principal thrust was directed at obtaining reliable chemical reaction and crack growth data to

confirm the concept of rate controlled crack growth and to identify the controlling process. Obvious deviations of the crack growth response curves (Fig. 6) from those of single rate controlling processes and the observed changes in fracture paths (or micromechanisms) led to the consideration of transfers of control and of the role of microstructure.

Models Based On Hydrogen Supply. Models for Stage II crack growth were proposed on the basis of extensive data on the kinetics of surface reactions and crack growth for high-strength steels in water/water vapor, hydrogen and hydrogen sulfide [45,46,50,52-62]. When the reactions are slow (e.g., in hydrogen and in water), Stage II crack growth rate is controlled by the rate of surface reactions. On the other hand, for very rapid reactions (e.g., in hydrogen sulfide), the growth rate is determined either by the rate of transport of the gases to the crack tip, or by the rate of diffusion of hydrogen to the embrittlement site. The models, expressing the specific dependence on gas pressure (p_o) and temperature (T), are as follows [44,63]:

Transport Control: $(da/dt)_{II} = C_t p_o / T^{1/2}$ (1)
(for Knudsen flow [64])

Surface Reaction Control: $(da/dt)_{II} = C_s p_o^m \exp(-E_s/RT)$ (2)

Diffusion Control: $(da/dt)_{II} = C_d p_o^{1/2} \exp(-E_d/2RT)$ (3)

The constants C_i contain chemical and physical quantities that relate to gas transport, surface reaction, etc., and reflect the susceptibility of specific alloys to embrittlement by specific

environments (viz., the embrittlement reaction term). E_s and E_d are the activation energies for surface reaction and hydrogen diffusion respectively. Good agreement with experimental observations in the low temperature region (Region A) is indicated in Fig. 6.

In these models, a single process is assumed to be in control, and the terms C_i are assumed to be sensibly constant. It is recognized that transfer of control from one process to another may occur as the environmental conditions are changed. The consequences of this transfer have been discussed [63]. In formulating these phenomenological models, simple (single step) reactions were implicitly assumed. Because the reactions tend to be more complex, these models are viewed as starting points for developing further understanding of environmentally assisted crack growth.

Partitioning of Hydrogen and Surface Phase Transformation. The observed decrease in sustained-load crack growth rate with increasing temperature in the "high temperature" region (Region C in Fig. 6) for carbon martensitic steels (such as, AISI 4340 steel) has been analyzed based on surface chemistry [46,65,66]. Similar analyses have been attempted to account for the much steeper decrease in crack growth rate for 18Ni maraging steels [67]. These analyses, however, have ignored the important role of microstructure and micromechanism in hydrogen embrittlement, or have made unrealistic assumptions regarding surface coverage by hydrogen. The models proposed on the basis of these analyses, therefore, cannot explain the observed changes in fracture

mode with temperature [49].

To quantitatively account for the role of hydrogen-microstructure interactions, a "hydrogen partitioning" model was developed [49]. The model suggested that the rate of hydrogen assisted crack growth is determined by two factors: (i) the rate of hydrogen supply to the fracture process zone, and (ii) the partitioning of hydrogen amongst different microstructural elements or traps (principally between prior-austenite grain boundaries and the martensitic matrix). The partitioning of hydrogen is controlled by hydrogen-trap interactions and determines the contribution by each element to the overall crack growth rate, which is the weighted average of rates of cracking along the different microstructural paths. This model is illustrated schematically in Fig. 7 for hydrogen assisted crack growth in a high strength steel. Detailed considerations and a derivation of the model are given in [49].

At low temperatures (in Region A of Fig. 6), hydrogen would reside primarily at grain boundaries and slip planes. Crack growth would tend to be predominantly intergranular (IG), and would conform to Eqns. (1) to (3). With increasing temperature (into Region C), the hydrogen supply processes remain in control, but hydrogen concentration at the grain boundaries and in the slip planes decreases and more hydrogen would reside in the martensite lattice. This temperature induced partitioning of hydrogen leads to increasing amounts of microvoid coalescence (MVC) and to slower crack growth rates. The change in crack

growth rate with temperature reflects a transfer of cracking mechanisms, rather than (or in addition to) a change in the process of hydrogen supply. The predicted temperature and pressure dependences for Stage II crack growth in high-strength steels were in good agreement with crack growth data for an AISI 4340 steel in hydrogen and in hydrogen sulfide (see, for example, Fig. 8) [49].

For the 18Ni maraging steels, a phase transition model was proposed to account for the abrupt decrease in crack growth rate that had been observed at the higher temperatures [50,68]. The model was based on the suggestion by Hart [69] that solute atoms can undergo a phase transformation at certain temperatures and pressures, and conformed with experimental observations.

Clearly, a number of factors can influence the kinetics of environmental crack growth. The hydrogen partitioning and surface phase transition models have provided some insight, and a clear indication of the need for a broadly based understanding, including that of the embrittlement mechanisms.

Fatigue Crack Growth

Based on the understanding developed for sustained-load crack growth, models for surface reaction and transport controlled fatigue crack growth were developed [58,59], and have been used successfully to explain the observed dependence of fatigue crack growth rates on cyclic load frequency and pressure in gaseous environments [56-59]. Insight obtained from this effort

has been applied to the consideration of corrosion fatigue in aqueous environments.

Superposition Model. Modeling was based on the proposition that the mechanical and environmental contributions could be decoupled such that the rate of crack growth in a deleterious environment, $(da/dN)_e$, may be written as the sum of three components, Eqn. (4) [40,70,71].

$$(da/dN)_e = (da/dN)_r(1 - \phi) + (da/dN)_c\phi + (da/dN)_{scc} \quad (4)$$

In this equation, $(da/dN)_r$ is the mechanical fatigue rate; $(da/dN)_c$ is the "pure" corrosion fatigue rate; ϕ as the fractional area of crack that is undergoing pure corrosion fatigue; and $(da/dN)_{scc}$ is the contribution of sustained-load crack growth. These rates may be composed of contributions from several concurrent micromechanisms. For simplicity, the sustained-load growth term is not included in the following discussions. Eqn. (4) is rewritten as follows [66]:

$$\begin{aligned}(da/dN)_e &= (da/dN)_r\,(1 - \phi) + (da/dN)_c\phi \\ &= (da/dN)_r + [(da/dN)_c - (da/dN)_r]\phi \end{aligned} \quad (5)$$

or,

$$(da/dN)_{cf} = [(da/dN)_c - (da/dN)_r]\phi \quad (6)$$

where $(da/dN)_{cf}$ denotes the incremental increase in growth rate above the reference level resulting from the embrittling environment.

In the limit for $\phi = 0$, or for a test in an inert environment, $(da/dN)_e = (da/dN)_r$ and corresponds to pure fatigue. For $\phi = 1$, corresponding to chemical reaction saturation [53,54], $(da/dN)_e = (da/dN)_{e,s} = (da/dN)_c$, and measured growth rates correspond to pure corrosion fatigue rates. In essence, the parameter ϕ represents material response to changes in environmental conditions. It is directly related to its counterpart, the fractional surface coverage (θ), in chemical modeling; i.e., $\phi = \theta$ [58,59]. The maximum in corrosion fatigue crack growth rate, therefore, corresponds to the maximum extent of chemical reaction ($\theta = 1$).

Chemical Modeling

Important understanding of corrosion fatigue crack growth response in gaseous environments was developed through chemical modeling (58,59) and through experimental verification of the role of gas transport and surface reactions on $(da/dN)_{cf}$ [56,57,72]. Similar understanding is being developed for aqueous environments [17,23-26].

Assuming that the environmental enhancement of fatigue crack growth results from embrittlement by hydrogen produced by the reactions of hydrogenous gases with freshly produced crack surfaces, models for transport and surface reaction were developed [58,59]. An analogous model for electrochemical reaction controlled crack growth was proposed for steels in aqueous environments, where the kinetics of reaction are assumed to be slow [73-75]. In these models, the environmental contribution is

assumed to be proportional to the extent of chemical or electrochemical reaction per cycle, which is given by the fractional surface coverage θ, and the crack growth rate $(da/dN)_{cf}$ is given as by Eqn. (6) with $\phi = \theta$.

Models for diffusion controlled growth (76) and strain induced hydride formation [77-79] have also been suggested. The latter model relates to metallurgical changes and the consequent effect on crack growth rates, and is considered later. Diffusion controlled crack growth occurs when the preceding transport and surface reaction processes are rapid, and must be considered outside of the context of limited surface coverage per cycle.

Transport controlled growth. For highly reactive gas-metal systems, crack growth is controlled by the rate of transport of gases to the crack tip [58,59]. The surface coverage (θ) is linearly proportional to pressure (p_o) and inversely proportional to frequency (f). The environmental contribution to fatigue crack growth is given by the following relationships:

$$(da/dN)_{cf} = [(da/dN)_c - (da/dN)_r]\cdot[(p_o/f)/(p_o/f)_s] \qquad (7a)$$
$$\text{for } (p_o/f) < (p_o/f)_s$$

$$(da/dN)_{cf} = [(da/dN)_c - (da/dN)_r] = \text{constant} \qquad (7b)$$
$$\text{for } (p_o/f) \geq (p_o/f)_s$$

The term $[(da/dN)_c - (da/dN)_r]$ is the maximum enhancement in the rate of cycle-dependent corrosion fatigue crack growth, and is a consequence of the finite extent of surface reaction (i.e., $\theta \rightarrow 1$) [56,57]. The saturation exposure, $(p_o/f)_s$, is a function

of gas pressure, temperature, and molecular weight of the gas, and of stress intensity level, load ratio, yield strength and elastic constants; through their influences on crack geometry and gas transport [58,59,72].

Surface and electrochemical reaction controlled growth. With less reactive systems, crack growth is controlled by the rate of surface or electrochemical reactions at the crack tip. For simple first-order reactions, the crack growth rate in gaseous environments is given by Eqn. (8) in terms of pressure, frequency and the reaction rate constant k_c [58,59].

$$(da/dN)_{cf} = [(da/dN)_c - (da/dN)_r]\cdot[1 - \exp(-k_c p_o/f)] \qquad (8)$$

A more general interpretation of surface coverage can be made to accommodate multi-step reactions, with the actual response reflecting the nature and kinetics of the individual reaction steps.

For aqueous environments, $(da/dN)_{cf}$ may be expressed as an analogue to Eqn. (8) [75]:

$$(da/dN)_{cf} = [(da/dN)_c - (da/dN)_r]\cdot[q/q_s] \qquad (9)$$

where q is the amount of electrochemical charge transferred per cycle; q_s is the "saturation" amount or that required to complete the reactions; and the ratio q/q_s is identified with θ.

Diffusion controlled growth. When transport and surface reaction processes are sufficiently rapid, the crack growth rate is determined by the rate of diffusion of hydrogen from the crack

tip to the "fracture process zone". According to Kim (76), $(da/dN)_{cf}$ is given by Eqn. (10):

$$(da/dN)_{cf} = A_o \exp(-H_B/RT)\cdot(p_o D/f)^{1/2}\Delta K^2 \qquad (10)$$

where A_o is an empirical constant, H_B is the binding enthalpy of hydrogen to dislocations, and R is the universal gas constant, D is the hydrogven diffusivity, and f is the frequency.

In the transport and reaction controlled models, a growth rate dependence upon ΔK^2 is implicitly assumed to reflect the expected proportionality between the sizes of the "hydrogen damaged" zone and the crack-tip plastic zone [59,72]. This dependence is explicitly incorporated in the diffusion controlled model [76]. The temperature dependence is reflected through its influence on the reaction rates, the fatigue process, the mechanical properties and on gas transport [58,59,73,74]. If the reaction mechanisms remain unchanged, the maximum enhancement in rate (or $(da/dN)_c$) is expected to remain constant. The temperature dependence for corrosion fatigue would be reflected principally through its frequency dependence, with the maximum remaining constant.

Experimental support. The transport and surface (and electrochemical) reaction controlled models have been examined by coordinated studies of the kinetics and mechanisms of gas-metal reactions, and of corrosion fatigue crack growth response as functions of pressure, temperature, and loading time (or frequency). Good agreement between these models and the experimental data on crack growth and surface and electrochemical reactions

has been obtained (see Figs. 9 to 11, for example). The transport controlled case is represented by aluminum and titanium alloys in water vapor (Fig. 9), and steels in hydrogen sulfide (Fig. 10) at low pressures; the reaction controlled case, by high strength steels in aqueous electrolytes (see Fig. 11, for example [80]).

It is recognized that the form of the crack growth rate response depends on the kinetics and on the specific nature and mechanism(s) of the reactions, and may reflect both transport and reaction control. For the case of reaction controlled crack growth, the response may reflect the fact that the reactions do not follow simple first-order kinetics, and the presence of more than one reaction step. For example, for the case of 7075-T651 aluminum alloy (Fig. 10), the additional enhancement at the higher pressures is surface reaction controlled and is attributed to a slow step in the reactions of water with segregated magnesium [81]. Similarly, the increase in rate observed on the 2-1/4Cr-1Mo steel in hydrogen sulfide at the higher pressures is surface reaction controlled, and is identified with the slower second step in the reactions of H_2S with iron [57,60]. A similar situation exists for crack growth of high-strength steels in water vapor and in aqueous solutions. The situation in water vapor may be further complicated by capillary condensation at the crack tip [53,73,74].

Evidence for diffusion-controlled crack growth is provided by data on titanium alloys (see Fig. 12, for example). At the higher frequencies, $(da/dN)_{cf}$ was found to be inversely propor-

tional to the square root of frequency [82]. This dependence, coupled with the known reactivity of titanium, is consistent with diffusion control. The abrupt decrease in growth rates at the lower frequencies is attributed to a hydride mechanism that depends on both strain and strain rate [29-31,36]. There is, however, no quantitative model for hydride induced crack growth.

Microstructural Modeling

The important role of different micromechanisms was discussed by Gerberich and Peterson (83). The role of micromechanism (or of microstructure) is explicitly incorporated in Eqns. (4) and (6). The implications of the model are as follows: (i) the partitioning of hydrogen to the various microstructural sites need not be uniform, and (ii) the fractional area of fracture surface (ϕ) produced by pure corrosion fatigue is equal to the fractional surface coverage (θ) for chemical reactions. The relationship between the microstructural and environmental parameters (ϕ and θ) was examined by Ressler (84) and by Gao et al (85).

For an AISI 4340 steel in water vapor (585 Pa) at room temperature, Ressler (84) determined the corrosion fatigue crack growth rate as a function of frequency (Fig. 13). Fractographic data show a change in fracture surface morphology with decreasing frequency from a predominantly transgranular mode (relative to the prior-austenite grains) to one that is predominantly intergranular, Fig. 14. By identifying the intergranular failure mode with pure corrosion fatigue and the transgranular mode with

mechanical fatigue, the fraction of pure corrosion fatigue (ϕ), was estimated from the microfractographs. A comparison was made between ϕ and θ, based on independent surface reaction measurements [51] and an adjustment of exposure to account for capillary condensation in the fatigue crack (Fig. 15). Agreement is excellent. A similar good correlation was reported by Gao et al [85] for a 7075-T651 aluminum alloy.

These results indicate the important role of microstructure, and of the interactions between the environmental and microstructural variables.

More work is needed to broaden the scope of this understanding, and to provide statistically reliable support. Nevertheless, the framework for understanding has been set in place.

IMPLEMENTATION OF THE FRACTURE MECHANICS APPROACH (1980s)

Significant complexities must be overcome in implementing the fracture mechanics approach for the quantitative prediction of component life to control environmentally assisted crack growth. During the 1980s, two critical issues emerged. Firstly, the principle of fracture mechanics similitude (that is, equal subcritical crack growth rates are produced by equal applied stress intensities) may be violated because of the effects of crack closure and variations in environmental chemistry within the crack. Secondly, the large number of relevant variables and their time-dependent interactions greatly complicate life predictions, particularly for lower strength materials which were not extensively characterized during the 1970s and where linear frac-

ture mechanics may not suffice.

Mechanistic understanding and scientific modeling provide the means for characterizing subcritical cracking in terms of a scalable crack tip driving force, for extrapolating short term data to predict long term component behavior, and for defining the effects of mechanical, chemical and metallurgical variables.

Fracture Mechanics Similitude

The use of fracture mechanics similitude to scale environmentally assisted crack growth rates, for different crack sizes and loadings, is permitted only if the following two conditions are met: (1) the applied driving force parameter (e.g., stress intensity factor) uniquely defines the stresses, strains and strain rates near the crack tip; and (2) the composition and conditions of the environment at the crack tip are constant for a given applied driving force parameter, irrespective of crack size and opening shape. Investigations of environmentally assisted crack growth at low stress intensities, in low strength or anisotropic materials, for small crack geometries and in complex embrittling environments demonstrate that the validity of similitude cannnot be always assumed [16-18,86-88]. The applied stress intensity basis shown in Figs. 1 and 2 may need to be modified to reflect the actual crack driving force, as described in the following subsections.

Crack Closure Problem. Premature contact of fatigue crack surfaces during unloading or crack closure reduces the effective crack driving force relative to the applied value (e.g., ΔK).

For corrosion fatigue, likely crack closure mechanisms include environmentally assisted crack deflection, intergranular cracking and enhanced surface roughness, enhanced plasticity, fluid pressure, and corrosion product wedging [89,90].

The effect of corrosion product wedging is shown in Fig. 16. Here, the reduction in fatigue growth rates at low mean stress is attributed to wedging by a thin surface oxide produced by fretting of the fracture surfaces in moist or oxygenated environments [91]. This closure mechanism is relevant when the crack tip opening displacements are small, and may become more pronounced because of enhanced (crevice) corrosion within fatigue cracks. The effect was documented for cathodically polarized steels in seawater [92,93].

For laboratory specimens, crack closure effects are accounted for through measurements of specimen compliance [89]. The implications of environment induced closure for component behavior, however, are unclear and require attention. Even though elementary micromechanical models have been proposed for specific closure mechanisms, the environment sensitive processes are poorly understood [90]. The problem is exacerbated by the time dependent nature of corrosion processes.

Small Crack Problem. Because of the importance of early crack formation and growth to component fatigue life, considerable emphasis has been placed on the fracture mechanics of small cracks through the 1980s [87]. Generally, stress corrosion and corrosion fatigue cracks sized below 1 to 5 mm have been found to grow unexpectedly rapidly relative to long cracks at the same K

level, and to grow below the threshold K level for long cracks [87,90,94,95]. This behavior must be understood in order to apply the fracture mechanics approach to predict environmental cracking life in components.

The observed crack size effect may be caused by inappropriate formulation of the mechanical driving force and by differences in crack tip environment. A variety of mechanisms and bounding crack sizes were identified [96]. For fatigue in benign environments, increased crack tip plasticity, underdeveloped crack wake closure, three dimensional crack shape and large scale yielding can increase growth rates of small cracks. Interactions with grain boundaries, on the other hand, can arrest growth. The same mechanisms may affect environmentally assisted cracking through changes in crack-tip environment, environmental modification of crack closure, or strain enhanced film rupture [90,95,97-99].

The occluded environments within short cracks can differ from the bulk and from those within long cracks. For the cases examined to date, the short crack environments appear to be more deleterious. Data for a high strength steel in aqueous chloride solution (Fig. 17) show that stress intensity similitude was not obeyed, with K_{Iscc} decreasing with crack size below about 1 mm [100]. Values for K_{Iscc} at the smallest crack size were about 1/3 those obtained with specimens containing 15 to 30 mm long cracks. This crack size effect is chemical in origin, and has been predicted successfully through calculations of solution pH, electrode potential and total rate of hydrogen production within

cracks of varying length, and the use of an empirical relationship between K_{Iscc} and adsorbed hydrogen concentration [100-102].

Gangloff showed that small corrosion fatigue cracks (below about 3 mm) grew at rates up to 10^3 times faster than long cracks at equivalent applied ΔK [103,104]. This effect is illustrated in Fig. 18 by comparing data for 25 to 40 mm long cracks with those of 0.1 to 3 mm long elliptical surface and through-thickness edge cracks for a high strength steel in aqueous 3% NaCl solutions. The concomitant absence of a crack size effect in vacuum and moist air further demonstrates the chemical origin of the breakdown in similitude. The chemical crack size effect has been confirmed by literature data, and by experiments with lower strength steels. The effect, however, decreased from a factor of 10^3 to 2 as the yield strength of the steel decreased [95].

The effect of crack geometry shown in Fig. 18 is qualitatively understood in terms of a complex interaction between mass transport by diffusion, ion migration and convection, and electrochemical reactions [94,104,105]. Initial effort at modeling this effect has been made, but needs to be supported by critical experiments [104-106]. Possible variations in crack chemistry and their effects on the growth of longer cracks must be considered.

In essence it is necessary to examine the coupled reaction and transport problem as a whole in dealing with the apparent violation of similitude. Turnbull has attempted to do this by modeling steady state reactions and mass transport in simple trapezoidally shaped cracks [107,108]. This work must be modified to include the important transient reaction kinetics dis-

cussed in a previous section, and must be related to the micromechanics of crack advance. Such an approach will provide the foundation for developing quantitative predictive methods for long term component service.

Life Prediction for Environmental Cracking

The time dependence of environmental crack growth, the many relevant variables and the complexities affecting similitude hinder fracture mechanics life prediction. None-the-less, the phenomenological and scientific foundations have been developed during the past 15 years. The challenge is to refine and integrate this understanding to produce methods which overcome the weaknesses of smooth specimen, time-indifferent design rules. Significant progress has been reported in this regard for stress corrosion and corrosion fatigue in nuclear systems, based on film rupture mechanistic modeling [109].

Recent advances and future directions for life prediction of steels cracking by hydrogen embrittlement are reviewed for static and cyclic loading.

Stress Corrosion Cracking. Stress corrosion cracking is sensibly predicted based on the threshold stress intensity (K_{Iscc}) concept, within the bounds summarized elsewhere [110]. Two variables critically affect K_{Iscc}: steel yield strength and hydrogen uptake.

Lower bound relationships between K_{Iscc} and yield strength are presented in Fig. 19, based on over 500 measurements reported during the past 20 years [111]. The beneficial effect of de-

creasing strength is shown for five specific environments. For constant strength, K_{Iscc}, correlates with the steady state concentration of dissolved hydrogen, produced by gaseous chemical or aqueous electrochemical reactions on the input surface of a steel foil and measured by a permeation experiment, as illustrated in Fig. 20 [111,112]. Such data, when employed with permeation based sensors of hydrogen uptake in plant components [113], enable conservative life predictions for environmental cracking under monotonic loading. This approach may be compromised by cyclic loading, unique microstructures and new environment chemistries [110,111].

Corrosion Fatigue. Significant progress was achieved in the 1980s for fracture mechanics predictions of long term corrosion fatigue in offshore structural applications, particularly large welded joints between low strength carbon steel tubulars [109,114]. The elements of this approach are reviewed.

(1) Data base. Corrosion fatigue cracking in the low alloy steel/aqueous environment system occurs at stress intensities well below K_{Iscc} and within the regime relevant to tubular joint performance, as illustrated by the data and arrow in Fig. 21 [93,115-119]. Crack growth is enhanced by reduced loading frequency and increased cathodic polarization; such effects must be understood to predict the long term (10^8 cycles at 0.1 Hz) life of cathodically protected tubulars.

(2) Hydrogen embrittlement models. The aim of mechanistic modeling is to predict corrosion fatigue crack growth rate as a

function of stress intensity, stress ratio, environment composition, microstructure, electrode potential and loading frequency. No single, quantitative model exists. The foundation has been established, however, by research on crack tip reactions and the frequency dependence of corrosion fatigue [44,59,75], on crack closure [89], on steady state crack chemistry modeling [100,102,105-108], and on hydrogen embrittlement [115,120]. Mechanisms for near-threshold corrosion fatigue have been proposed also [90,91,93,94,115,121], however, quantitative formulations and experimental evaluations are lacking.

(3) Stress intensity and life predictions. To date, only approximate K solutions for complex tubular joints have been developed [122]. Such equations were integrated with laboratory crack growth rate data (Fig. 21) to yield the prediction shown in Fig. 22 [122].

(4) Full scale component testing. Sophisticated capabilities exist in several countries to conduct fatigue and corrosion fatigue experiments with large welded tubular joints, and to monitor crack growth continuously by electrical potential techniques [123-125]. As shown in Fig. 22, fatigue life data on full-scale joints are in excellent agreement with fracture mechanics predictions for cycle dependent cracking in moist air. Measurements of surface crack shape development are also consistent with model predictions.

Limited corrosion fatigue experiments on full-scale joints demonstrate the deleterious effect of the seawater environment,

potential problems due to cathodic protection and the inability of simple cycle based fatigue design rules to adequately describe tubular life [109]. Modeling of these effects requires improved crack growth rate data, mechanistic models and understanding of similitude, particularly for near threshold corrosion fatigue.

OUTSTANDING ISSUES AND NEW DIRECTIONS

The foregoing sections provide a perspective summary of the modeling effort to quantitatively connect chemical and physical processes with environmental crack growth response. From an initial effort that was narrowly focused on the rate controlling processes for crack growth in steels exposed to gaseous environments, ensuing studies broadened the understanding to cracking in high-strength aluminum and titanium alloys, and extended the approach to the complex problem of crack growth in aqueous environments. The simplified models serve as a framework for research and design, as illustrated for offshore structures. They serve also as a basis for furthering the understanding of environmentally assisted crack growth. Results from these studies will aid in the development of alloys and of methods to minimize sensitivity to environmentally assisted cracking, and of procedures for making reliable predictions of long-term service. Fracture mechanics has played a major role in the development of this understanding. Significant issues remain to be resolved.

(i) Detailed understanding of the kinetics and mechanisms of surface/electrochemical reactions with clean metal surfaces is needed, over a broad range of environmental conditions: (a) to

establish the form and quantity of hydrogen that is produced, and the fraction that enters the material to effect embrittlement, (b) to explore and confirm the indicated transfer of rate controlling processes with changes in environmental conditions, and (c) to determine the relationship between the kinetics of surface reactions and crack growth response to improve the predictive capability of crack growth models.

(ii) For environmentally assisted crack growth in aqueous environments, the traditional electrochemical measurement of polarization response is inadequate. A new technique for measuring the kinetics of equilibration reactions at the crack tip has been developed. These measurements, however, must be coupled with a detailed understanding of the reaction mechanisms and modeling of the crack tip chemistry.

(iii) Greater effort is needed to understand the factors and processes that control or inhibit electrochemical reactions of bare, straining metal surfaces with electrolytes.

(iv) Quantitative understanding of the physical-chemical interactions between hydrogen and metal (i.e., the embrittlement mechanisms) is needed to establish the roles of microstructure and of other metallurgical variables in determining the rate of crack growth, or the degree of susceptibility.

(v) Better understanding of the influences of alloying and impurity elements, and of microstructure is needed. It is essential to determine whether such influences on environmental cracking result from alterations of the reaction kinetics (chemical effects), from their influence on the mechanical properties of

alloys (physical effects), or both (physical-chemical effects).

(vi) Better understanding of the processes that control environmental crack initiation and early growth (viz., threshold and Stage I crack growth) is needed.

(vii) Mechanistic descriptions of crack chemistry, transient reactions and micromechanical embrittlement must be integrated to produce a predictive model of environmentally assisted crack growth rate. The model must quantitatively predict both specimen and component cracking performance, and must be amenable to experimental confirmations and mechanistic refinements.

(viii) Experimental research and modeling must be exploited to develop in-situ monitors of environmental crack growth in complex components. Sensors for hydrogen uptake from service environments must be further developed and implemented.

(ix) New experimental methods must be developed for direct measurement of environmental damage processes at the crack tip.

(x) Research on environmentally assisted cracking must be extended to include novel monolithic and composite materials.

Summary

Experimental and analytical work in the past decade has contributed significantly to both the phenomenological and mechanistic understanding of environmentally assisted crack growth. Crack growth response reflects the complex interplay among chemical, mechanical and metallurgical factors, and is dependent on the rate controlling processes, and on the micromechanisms for crack growth and the mechanisms of the relevant chemical reac-

tions. On the basis of this understanding, modeling of environmentally assisted crack growth, under sustained-load and in fatigue, has been made. This modeling effort has placed the study of this technologically important problem on a sound footing, and provides a framework for new understanding and for the development and utilization of data in design. To make significant further advances in understanding, continued emphasis on multidisciplinary approaches which incorporate chemistry, physics, materials science and fracture mechanics, and long-term support are essential.

ACKNOWLEDGEMENT

This work is supported by the Office of Naval Research under Contract N00014-83-K-0107 NR 036-097 and by the National Aeronautics and Space Administration, Langley Research Center, Research Grant NAG-1-745.

REFERENCES

1. Brown, B. F., in Stress-Corrosion Cracking in High Strength Steels and in Titanium and Aluminum Alloys, ed., B. F. Brown, U. S. Naval Research Laboratory, Washington, DC (1972), pp. 2-16. (Library of Congress Catalog Card No. 72-600053)

2. Haigh, B. P., J. Inst. Metals, Vol. 18, 1917, p. 55.

3. Gough, H. J. and Sopwith, D. G., J. Inst. Metals, Vol. 49, 1932, p. 93.

4. The Theory of Stresss Corrosion Cracking in Alloys, ed., J. C. Scully, NATO, Brussels, Belfium, 1971.

5. Fundamental Aspects of Stress Corrosion Cracking, NACE-1, eds., R. W. Staehle, A. J. Forty, and D. van Rooyen, Natl. Assoc. Corro. Engrs., Houston, TX, 1969.

6. Corrosion Fatigue: Chemistry, Mechanics and Microstructure, NACE-2, eds., O. F. Devereux, A. J. McEvily, and R. W. Staehle, Natl. Assoc. Corro. Engrs., Houston, TX, 1972.

7. Stress Corrosion Cracking and Hydrogen Embrittlement of Iron Base Alloys, NACE-5, eds., R. W. Staehle, J. Hochmann, R. D. McCright and J. E. Slater, Natl. Assoc. Corro. Engrs., Houston, TX, 1978.

8. L'Hydrogene Dans Les Metaux, eds., J. P. Fidelle, and M. Rapin, Commissariat Energie Atomique, France, 1967.

9. Hydrogen in Metals, eds., I. M. Bernstein and A. W. Thompson, Am. Soc. Metals, Metal Park, OH, 1974.

10. Effect of Hydrogen on Behavior of Materials, eds., A. W. Thompson and I. M. Bernstein, Am. Soc. Metals, Metal Park, OH, 1976.

11. Hydrogen in Metals, Proc. of Second Japan Inst. of Metals Inter. Symposium (JIMS-2), Suppl. to Trans. Japan Inst. Metals, Vol. 21, 1980.

12. Environment-Sensitive Fracture of Engineering Materials, ed., Z. A. Foroulis, The Metall. Soc. AIME, New York, 1979.

13. Hydrogen Embrittlement and Stress Corrosion Cracking, a Festshrift,eds., R. Gibala and R. F. Hochmann, Am. Soc. Metals, Metals Park, OH, 1984.

14. Wei, R. P., in Environmental Degradation of Engineering Materials in Aggressive Environments, eds., M. R. Loutrhan, Jr., R. P. McNitt and R. D. Sisson, Jr., Virginia Polytechnic Institute and State University, Blacksburg, VA, 1981, pp. 73-81, Vol. 2.

15. Environment-Sensitive Fracture: Evaluation and Comparison of Test Methods, ASTM STP 821, eds., S. W. Dean, E. N. Pugh, and G. M. Ugiansky, American Society for Testing and Materials, 1916 Race St., Philadelphia, PA, 19103, 1984.

16. Embrittlement by the Localized Crack Environment, ed., R. P. Gangloff, The Metall. Soc. AIME, New York, 1984.

17. Modeling Environmental Effects on Crack Initiation and Propagation, eds., R. H. Jones and W. W. Gerberich, The Metall. Soc. AIME, Warrendale, PA, 1986.

18. Corrosion Fatigue Technology, ASTM STP 642, eds., H. L. Craig, Jr., T. W. Crooker and D. W. Hoeppner, ASTM, Philadelphia, PA (1978).

19. Hydrogen Effects in Metals, eds., I. M. Bernstein and A. W. Thompson, TMS-AIME, Warrendale, PA, p. 1005 (1981).

20. Basic Questions in Fatigue, Vols. I and II, ASTM STP, eds., R. P. Wei, J. T. Fong, R. J. Fields, and R. P. Gangloff, ASTM, Philadelphia, PA, in press (1987).

21. Environmental Degradation of Engineering Materials-III, eds., M. R. Louthan, R. P. McNitt and R. D. Sisson, Pennsylvania State University, 1987.

22. Mechanisms of Environmemt Sensitive Cracking of Materials, eds., P. R. Swann, F. P. Ford and A. R. C. Westwood, The Metals Society, London, 1977.

23. Corrosion Fatigue, ASTM STP 801, eds., T. W. Crooker and B. N. Leis, Am. Soc. Testing Matls., Philadelphia, PA, 1983.

24. Staehle, R. W., Final Report on "Stress Corrosion Cracking of High Strength Alloys", AFML-TR- , 1970 (to be completed).

25. Brown, B. F. and Beachem, C. D., Corro. Sci., Vol. 5, 1965, pp. 745-750.

26. Brown, B. F., Mater. Res. Stand., Vol. 6, No. 3, 1966, p. 129.

27. Johnson, H. H. and Paris, P. C., Eng. Fract. Mech., Vol. 1, 1968, pp. 3-45.

28. Smith, H. R., Piper, D. E. and Downey, F. K., Eng. Fract. Mech., Vol. 1, 1968, pp. 123-128.

29. Feeney, J. A., McMillan, J. C. and Wei, R. P., Metall. Trans., Vol. 1, 1970, pp. 1741-1757.

30. Wei, R. P., in Fundamental Aspects of Stress Corrosion Cracking, NACE-1, eds., R. W. Staehle, A. J. Forty and D. van Rooyen, Natl. Assoc. Corro. Engrs., Houston, TX, 1969, pp. 104-112.

31. Steigerwald, E. A., "Delayed failure of high-strength steel in liquid environments", Proc. A.S.T.M. 60, 1960, p. 750.

32. Hanna, G. L., Troiano, A. R., and Steigerwald, E. A., ASM Trans. Quarterly , Vol. 57, 1964, p. 658.

33. Johnson, H. H. and Willner, A. M., Applied Mater. Res., Vol. 1, 1965, p. 34.

34. Hancock, G. G. and Johnson, H. H., Trans. Metall. Soc. AIME, Vol. 236, 1966, p. 513.

35. Bradshaw, F. J. and Wheeler, C., Applied Mater. Res., Vol. 5, 1966, p. 112.

36. Hartman, A., Inter. J. Fract. Mech., Vol. 1, 1965, p. 167.

37. Wei, R. P., Talda, P. M. and Li, Che-Yu, in Fatigue Crack Propagation, ASTM STP 415, Am. Soc. Testing Mater., Philadelphia, PA, 1967, pp. 460-485.

38. Wei, R. P., Novak, S. R. and Williams, D. P., Mater. Res. Stand., Vol. 12, 1972, p. 25.

39. Novak, S. R. and Rolfe, S. T., Corrosion, Vol. 26, No. 4, 1970, pp. 121-130.

40. Wei, R. P., in Fatigue Mechanisms, ASTM STP 675, ed., J. T. Fong, Am. Soc. Testing Mater., Philadelphia, PA, 1979, pp. 816-840.

41. Wei, R. P., in "Steels", ARPA Coupling Program on Stress Corrosion Cracking: (Seventh Quarterly Report), NRL Memorandum Report 1941, Naval Research Laboratory, Washington, DC, October 1968, p. 49.

42. Speidel, M. O., "Current Understanding of Stress Corrosion Crack Growth in Aluminum Alloys", in The Theory of Stress Corrosion Cracking in Alloys, ed., J. C. Scully, NATO Scientific Affairs Division, Brussels, 1971, pp. 289-344.

43. Wei, R. P., Klier, K., Simmons, G. W. and Chou, Y. T., in Hydrogen Embrittlement and Stress Corrosion Cracking, eds., R. Gibala and R. F. Hehemann, American Society for Metals, Metals Park, OH, 1984, pp. 103-133.

44. R. P. Wei and Ming Gao: in Hydrogen Degradation of Ferrous Alloys, eds., R. A. Oriani, J. P. Hirth and M. Smialowski, pp. 579-607; Noyes Publications, Park Ridge, N. J., 1985.

45. Williams, D. P. and Nelson, H. G., Metall. Trans., Vol. 1, 1970, p. 63.

46. Nelson, H. G., Williams, D. P. and Tetelman, A. S., Metall. Trans., Vol. 2, 1971, p. 953.

47. Wei, R. P., Inter. J. Fract. Mech., Vol. 4, 1968, pp. 159-170.

48. Wei, R. P. and Landes, J. D., Mater. Res. Stand., Vol. 9, No. 7, 1969, pp. 25-28.

49. Gao, M. and Wei, R. P., Met. Trans. A, Vol. 16A, 1985, pp. 2039-2050.

50. Gangloff, R. P. and Wei, R. P., Met. Trans. A, Vol. 8A, 1977, pp. 1043-1053.

51. Simmons, G. W., Pao, P. S. and Wei, R. P.: Met. Trans A, 9A (1978) p. 1147.

52. Simmons, G. W. and Dwyer, D. J.: Surf. Sci., 48 (1975) p.373.

53. Dwyer, D. J., Simmons, G. W. and Wei, R. P.: Surf. Sci., 64 (1977) p. 617.

54. Dwyer, D. J.: Ph. D. Dissertation, Lehigh University, 1977.

55. Wei, R. P. and Simmons, G. W.: in Stress Corrosion Cracking and Hydrogen Embrittlement of Iron Base Alloys, eds., R. W. Staehle, J. Hochmann, R. D. McCright and J. E. Slater, pp. 751-765; NACE-5, Nat. Assoc. Corro. Engrs., Houston, TX, 1979.

56. Wei, R. P., Pao, P. S., Hart, R. G., Weir, T. W. and Simmons, G. W.: Met. Trans A, 11A (1980) pp. 151-158.

57. Brazill, R. Simmons, G. W. and Wei, R. P., J. Engr. Matls. & Tech., Trans. ASME, 101 (July 1979) pp. 199-204.

58. Weir, T. W., Simmons, G. W., Hart, R. G. and Wei, R. P.: Scripta Met., 14 (1980) pp. 357-364.

59. Wei, R. P. and Simmons, G. W.: in FATIGUE: Environment and Temperature Effects, eds., John J. Burke and Volker Weiss; Sagamore Army Materials Research Conference Proceedings, 27 (1983) pp. 59-70.

60. Lu, M., Pao, P. S., Weir, T. W., Simmons, G. W. and Wei, R. P., Met. Trans. A, 12A (1981) pp. 805-811.

61. Lu, M., Pao, P. S., Chan, N. H., Klier, K. and Wei, R. P., in Hydrogen in Metals, Suppl. to Trans. Japan Inst. Metals, 21 (1980) p. 449.

62. Chan, N. H., Klier, K. and Wei, R. P., in Hydrogen in Metals, Suppl. to Trans. Japan Inst. Metals, 21 (1980) p. 305.

63. Wei, R. P., in Hydrogen Effects in Metals, eds., I. M. Bernstein and A. W. Thompson, p. 677; The Metall. Soc.-AIME, Warrendale, PA, 1981.

64. Dushman, S., "Molecular Flow", in Scientific Foundations of Vacuum Technique, 2nd ed., ed., J. M. Lafferty, Wiley, 1962, pp. 87-104.

65. Pasco, R. W. and Ficolora, P. J., Scripta Met., 15 (1980) p. 1019.

66. Pasco, R. W., Sieradzki, K. and Ficalora, J. P., Scripta Met., 16, 1982, p. 881.

67. Chan, N. H., Klier, K. and Wei, R. P., Scripta Met., Vol. 12, 1978, pp. 1043-1046.

68. Pao, P. S. and Wei, R. P., Scripta Met., 11 (1977) p. 515-520.

69. Hart, E. W., in The Nature and Behavior of Grain Boundaries, Hsun Hu, ed., Plenum Publ. Corp., New York, 1970, p. 155.

70. Wei, R. P. and Landes, J. D.: Mater. Res. Stand., 9 (7) (1969) pp. 25-28.

71. Wei, R. P. and Gao, Ming, Scripta Met., 17 (1983) pp. 959-962.

72. Shih, True-Hwa and Wei, R. P., Engr. Frac. Mech., 18 (4) (1983) pp. 827-837.

73. Wei, R. P. and Shim, G., in Corrosion Fatigue, ASTM STP 801, eds., T. W. Crooker and B. N. Leis, Am. Soc. Testing & Mater., Philadelphia, PA 19103, pp. 5-25.

74. Shim, Gunchoo, and Wei, R. P., Mats. Sci. & Engr., Vol. 86, 1986, pp. 121-135.

75. Wei, R. P., "Corrosion Fatigue Crack Growth", Proceedings of International Symposium on Microstructure and Mechanical Behaviour of Materials, 21-24 Oct., 1985, Xi'an, People's Republic of China, E.M.A.S., Warley, England (to be published).

76. Kim, Y. H., Speaker, S. M., Gordon, D. E., Manning, S. D., and Wei, R. P., Naval Air Development Center (604), Warminster, PA, Report No. NADC-83126-60, Vol. I, March, 1983.

77. Pao, P. S., and Wei, R. P., in Titanium: Science and Technology, eds., G. Lutjering, U. Zwicker and W. Bunk, FRG: Deutsche Gesellschaft Fur Metall-kunde e.V., 1985, p. 2503.

78. Birnbaum, H. K., "On the mechanisms of hydrogen related fracture in metals", Proc. of ONR Workshop on Environment-Sensitive Fracture of Metals and Alloys, Washington, DC, June 3, 1985 (to be published).

79. Peterson, K. P., Schwanebeck, J. C., and Gerberich, W. W., Met. Trans. A, Vol. 9A, 1978, p. 1169.

80. Nakai, Y., Alavi, A., and Wei, R. P., "Effects of Frequency and Temperature on Short Fatigue Crack Growth in Aqueous Environments", Submitted for publication in Met. Trans. A.

81. Wei, R. P., Gao, M. and Pao, P. S., Scripta Met., Vol. 18, 1984, pp. 1195-1198.

82. Chiou, S., and Wei, R. P., "Corrosion Fatigue Cracking Response of Beta Annealed Ti-6Al-4V Alloy in 3.5% NaCl Solution", Report No. NADC-83126-60 (Vol. V), U. S. Naval Air Development Center, Warminster, PA, 30 June 1984.

83. Gerberich, W. W., and Peterson, K. A., in Micro and Macro Mechanics of Crack Growth, eds., K. Sadanada, B. B. Rath and D. J. Michel, The Metall. Soc. of AIME, Warrendale, PA, 1982, pp. 1-17.

84. Ressler, D., "An Examination of Fatigue Crack Growth In AISI 4340 Steel in Respect to Two Corrosion Fatigue Models", M.S. Thesis, Dept. of Mech. Engg. & Mechanics, Lehigh University, Bethlehem, PA, 1984.

85. Gao, M., Pao, P. S., and Wei, R. P., in FRACTURE: Interactions of Microstructure, Mechanisms and Mechanics, eds., J. M. Wells and J.D. Landes, The Metall. Soc. of AIME, Warrendale, PA, 1985, pp. 303-319.

86. Fatigue Crack Growth Threshold Concepts, eds., David Davidson and Subra Suresh, TMS-AIME, Warrendale, PA, 1984.

87. Small Fatigue Cracks, eds., R.O. Ritchie and J. Lankford, TMS-AIME, Warrendale, PA, 1986.

88. Aluminum-Lithium Alloys II, eds., T.H. Sanders, Jr. and E.A. Starke, Jr., TMS-AIME, Warrendale, PA, 1984.

89. Suresh, S. and Ritchie, R. O., in Fatigue Crack Growth Threshold Concepts, eds., David Davidson and Subra Suresh, TMS-AIME, Warrendale, PA, 1984, pp. 227-261.

90. Gangloff, R. P. and Ritchie, R. O., in Fundamentals of Deformation and Fracture, eds., B.A. Bilby, K.J. Miller and J.R. Willis, Cambridge University Press, Cambridge, UK, 1985, pp. 529-558.

91. Suresh, S., Zamiski, G. F. and Ritchie, R. O., Metall. Trans. A., Vol. 12A, 1981, pp. 1435-1443.

92. Hartt, W. H., Culberson, C. H. and Smith, S. W., Corrosion, Vol. 40., 1984, pp. 609-618.

93. Thorpe, T. W., Scott, P. M., Rance, A. and Silvester, D., Intl. J. Fatigue, Vol. 5., 1983, pp. 123-133.

94. Gangloff, R. P. and Duquette, D. J., in Chemistry and Phyics of Fracture, eds., R.M. Latanision and R.H. Jones, Martinus Nijhoff Publishers BV, Netherlands, in press, 1987.

95. Gangloff, R. P. and Wei, R. P., in Small Fatigue Cracks, eds., R.O. Ritchie and J. Lankford, TMS-AIME, Warrendale, PA, 1986, pp. 239-264.

96. Ritchie, R. O. and Lankford, J., Matls. Sci. Engr., Vol. 84, 1986.

97. Tanaka, K. and Wei, R. P., Engr. Fract. Mech., Vol. 21, 1985, p. 293-305.

98. Zeghloul, A., and Petit, J., in Small Fatigue Cracks, eds., R.O. Ritchie and J. Lankford, TMS-AIME, Warrendale, PA, 1986, pp. 225-235.

99. Ford, F. P. and Hudak, Jr., S. J., in Small Fatigue Cracks, eds., R.O. Ritchie and J. Lankford, TMS-AIME, Warrendale, PA, 1986, pp. 289-308.

100. Gangloff, R. P. and Turnbull, A., in Modeling Environmental Effects on Crack Initiation and Propagation, eds., R.H. Jones and W.W. Gerberich, TMS-AIME, Warrendale, Pa., 1986, pp. 55-81.

101. Clark, Jr., W. G., in Cracks and Fracture, ASTM STP 601, ASTM, Philadelphia, PA, 1976, pp. 138-153.

102. Brown, B.F., in Stress Corrosion Cracking and Hydrogen Embrittlement of Iron Based Alloys, eds., J. Hochmann, J. Slater, R.D. McCright and R.W. Staehle, NACE, Houston, TX, 1976, pp. 747-751.

103. Gangloff, R. P., Res. Mech. Let., Vol. 1, 1981, pp. 299-306.

104. Gangloff, R. P., Metall. Trans. A., Vol. 16A., 1985, pp. 953-969.

105. Gangloff, R. P., in Embrittlement by the Localized Crack Environment, ed., R.P. Gangloff, TMS-AIME, Warrendale, PA, 1984, pp. 265-290.

106. Gangloff, R. P., in Critical Issues in Reducing the Corro sion of Steel, eds., H. Leidheiser, Jr. and S. Haruyama, NSF/JSPS, Tokyo, Japan, 1985, pp. 28-50.

107. Turnbull, A. and Ferriss, D. H., in Proc. Conf. Corrosion Chemistry within Pits, Crevices and Cracks, ed., A. Turnbull, NPL, Teddington, UK, in press, 1987.

108. Turnbull, A., in Embrittlement by the Localized Crack Environment, ed., R.P. Gangloff, TMS-AIME, Warrendale, PA, 1984, pp. 3-48.

109. Andresen, P. L., Gangloff, R. P., Coffin, L. F. and Ford, F. P., in Fatigue 87, eds., R.O. Ritchie and E.A. Starke, Jr., EMAS, West Midlands, England, in press, 1987.

110. "Characterization of Environmentally Assisted Cracking for Design", National Materials Advisory Board, Report NMAB-386, 1982.

111. Gangloff, R. P., in Corrosion Prevention and Control, Proc. 33rd Sagamore Army Materials Research Conference,, ed., S. Isserow, U.S. Army Materials Technology Laboratory, Watertown, MA, in press, 1987.

112. Yamakawa, K., Tsubakino, H. and Yoshizawa, S., in Critical Issues in Reducing the Corrosion of Steel, eds., H. Leidheiser, Jr. and S. Haruyama, NSF/JSPS, Tokyo, Japan, 1985, pp. 348-358.

113. Yamakawa, K., Harushige, T. and Yoshizawa, S., in Corrosion Monitoring in Industrial Plants Using Nondestructive Testing and Electrochemical Methods, ASTM STP 908, eds., G.C. Moran and P. Labine, ASTM, Philadelphia, PA, 1986, pp. 221-236.

114. Dover, W. D. and Dharmavasan, S. in Fatigue 84, ed., C.J. Beevers, EMAS, West Midlands, England, 1984, pp. 1417-1434.

115. Austen, I.M. and Walker, E. F., in Fatigue 84, ed., C.J. Beevers, EMAS, West Midlands, England, 1984, pp. 1457-1469.

116. Cialone, H. J. and Holbrook, H. J., Metall. Trans. A., Vol. 16A, 1985, pp. 115-122.

117. Vosikovsky, O. and Cooke, R. J.,Int. J. Pres. Ves. & Piping, Vol. 6., 1978, pp. 113-129.

118. Vosikovsky, O. J. Test. Eval., 1978, pp.175-182.

119. Vosikovsky, O. J. Test. Eval., Vol. 8., 1980, pp. 68-73.

120. Scott, P. M., Thorpe, T. W. and Silvester, D.R.V., Corrosion Science, Vol. 23., No. 6, 1983, pp. 559-575.

121. Duquette, D. J. and Uhlig, H. H., Trans. ASM, Vol. 61., 1968, pp. 449-456.

122. Hudak, S. J., Burnside, O. H. and Chan, K. S., J. Energy Resources Tech., ASME Trans., Vol. 107, 1985, pp. 212-219.

123. Fatigue in Offshore Structural Steels, Thomas Telford, Ltd., London, 1981.

124. Proceedings of the International Conference on Steel in Marine Structures, Comptoir des produits Siderurgiques, Paris, 1981.

125. Proceedings Institute of Mechanical Engineers Conference on Fatigue and Crack Growth in Offshore Structures, Inst. Mech. Engr., London, 1986.

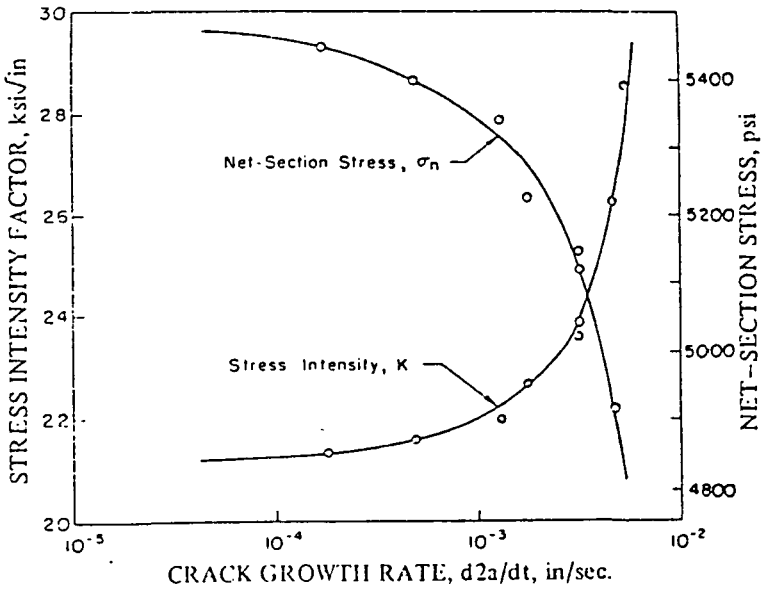

Fig. 1 - Stress intensity factor and net-section stress versus crack growth rate for a wedge-force-loaded specimen [28].

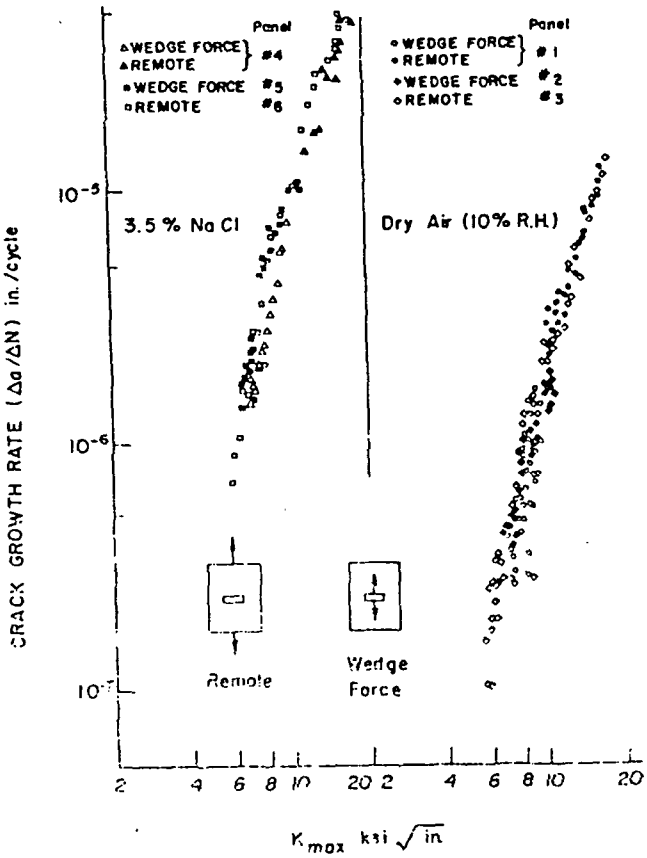

Fig. 2 - Compatibility data for aluminum alloy 7075-T6 upon intensity factor.

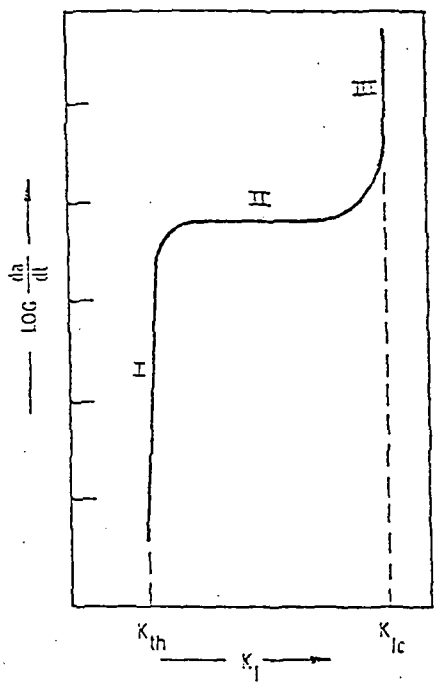

Fig. 3 - Schematic of monotonic load environment enhanced crack growth response.

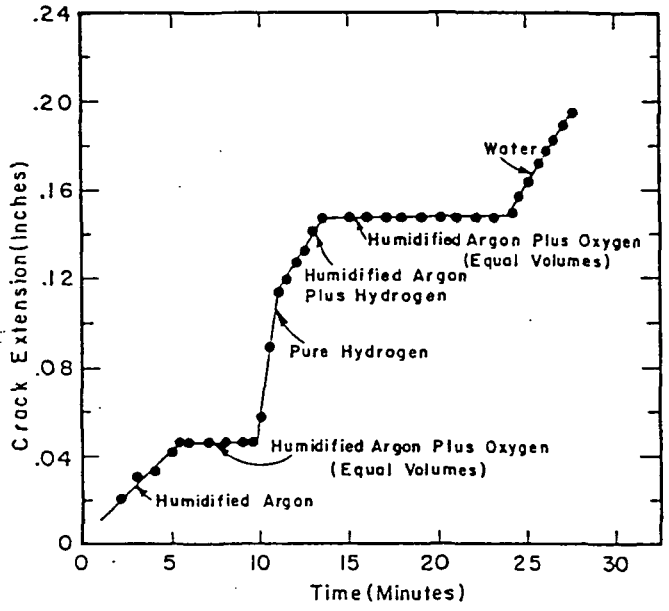

Fig. 4 - Subcritical crack growth in different water, water vapor, hydrogen, and oxygen environments, H-11 steel, 230 ksi yield strength [34].

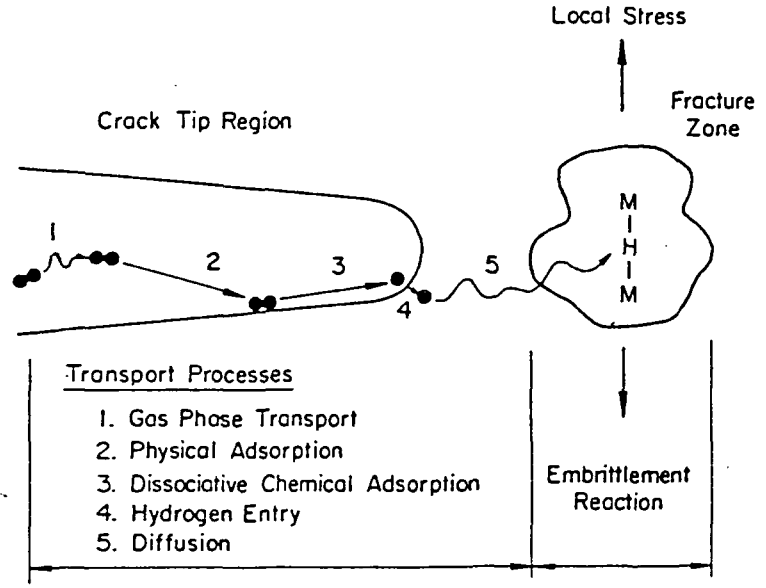

Fig. 5 - Schematic illustration of sequential processes in environmental enhancement of crack growth by hydrogenous gases. Embrittlement by hydrogen is assumed and is schematically depicted by the metal-hydrogen-metal bond.

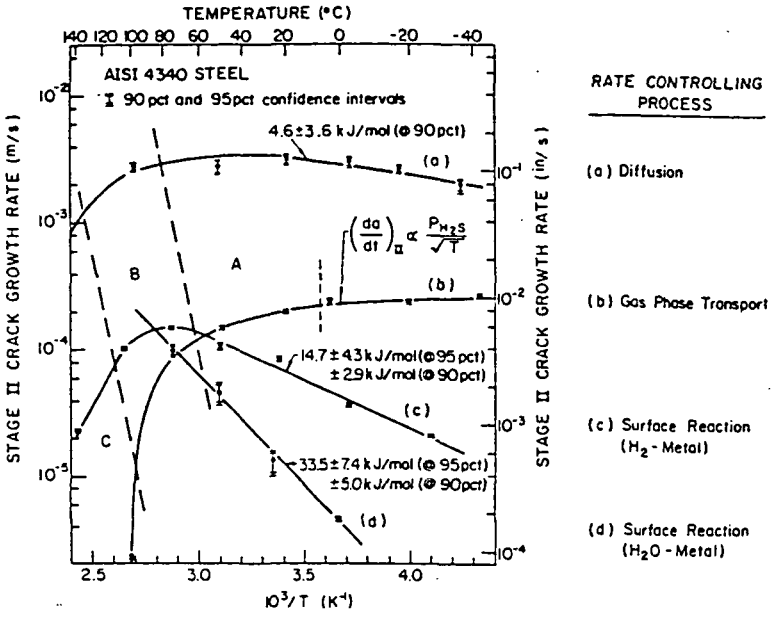

Fig. 6 - Temperature dependence for Stage II crack growth and the corresponding rate controlling processes at low temperatures for AISI 4340 steel in various hydrogenous environments: (a) H_2S at 2.66 kPa, (b) H_2S at 0.13 kPa, (c) H_2 at 133 kPa, and (d) H_2O (liquid) [51,60,61].

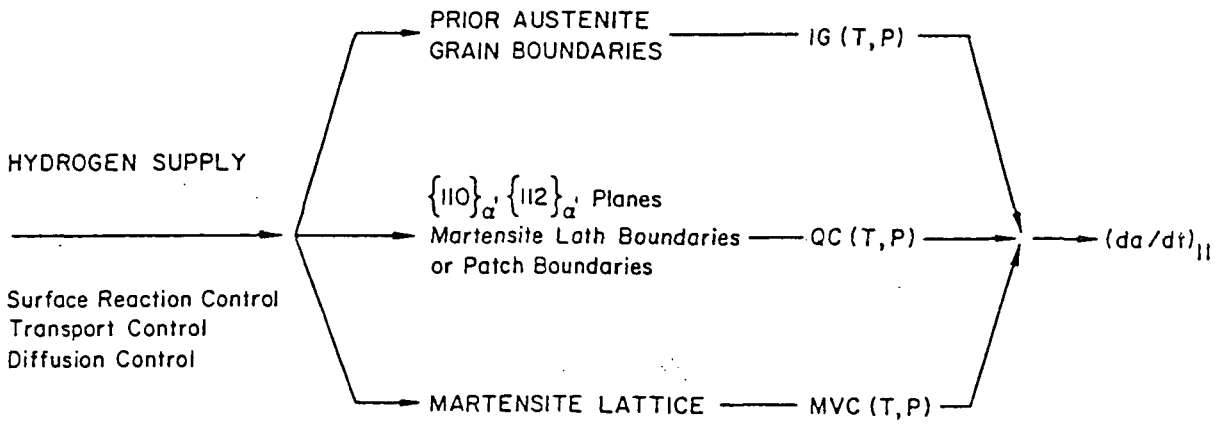

Fig. 7 - Schematic illustration of the partitioning of hydrogen and its relationship to hydrogen supply and the resulting Stage II crack growth rate [49].

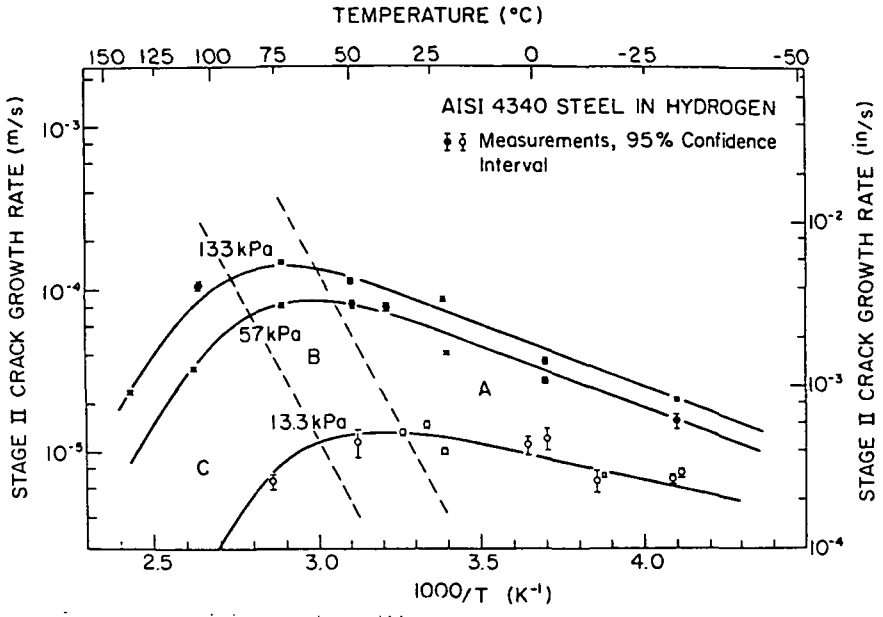

Fig. 8 - Comparison between model predictions sustained load and crack growth data on AISI 4340 steel tested in hydrogen at different pressures and temperatures [49,61].

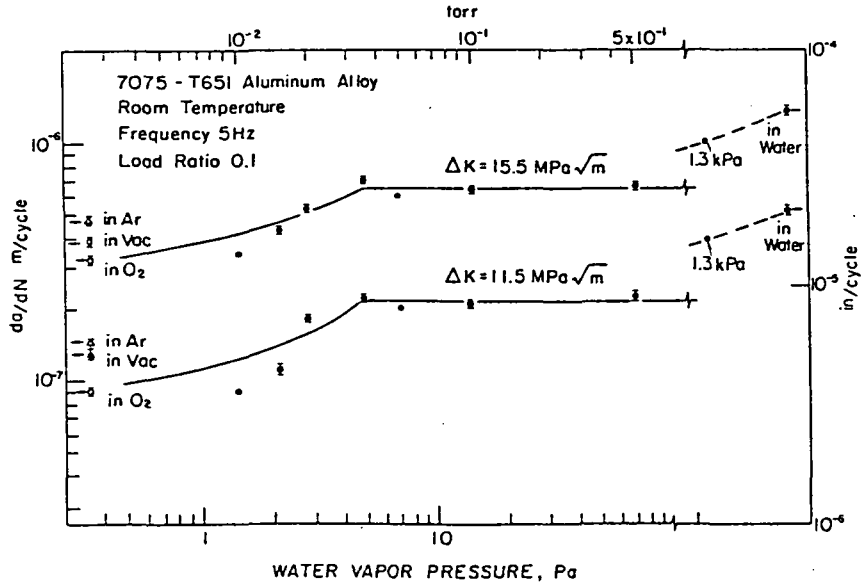

Fig. 9 - The influence of water vapor pressure and of other environments on fatigue crack growth in 7075-T651 (AlMgZn) alloy at room temperature. The solid lines represent predictions of a model for transport-controlled crack growth. The dashed lines indicate surface-reaction-controlled growth and reflect the influence of segregated magnesium [85].

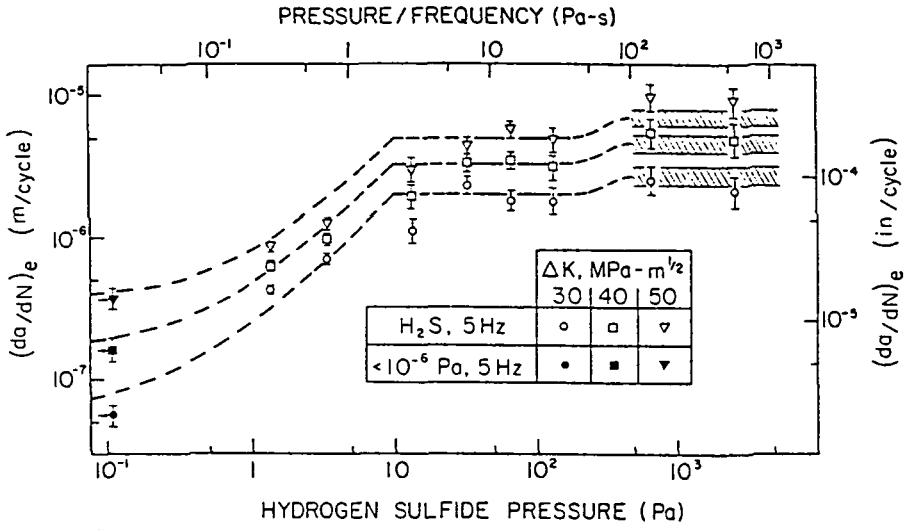

Fig. 10 - The influence of hydrogen sulfide pressure on fatigue crack growth in a 2-1/4Cr-1Mo (A542 Class 2) steel at room temperature. The dashed lines represent predictions of a model for transport-controlled crack growth. The solid lines indicate surface-reaction-controlled growth and reflect the second step of hydrogen sulfide-iron surface reactions.

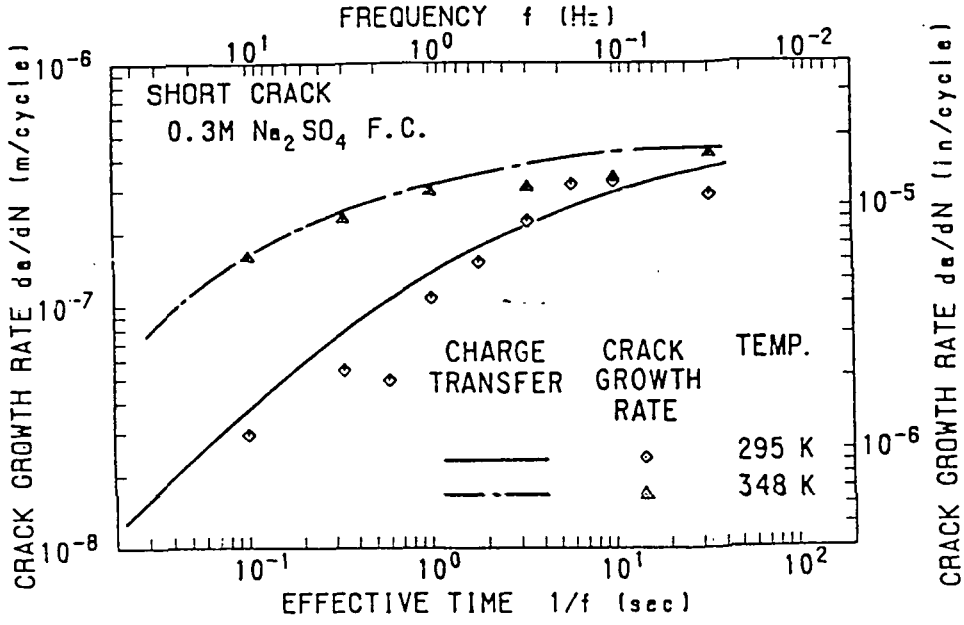

Fig. 11 - The influence of frequency and temperature on fatigue crack growth for NiCrMoV steel in 0.3N Na_2SO_4 solution [80].

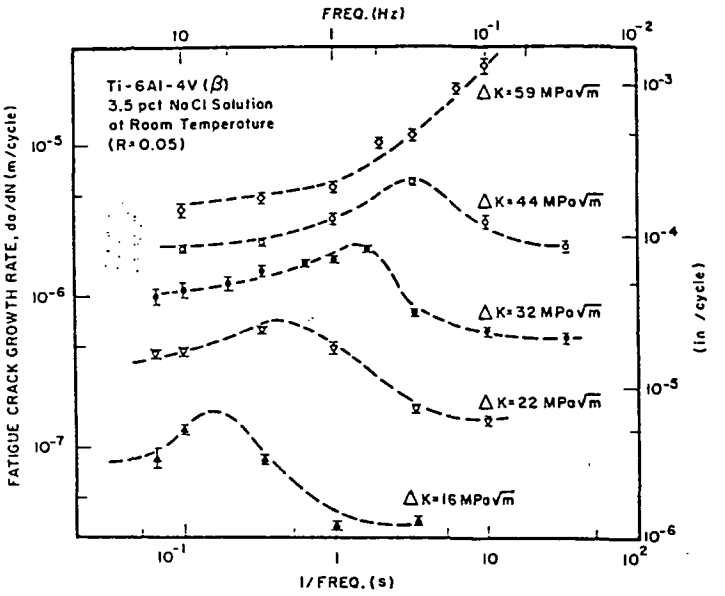

Fig. 12 - The influence of frequency on fatigue crack growth in a Ti-6Al-4V alloy exposed to 0.6M NaCl solution at room temperature and R = 0.1 [83].

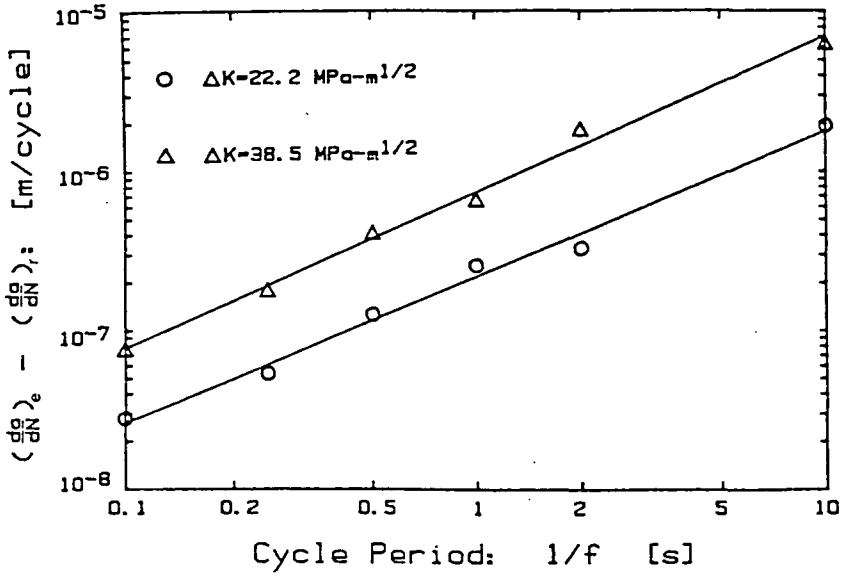

Fig. 13 - Influence of frequency on fatigue crack growth rate for an AISI 4340 steel in water vapor at 585 Pa at room temperature [84].

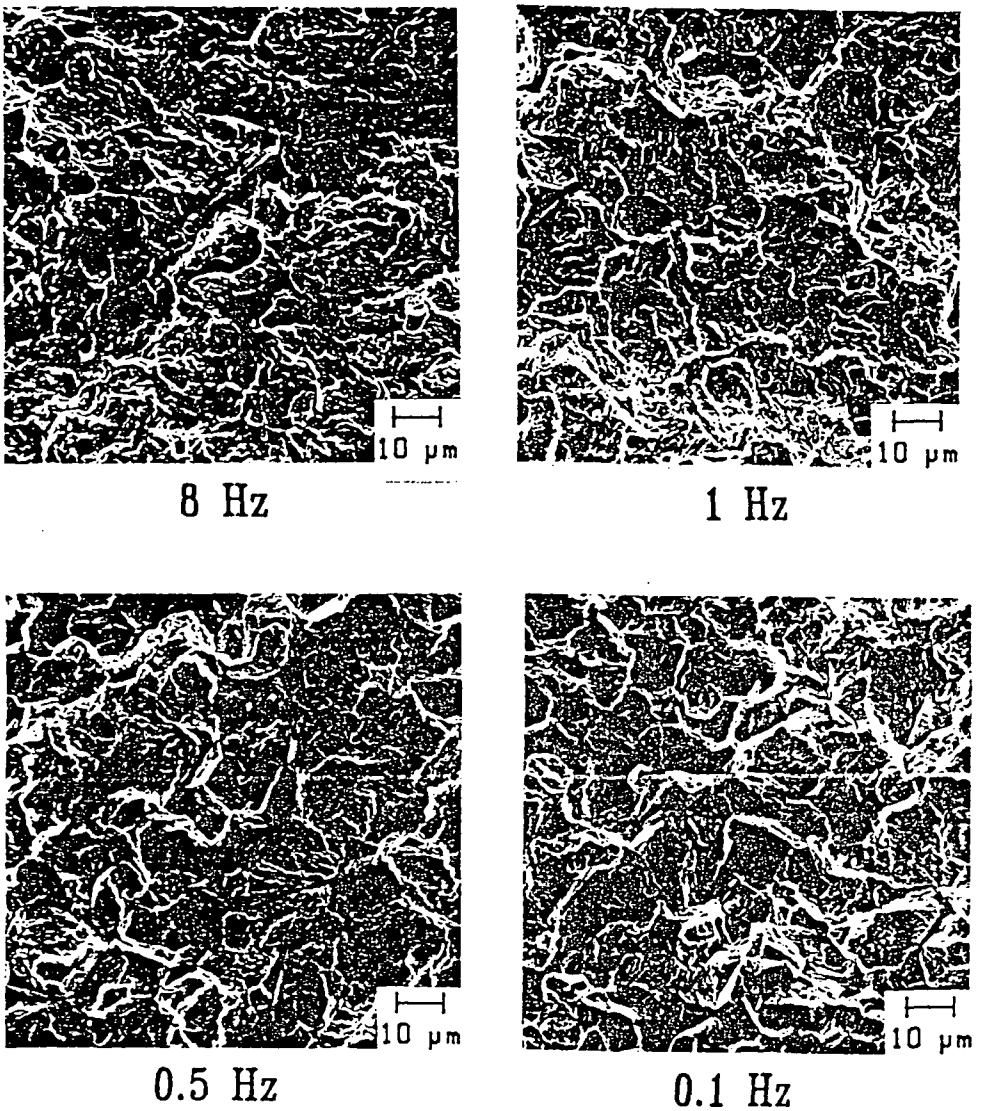

Fig. 14 - Microfractographs of AISI 4340 steel stressed in water vapor, showing changes in fracture surface morphology with frequency [84].

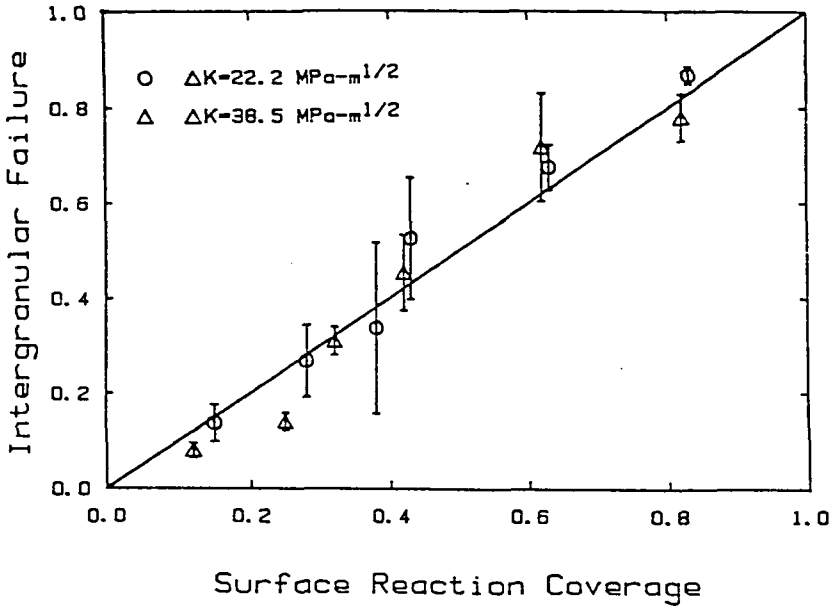

Fig. 15 - Correlation between surface coverage and fraction of intergranular failure (or ϕ) for AISI 4340 steel.

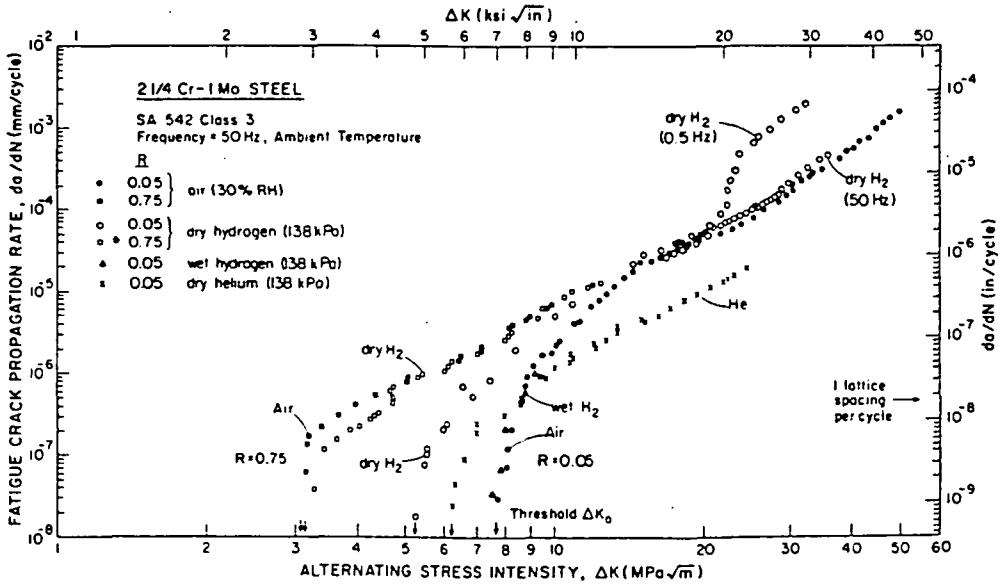

Fig. 16 - Oxide induced closure and hydrogen embrittlement effects on corrosion fatigue crack propagation in a low strength bainitic steel exposed to moist, oxidizing and dry gaseous environments. (after Ritchie et al. [91])

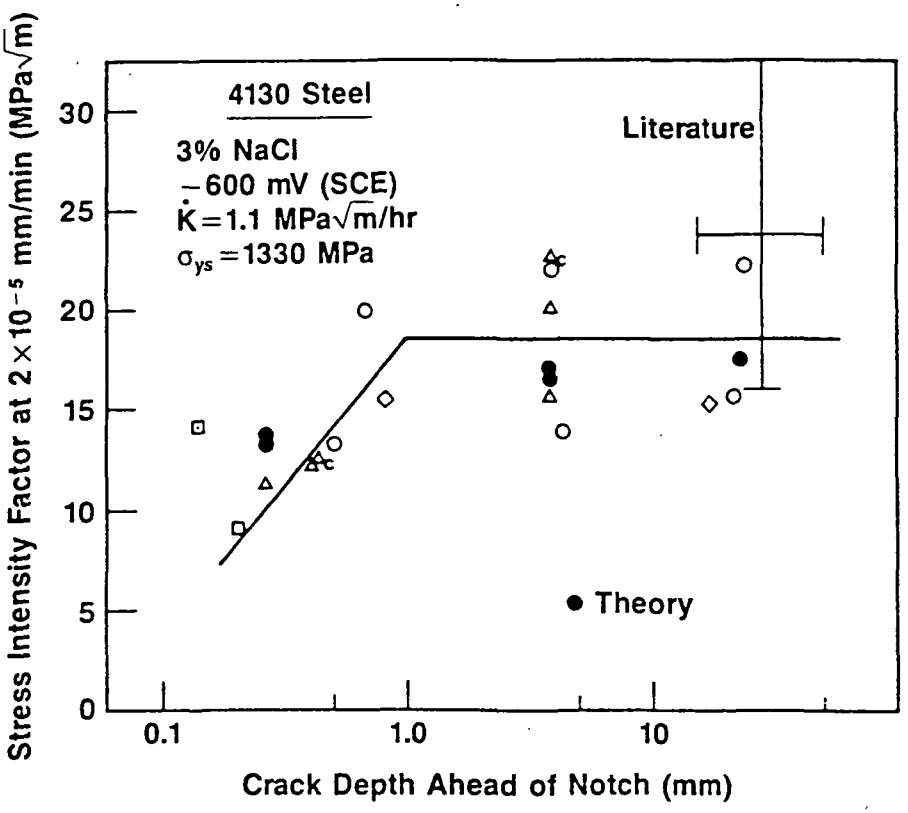

Fig. 17 - The measured and predicted effect of precrack depth on the threshold stress intensity for stress corrosion cracking of high strength steel exposed to 3% NaCl. (after Gangloff and Turnbull [100])

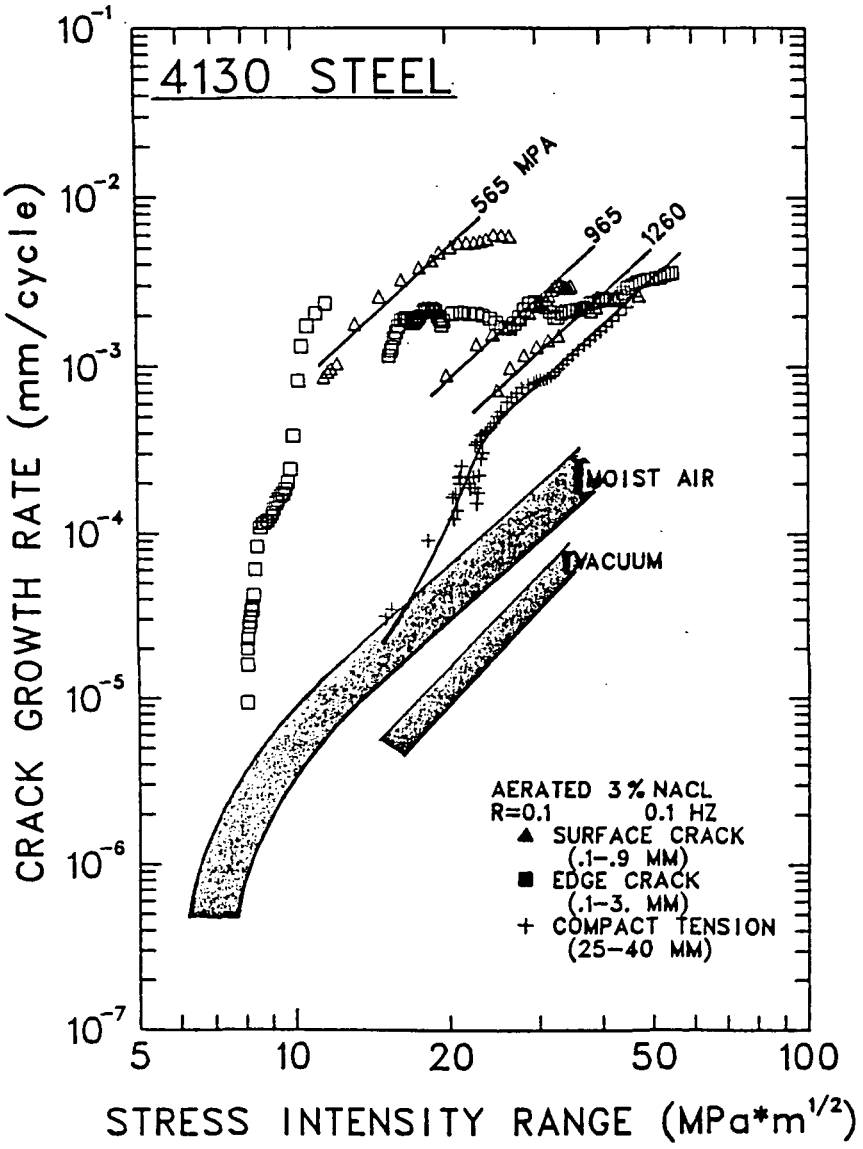

Fig. 18 - The effect of short crack size on corrosion fatigue propagation rates in high strength steel in 3% Nacl. Applied stress ranges are shown for surface cracks. (after Gangloff [104])

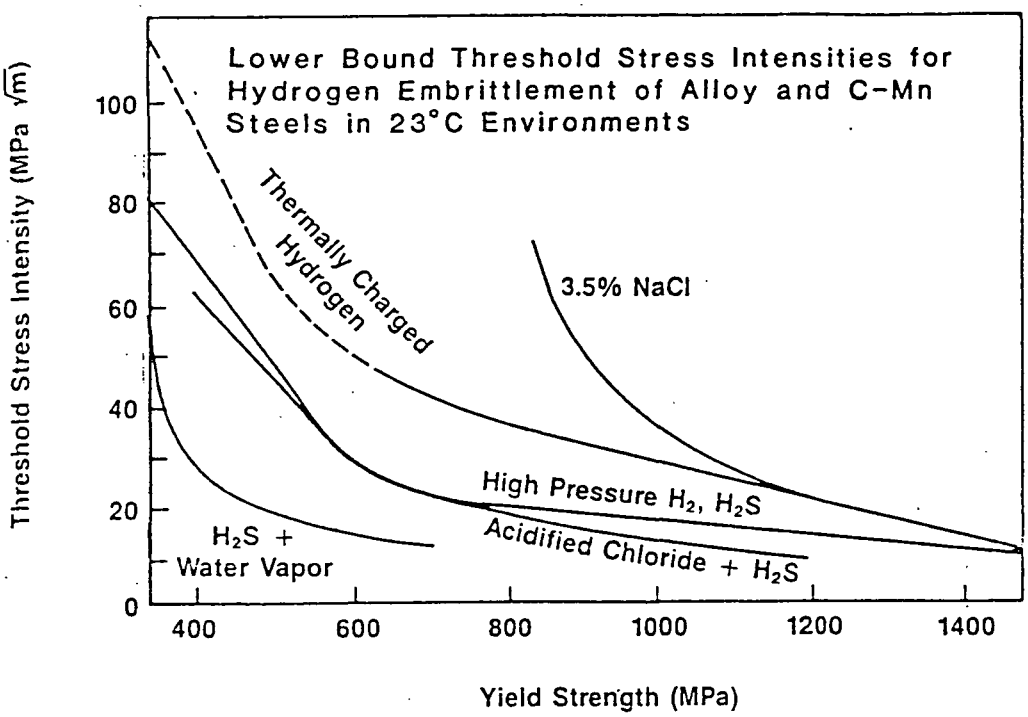

Fig. 19 - Lower bounds on K_{ISCC}-σ_{ys} for ferrite-pearlite, bainitic and tempered martensitic steels stressed in five hydrogen producing environments. Over 500 measurements are represented. (after Gangloff [111])

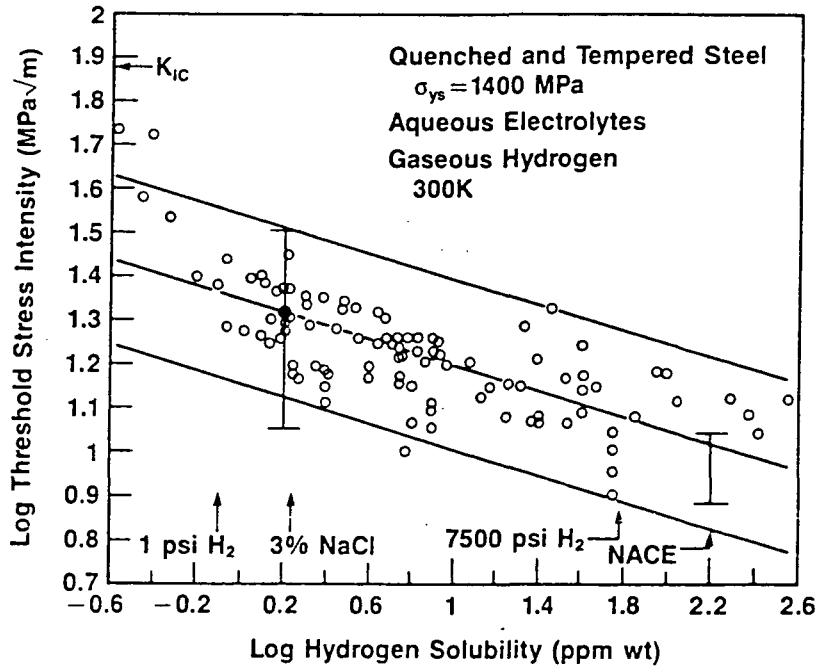

Fig. 20 - Correlation between K_{ISCC} and hydrogen uptake for high strength steels fractured in gaseous hydrogen and electrolytes. (after Gangloff [111])

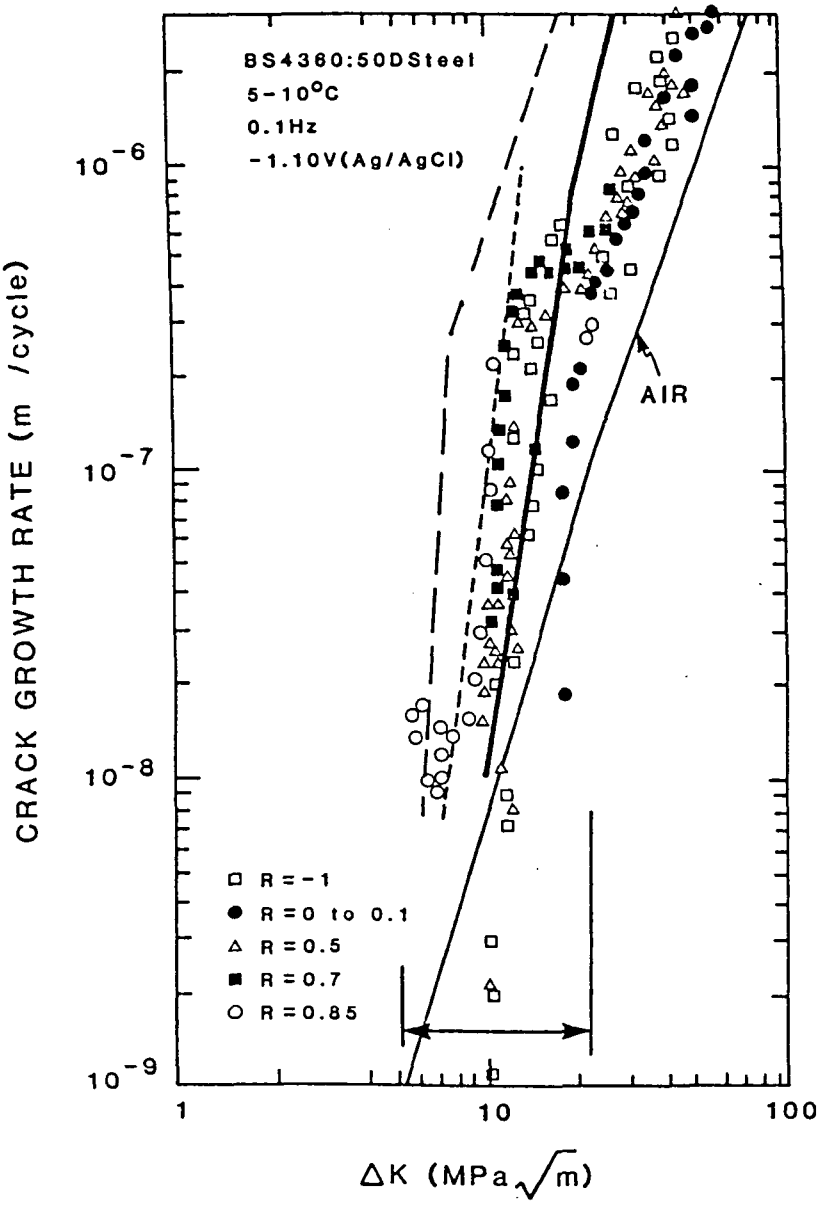

Fig. 21 - Corrosion fatigue crack growth rate versus ΔK for low strength BS4360:50D C-Mn steel in seawater after Scott et al. [93]; seawater + H_2S — — — — [115], oil + H_2S ——— [117], and high pressure H_2 --------[116].

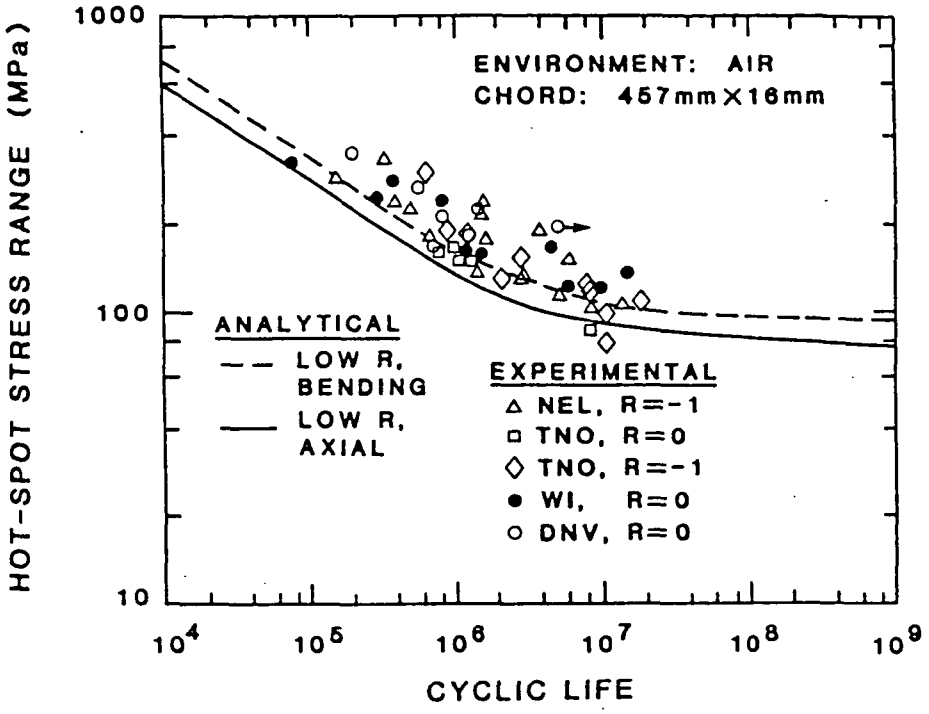

Fig. 22 - Fracture mechanics life prediction for fatigue crack propagation in welded tubular joints exposed to moist air and compared to full scale component measurements [121].

AQUEOUS ENVIRONMENT EFFECTS ON INTRINSIC CORROSION FATIGUE CRACK PROPAGATION IN AN Al-Li-Cu ALLOY

ROBERT S. PIASCIK AND RICHARD P. GANGLOFF
Department of Materials Science
University of Virginia
Charlottesville, VA 22901 USA

INTRODUCTION

The objective of this research is to characterize and understand intrinsic fatigue crack propagation in advanced aluminum-lithium based alloys, with emphasis on the damage mechanisms for environmentally assisted transgranular cracking.

While the importance of complex extrinsic (namely crack closure, delamination and crack deflection) contributions to fatigue crack propagation (FCP) in Al-Li alloys is established (1), gaseous and aqueous environmental effects have not been examined. In this study, fracture mechanics experiments; developed to characterize intrinsic FCP for benign environment exposure and based on short crack, programmed stress intensity methods (2); are extended to investigate the effect of aqueous sodium chloride. Emphasis is placed on electrochemical control of the environment and on high resolution measurements of fatigue crack length changes in response to chemical variations.

EXPERIMENTAL PROCEDURE

A 3.8 cm thick plate of an advanced Al-Li-Cu-Zr alloy (AA 2090) was studied in the rolled, unrecrystallized, peakaged

Submitted for publication in: "Proceedings, World Congress on Environmental Cracking of Metals", M. B. Ives and R. P. Gangloff, eds., NACE, Houston, TX (1989).

condition. Alloy composition, heat treatment, mechanical properties and microstructure, defined by optical and transmission electron metallography, are summarized in Table 1.

Corrosion behavior was characterized by potentiodynamic polarization experiments at a scan rate of 9.6 mV/min in helium deaerated, aqueous NaCl at pH 8 and 297 K (3). Corrosion fatigue experiments were conducted with specimens which were fully immersed in flowing (30 ml/min), helium deaerated, 1% NaCl (pH 8) in a sealed plexiglass chamber. Electrode potential was maintained constant by a Wenking potentiostat and platinum counter electrodes isolated from the solution through asbestos frits.

Crack propagation experiments were conducted with single edge notched specimens (10.16 mm wide, 2.54 mm thick, 0.25 or 0.89 mm notch depth) machined in the LT orientation at the one-third position in the plate. Pinned, freely rotating grips were employed, consistent with the stress intensity solution (4). The growth of short edge cracks, sized between 0.25 and 5 mm, was monitored continuously by a direct current electrical potential method including 8 to 12 amps current, 0.1 uV potential measurement resolution and an analytical calibration relation (5). This method has been successfully applied to short cracks in aluminum alloys, with better than 3 um crack growth resolution and long term (10 day) stability for near threshold growth rate measurements (2).

Intrinsic and transient or steady-state corrosion fatigue crack propagation is studied for both the moderate stress

intensity (ΔK) Paris regime and near threshold growth rates. Edge cracked specimens are stressed cyclically (sine waveform; 0.07 Hz < frequency < 20 Hz; 0.05 < stress ratio < 0.95) in a closed loop servohydraulic machine operated in load control. Employing computer measurement and feedback control, ΔK is maintained constant over segments of growing crack length (about 0.5 to 1 mm), with step reductions in ΔK at constant K_{max}, producing increasing stress ratio (R). Crack growth rates (da/dN) are calculated by linear regression analysis of crack length versus load cycles data. For a single specimen, the load sequence initially probes high ΔK, low R cracking; followed by near threshold ΔK, high R fatigue for deeper crack depths. Short crack length for the former and high stress ratio for the latter conditions minimize complicating extrinsic effects. Continuous reductions in ΔK at constant K_{max} provide an effective characterization of intrinsic fatigue crack growth (6). The procedure based on decreasing ΔK/step increasing R more effectively characterizes transient to steady state crack propagation associated with ΔK changes, electrochemical variables and microstructure.

RESULTS AND DISCUSSION

Corrosion Characteristics

Potentiodynamic polarization data are summarized in Fig. 1a for peakaged alloy 2090 exposed to deaerated and oxygen containing 1% NaCl solutions. In oxygen containing environments, the open circuit potential of alloy 2090 is near the breakaway potential, resulting in extensive surface pitting. Deaeration of

the NaCl solution limits the oxygen reduction reaction and shifts the open circuit potential in the cathodic direction forming a passive region extending from -1.0 V to -0.7 V (SCE). At passive region potentials, general corrosion and pitting are greatly reduced; constituent particles are none-the-less primary sites for sub-breakaway pitting. Long term (8 day) constant potential experiments performed at -0.760 V SCE in deaerated 1% NaCl reveal that T_1 precipitates, concentrated at subgrain boundaries, and constituent particles are sites of localized attack, Fig. 1b.

Corrosion fatigue experiments were performed in deaerated 1% NaCl to limit fracture surface corrosion and pitting, to reduce crevice corrosion at the electrical potential probes and to minimize electrolyte IR-type errors in measured potential. Since the open circuit potential of alloy 2090 varies by 100 to 400 mV during long term exposure, fatigue experiments were performed at a constant anodic potential of -0.760 V (SCE) and a cathodic potential of either -1.160 or -1.120 V (SCE).

Intrinsic Fatigue Crack Growth (Moist Air)

The intrinsic fatigue crack growth characteristics of alloy 2090 in moist air are shown in Fig. 2a. The data points (□) labeled with ΔK in $MPa \cdot m^{1/2}$ and R were calculated from the (a) versus (N) response shown in Fig. 2b, and which shows the seven constant ΔK levels of linear crack growth obtained by step increases in R at a constant K_{max} of 17 $MPa \cdot m^{1/2}$. Specifically note that the linear crack growth for the low ΔK region (ΔK=1.68/R=0.90) reveals no evidence of delay retardation, demonstrating that load shedding at constant K_{max} does not induce

overload effects presumably because the maximum or forward loading plastic zone size is constant.

Also plotted in Fig. 2a are the results of a continuously ($C=-177\ m^{-1}$) decreasing ΔK experiment at constant K_{max}. Above the near threshold regime, good agreement is observed between the constant ΔK-step increased R and continuously decreasing ΔK constant K_{max} techniques. The constant ΔK results exhibit crack growth below the threshold stress intensity indicated by the continuous load shedding experiment. The data contained in Fig. 2a are in excellent agreement with literature results for alloy 2090 (1,2,6) and represent the intrinsic FCG behavior of this alloy.

Aqueous Corrosion Fatigue

Intrinsic CF Characteristics. Shown in Fig. 3 is a comparison of the intrinsic corrosion fatigue crack growth characteristics of alloy 2090 in moist air, deaerated 1% NaCl (-0.760 V and -1.160 V SCE) and deaerated 1% NaCl+0.05M Li_2CO_3 (-0.760 V SCE). All experiments were performed at a cyclic frequency of 5 Hz, using the constant ΔK-step increased R/constant K_{max} method and a ΔK-step sequence similar to that shown in Fig. 2b. These results show that alloy 2090 exhibits a moderate environmental effect at high levels of ΔK where differences in crack growth rate are less than three-fold. Near threshold, considerable differences in fatigue crack growth are observed, with a factor of ten increase in da/dN revealed by comparing 1% NaCl with anodic polarization (-0.760 V SCE) and moist air. Anodic polarization with NaCl produced the largest corrosion fatigue effect. In contrast, at

moderate to high levels of ΔK, cathodic potential (-1.160 V SCE) reduced fatigue crack growth to a level slightly greater than that observed for moist air. Cathodic potential at low ΔK produced crack arrest above the moist air threshold. The addition of Li_2CO_3 to 1% NaCl (-0.760 V SCE) retarded crack growth; the reduction is not as dramatic as that produced by mild cathodic potential.

Corrosion fatigue experiments performed in aqueous 1% NaCl at constant anodic potential (-0.760 V SCE) show that peakaged alloy 2090 exhibits increased resistance to transgranular corrosion fatigue crack growth, by a factor of three, when compared to alloy 7075-T651 (2).

Frequency Effects. The classical frequency effect observed for high strength aluminum alloys at higher ΔK and characteristic of hydrogen environment embrittlement (7,8), namely increased corrosion fatigue crack growth rate with decreased frequency, is not observed for alloy 2090. In deaerated 1% NaCl solution (-0.760 V SCE), alloy 2090 exhibits mildly increased corrosion fatigue crack growth rates with increased frequency at high cyclic stress intensity and little frequency effect at low ΔK, as shown in Figs. 4, and 5.

Fig. 4 reveals the fatigue crack growth rate characteristics of alloy 2090 in 1% NaCl (-0.760 V SCE), at a frequency of 5 and 0.1 Hz. Plotted are the results of a constant ΔK-step increasing R/constant K_{max} test performed at a frequency of 5 Hz and three experiments performed at constant ΔK and R, at 0.1 and 5 Hz. Arrows indicate the increase in crack growth rate, at

constant ΔK, as the frequency was changed from 0.1 to 5 Hz. Best fit lines are drawn for the 5 and 0.1 Hz data, revealing a factor of 2 increase in fatigue da/dN at high ΔK and no change in crack growth at low levels of ΔK.

The changes in slope of the crack length versus cycles plot, Fig. 5a, highlight the changes in da/dN for three frequency. At high constant ΔK (9.9 $MPa \cdot m^{1/2}$), a factor of two decrease in fatigue crack growth rate is observed when decreasing the cyclic frequency from 5 to 0.1 Hz. Similar results were reported by Yoder and coworkers for alloy 2090 in aerated 3.5% NaCl (9).

At low cyclic stress intensities, distinct changes in fatigue crack growth as a function of frequency are not observed. Fig. 5b is a comparison of the average crack growth rate versus frequency, and includes the variation in crack growth rate (calculated with a point secant method) and the sequence in which the experiments were conducted for two specimens. At low ΔK, no difference in fatigue crack growth rate is observed for cyclic frequencies of 0.2, 1, 5, and 20 Hz. As much as a factor of 1.6 increase in da/dn is suggested by the a-N data for the 0.07 Hz condition and a 35% reduction in rate is recorded for the last portion of the constant ΔK experiment. The origin of the low frequency result is unclear. Fractographic analysis revealed evidence of increased dissolution for this long term experiment (0.25 mm of crack extension in 8 days), possibly related to an increased driving force for fatigue; however; long term electrical potential system variations may have contributed to part or all of the increased growth rate. The reduction in da/dN

for segment 6 is attributed to a chemical or mechanical history dependence associated with crack length and shape (10). These factors complicate characterizations of moderate frequency effects in corrosion fatigue. The important point to be made in Fig. 4 and 5 is that corrosion fatigue in AA 2090 is not exacerbated by decreasing frequency; to the contrary, the opposite trend is likely, particularly at higher ΔK.

Polarization Effects. The results of constant ΔK experiments show that corrosion fatigue crack growth in 1% NaCl is mitigated by cathodic polarization. Fig. 6a reveals that, at constant ΔK (2.2 MPa·m$^{1/2}$, R=0.8) and anodic polarization (-0.760 V SCE), a constant crack growth rate is maintained to a crack length of 2.05 mm. Here, a cathodic potential of -1.160 V (SCE) was applied, resulting in crack arrest. At 1.0 million load cycles a potential of -0.760 V (SCE) was again applied. 76 hours or 2.2 million cycles elapsed before crack growth resumed, achieving a steady state rate similar to the initial anodic condition. A second cathodic polarization of -1.160 V (SCE) reproduced crack arrest.

Cathodic polarization also reduced rates of corrosion fatigue at high cyclic stress intensity (9.6 MPa·m$^{1/2}$, R=0.1), as shown in Fig. 6b. After initial cracking at -0.760 V (SCE), a mild reduction in da/dN was produced by polarization to -1.160 V (SCE), and a significant, time dependent retardation in crack growth was observed at a cathodic potential of -1.260 V (SCE). At a crack length of 3.12 mm, the applied stress intensity range was decreased to a ΔK of 2.1 MPa·m$^{1/2}$ at R=0.9 with K_{max}

maintained constant. A slow recovery to a constant growth rate was observed at an anodic potential of -0.760 V (SCE). Crack growth arrest occurred due to cathodic polarization at -1.160 V (SCE), reproducing the results shown in Fig. 6a. The results of constant ΔK and R experimentation, Fig. 6, are consistant with the single specimen constant ΔK-step increased R results presented in Fig. 3.

The reduction in corrosion fatigue crack growth of alloy 2090 by cathodic polarization is consistent with the findings of other researchers. Cathodic polarization of alloy 7075 in aqueous 3.5% NaCl reduced corrosion fatigue crack propagation, only at ΔK=11 MPa$\cdot m^{1/2}$, (11), and the enhanced stress corrosion cracking resistance of conventional 2000 and 7000 series alloys due to cathodic polarization is documented (12). Consistent with the above results, although not conclusive, the smooth specimen fatigue life of an Al-4.2Mg-2.1Li alloy was increased by mild cathodic potential (13).

Ion Addition Effects. The experimental results shown in Fig. 7 demonstrate that a lithium carbonate (Li_2CO_3) addition to 1% NaCl reduces the rate of transgranular corrosion fatigue crack growth at constant ΔK, pH and potential. At a cyclic stress intensity of 2.3 MPa$\cdot m^{1/2}$ (R=0.87) and an anodic potential of -0.760 V (SCE), a constant crack growth rate was initially established in deaerated 1% NaCl (pH=8.1). No change in crack growth is observed as the solution pH is adjusted from 8.1 to 10.4. At a crack length of 1.90 mm, the cell environment was changed by continuously pumping deaerated 1% NaCl-0.05M Li_2CO_3 (pH=10.4)

solution from a separate reservoir. After purging the cell with flowing 1% NaCl-0.05M Li_2CO_3, the experiment was resumed, resulting in a reduced fatigue crack growth rate. This beneficial effect was reproduced at two higher ΔK levels, Fig. 3.

Fractographic Analysis. A comparison of the fracture surface morphologies for moist air and deaerated 1% NaCl (-0.760 V SCE) environments is shown in Fig. 8. Both fracture surfaces represent crack growth at low cyclic stress intensity. In moist air, Fig. 8a, the transgranular fracture surface is crystallographic with intermittent regions of flat and deflected crack growth exhibiting a ductile appearance. The transgranular fracture morphology for 1% NaCl, Fig. 8b, is characterized by a flat "cleavage type" fracture surface exhibiting little evidence of ductility (11). Detailed examination of the fatigue crack-final overload fracture interface region revealed little evidence of corrosion. Small and widely dispersed regions of sub grain boundary corrosion, similar to that shown in Fig. 1b, were observed. No evidence of corrosion was observed along high angle grain boundaries.

The fracture surface morphology for aqueous NaCl depends on cyclic stress intensity range. At high ΔK (15 $MPa \cdot m^{1/2}$) severe planar crack surface deflections are dominant. Here fatigue crack growth is possibly due to decohesion along intense slip bands. As stress intensity range decreases, the amount of crack tip deflection is reduced and the fracture surface is characterized by increased areas exhibiting a flat crystallographic appearance.

MECHANISTIC IMPLICATIONS

Many mechanisms have been proposed for environmental fracture of aluminum alloys including: hydrogen embrittlement, adsorbate decohesion, film rupture/dissolution, film induced slip irreversibility, enhanced localized plasticity, and crack tip blunting (7,8,11,12,14,15). Paris regime corrosion fatigue has been emphasized; the effects of aqueous environments on near threshold cracking have not been considered. For the former, a cleavage fracture morphology was circumstantially linked to both hydrogen embrittlement and surface film effects. Hydrogen from cathodic reduction in electrolytes and chemical reactions in water vapor is held to embrittle aluminum with contributions from dislocation and grain boundary transport processes. Alternately, surface films suppress plastic deformation by blocking the crack tip emission of dislocations; the local normal stress is elevated causing cleavage.

Based on the experimental observations of FCP response to ΔK, frequency, cathodic polarization and Li_2CO_3 addition, we speculate that surface films play an important role in crack tip damage during transgranular corrosion fatigue of Al-Li-Cu alloys. Faster crack growth is correlated with those environmental conditions which are likely to favor less protective crack tip surface films. While hydrogen embrittlement may contribute to crack propagation, the frequency and cathodic polarization dependencies observed for AA 2090 are opposite to the classical relationships which are diagnostic of this failure mechanism, as discussed for 7000 series alloys (7,8,12).

Increased crack growth rates with increased frequency suggest that time dependent chemical reactions and mass transport are rapid and do not limit crack tip environmental damage. Considering mechanical rate effects, crack tip cyclic strain rate is approximately proportional to loading frequency and stress intensity range raised to a power on the order of 5 (16). At high ΔK, mechanical film disruption provides a plausible explanation for the mild increase in crack growth with increasing frequency. Here, crack tip strain rate increases with increasing frequency, the film is locally breached more frequently favoring transient dissolution or hydrogen production reactions, and crack extension per unit time and cycle increases. Near threshold, crack tip deformation may further localize, however, the average crack tip strain rate decreases strongly. The diminished effect of frequency suggests that the latter effect dominates for AA 2090 in aqueous chloride. The environmental effect is strong near threshold, suggesting that chemical factors control surface film formation and environmental crack advance.

The beneficial effect of a surface film is likely to be chemical in origin. Film or corrosion product induced crack closure is not operative because the environmental influences are observed at stress ratios above 0.85 and for short crack wakes. Secondly, there is no evidence that surface films promote irreversible dislocation damage (14). Rather, we speculate that films interfere with crack tip environmental reactions (hydrogen production or dissolution), resulting in a significant reduction in fatigue crack growth rate. Once the film is damaged by

chemical or mechanical means, such as localized anodic pitting dissolution or slip step formation, the film no longer acts as a barrier; the alloy is rendered susceptible to brittle crack growth.

Although experimental evidence strongly suggests that surface films play a primary role in crack tip damage during transgranular fatigue of alloy 2090 in aqueous environments, further work must be performed to understand the roles of hydrogen and transient localized anodic dissolution. Gaseous environment corrosion fatigue experiments and high resolution fractographic analyses are being conducted in this regard (2).

CONCLUSIONS

The high resolution potential difference technique, short crack specimen geometry and constant ΔK-step increased R/constant K_{max} approach successfully characterizes intrinsic fatigue crack growth in complex aluminum-lithium based alloys exposed to aggressive aqueous environments.

Al-Li-Cu alloy 2090, peak aged, is susceptible to corrosion fatigue crack propagation in aqueous 1% NaCl under anodic polarization. At low ΔK/high R, near threshold crack growth rates are significantly increased, with growth occurring by a cleavage process. High ΔK/low R growth rates are increased by the environment, with highly deflected slip band cracking the dominate microscopic mode. Environmental effects on AA 2090 are less severe than those reported for high strength AA 7075.

Crack tip films play an important role in corrosion fatigue damage, as evidenced by: (1) increased da/dN with increased

cyclic frequency, particularly at high ΔK, (2) retarded crack growth due to cathodic polarization in NaCl and (3) reduced da/dN due to Li_2CO_3 additions.

ACKNOWLEDGEMENT

The research support provided by the NASA-Langley Research Center, grant NAG-1-745 with D.L. Dicus as monitor, is gratefully acknowledged. Alloy 2090 was provided by E.L. Colvin, Alcoa Technical Center.

REFERENCES

1. K.T. Venkateswara Rao, W. Yu and R.O. Ritchie, Metall. Trans., Vol. 19A, pp. 549-561 and pp. 563-569 (1988).

2. R.S. Piascik and R.P. Gangloff, "Environmental Assisted Degradation Mechanisms in Al-Li Alloys", Report No. UVA/528266/MS88/101, University of Virginia (1988).

3. ASTM G5-82,"Standard Reference Method for Making Potentiostatic and Potentiodynamic Anodic Polarization Measurements", 1985 Annual Book of ASTM Standards-Methods and Analytical Procedure, ASTM, Philadelphia, PA, Vol. 3, pp. 123-133 (1985).

4. H. Tada, P. Paris and G.I. Irwin, The Stress Analysis of Cracks Handbook, Del Research Corp., St. Louis, MO, pp. 2.10-2.11 (1985).

5. R.P. Gangloff, Advances in Crack Length Measurements, C.J. Beevers, ed., EMAS, UK, pp. 175-229 (1982).

6. W.A. Herman, R.W. Hertzberg, and R. Jaccard,"A Simplified Laboratory Approach for the Prediction of Short Crack Behavior in Engineering Structures", The Journal of Fatigue and Fracture of Engineering Materials and Structures, in press (1988).

7. H.J.H. Holroyd and D. Hardie, Corr. Sci., Vol.23, No.6, pp. 527-546 (1983).

8. M.Gao, P.S. Pao and R.P. Wei, "Chemical and Metallurgical Aspects of Environmentally Assisted Fatigue Crack Growth In 7075-T651 Aluminum Alloy, Metall. Trans. A, in press (1987).

9. G. R. Yoder, P.S. Pao, M.A. Imam and L.A. Cooley, Intl. SAMPE Metals Conf. Ser., Vol.1, pp. 25-36 (1987).

10. R.P. Gangloff and D.J Duquette, Chemistry and Physics of Fracture, R.M. Latanision and R.H. Jones, eds., NATO Series E, No.130, pp. 612-645 (1987).

11. R.E. Stotz and R.M. Pelloux, Met. Trans, Vol. 3, pp. 2433-2441 (1972).

12. N.J.H. Holroyd and G.M. Scammans, Environment-Sensitive Fracture, ASTM 821, S.W. Dean, E.N, Pugh and G.W. Ugiansky, eds., American Society for Testing and Materials, pp. 202-241 (1984).

13. R.E. Ricker and D.J. Duquette, "The Use of Electrochemical Potential to Control and Monitor Fatigue of Aluminum Alloys, Corrosion 85, 1985, NACE, Publications Dept., Houston, TX, Paper # 354.

14. K.V. Jata and E.A. Starke, Jr., Metall. Trans. A, Vol. 17A, pp. 1011-1026 (1986).

15. D.L. Davidson and J. Lankford, Fat. Engr. Matls. and Struc., Vol. 6, pp. 241-256 (1983).

16. S.J. Hudak, Jr., D.L. Davidson and R.A. Page, Embrittlement by the Localized Crack Environment, R.P. Gangloff, ed., TMS-AIME, Warrendale, PA, pp. 173-198 (1984).

17. J.G. Craig, R.C. Newman, M.R. Jarrett and N.J. H. Holroyd, Journal De Physique, Vol. C3, No. 9/48, pp. 825-833 (1987).

18. J. Gui and T.M. Devine, Scripta Metall., Vol. 21, pp. 853-(1987).

Figure Captions

Fig.1 (a) Potentiodynamic polarization of alloy 2090 in aerated and deaerated 1% NaCl. (b) A photomicrograph of alloy 2090 exposed to deaerated 1% NaCl for 8 days at - 0.760 V (SCE). Note subgrain boundary, T_1 precipitate, corrosion (arrows) and constituent particle pitting.

Fig.2 (a) A comparison of constant ΔK-step increased R/constant K_{max} results with decreasing ΔK-constant K_{max} data. (b) Crack length versus loading cycles plot for the decreasing ΔK-increasing R/constant K_{max} results in Fig. 2a.

Fig.3 The corrosion fatigue crack growth characteristics of alloy 2090 in aqueous 1% NaCl at constant anodic (-0.760 V SCE) and cathodic (-1.160 V SCE) potentials, 1% NaCl + 0.05M Li_2CO_3 (-0.760 V SCE), and moist air environments.

Fig.4 The effect of cyclic loading frequency on the intrinsic corrosion fatigue crack growth of alloy 2090 exposed to 1% NaCl at constant anodic potential.

Fig.5 (a) The effect of frequency on corrosion fatigue crack propagation in alloy 2090 at high ΔK. (b) The dependence of corrosion fatigue crack growth rate on cyclic frequency at high and low ΔK.

Fig.6 The effect of cathodic polarization on intrinsic corrosion fatigue crack growth in alloy 2090 at constant ΔK level of (a) 2.2 $MPa \cdot m^{1/2}$ for high R and (b) 9.6 and 2.1 $MPa \cdot m^{1/2}$ for low and high R conditions, respectively, in 1% NaCl.

Fig.7 The effect of Li_2CO_3 addition and pH change on the intrinsic fatigue crack growth of alloy 2090 in 1% NaCl at constant anodic potential and constant cyclic stress intensity.

Fig.8 A comparison of the fracture morphology due to corrosion fatigue at low ΔK in (a) moist air at 2.5 $MPa \cdot m^{1/2}$ and (b) deaerated 1% NaCl (-0,760 V SCE) at 2.2 $MPa.m^{1/2}$. Crack growth is from right is from right to left, with the fatigue crack-final overload fracture interface shown.

TABLE 1 Material Properties

Chemical Composition:

Li	Cu	Zr	Fe	Si	Mn
2.14	2.45	0.09	0.05	0.04	0.00
Mg	Cr	Ni	Ti	Na	Zn
0.00	0.00	0.00	0.01	0.001	0.01

Material Condition:

Solutionized quenched and stretched.
Peakaged 190°C - 4hrs

Mechanical Properties:(Long-Transverse)

Yield	Ultimate
496 MPa	517 MPa

Microstructure:

Grain size - 3.3 mm (transverse)
- 0.11 mm (short transverse)
Subgrain size - 15 um (transverse)
- 5 um (short transverse)
Precipitate morphology
δ' - Al_3Li, Θ' - Al_2Li, T_1 - Al_2CuLi, T_2 - Al_6CuLi_3,
Matrix phases - δ', T_1, Θ'
Sub grain boundary - T_1
High angle grain boundary - T_2

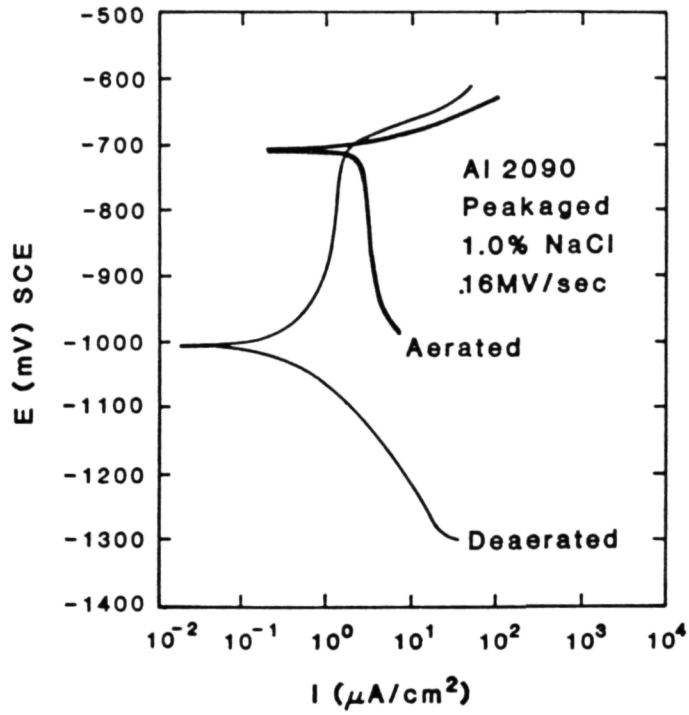

(a)

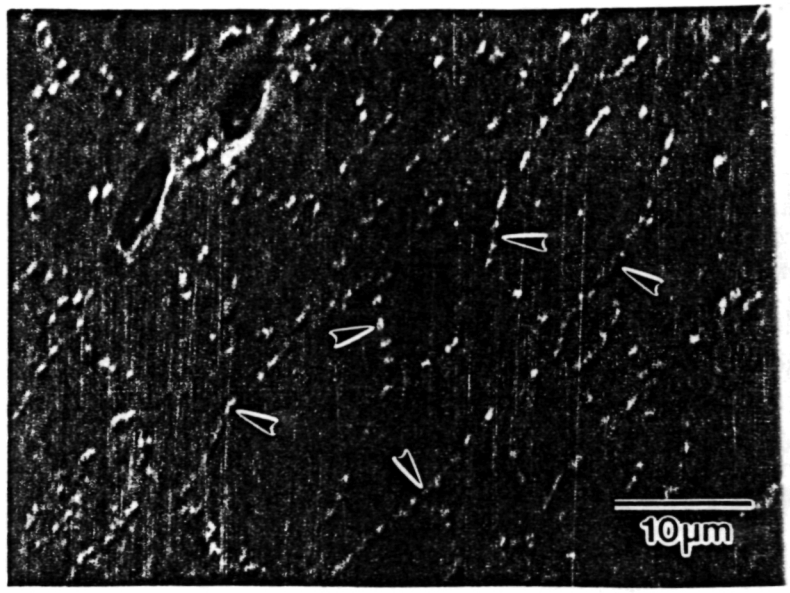

(b)

Figure 1

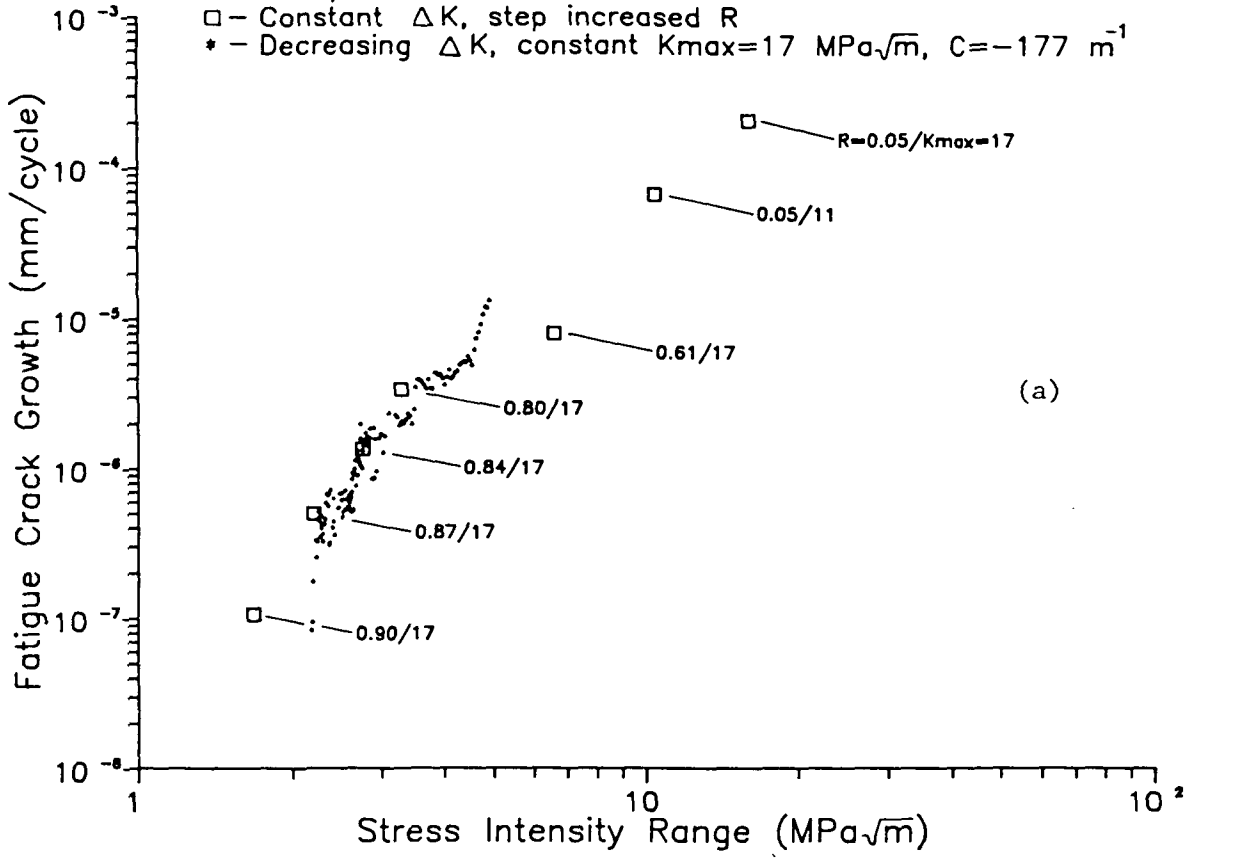
ALLOY 2090 Peakaged, L-T
Moist Air, 5 Hz
□ – Constant ΔK, step increased R
* – Decreasing ΔK, constant Kmax=17 MPa√m, C=–177 m⁻¹
R=0.05/Kmax=17
0.05/11
0.61/17
0.80/17
0.84/17
0.87/17
0.90/17
(a)
Fatigue Crack Growth (mm/cycle)
Stress Intensity Range (MPa√m)

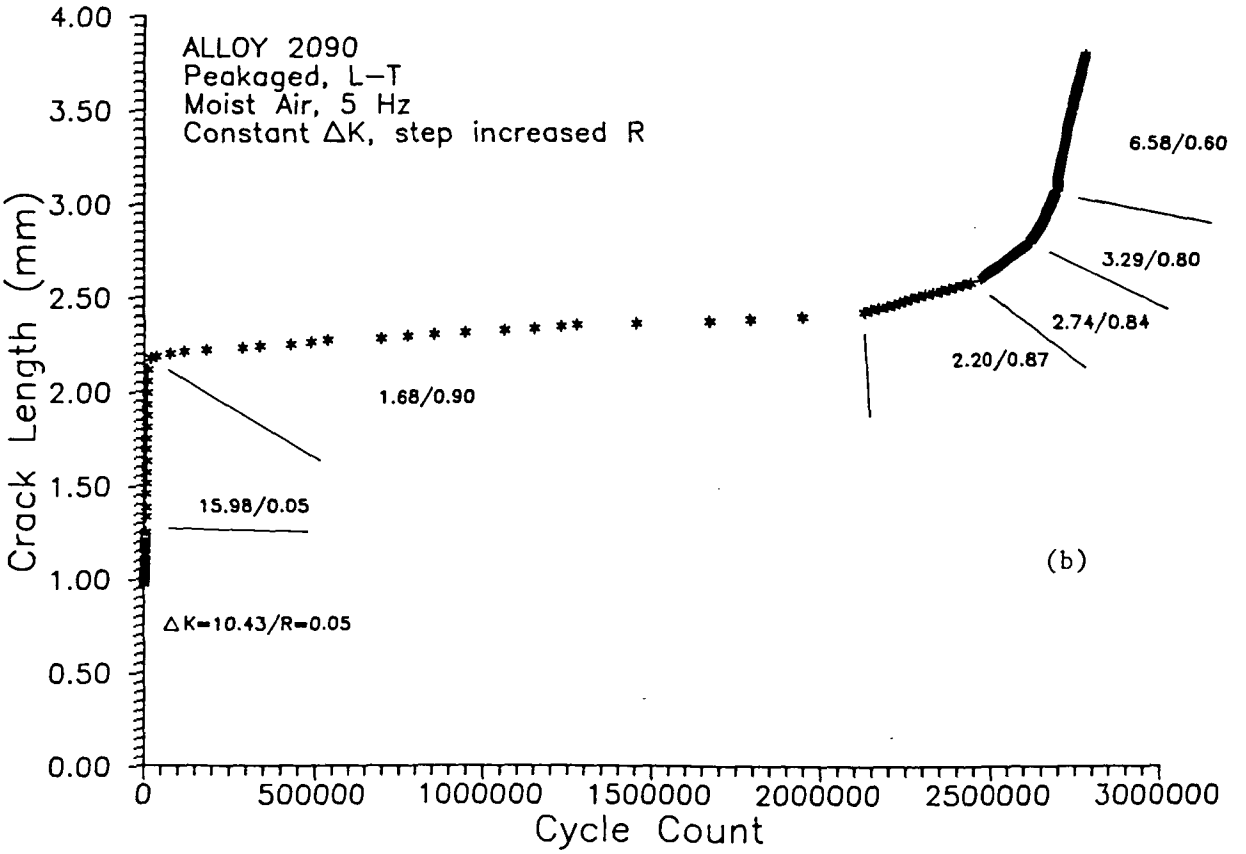
ALLOY 2090
Peakaged, L-T
Moist Air, 5 Hz
Constant ΔK, step increased R
6.58/0.60
3.29/0.80
2.74/0.84
2.20/0.87
1.68/0.90
15.98/0.05
ΔK=10.43/R=0.05
(b)
Crack Length (mm)
Cycle Count

Figure 2

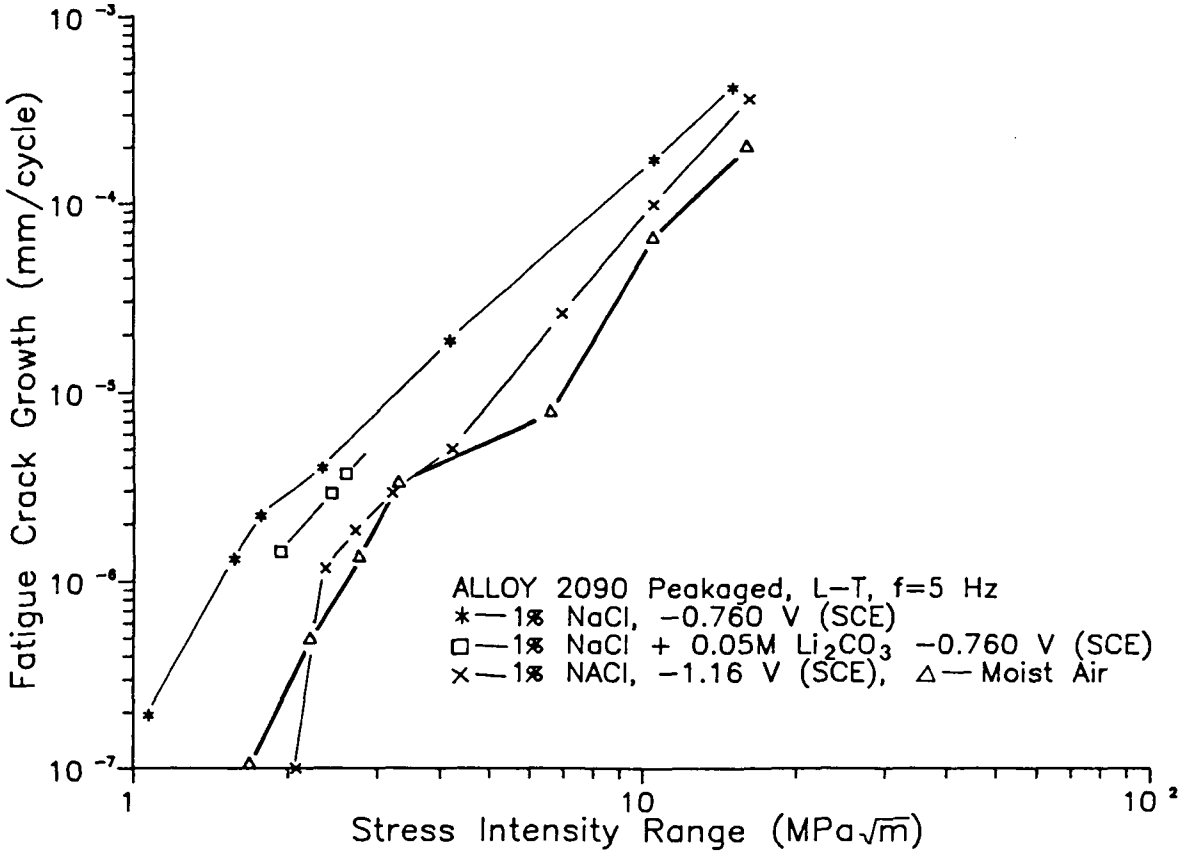
Fatigue Crack Growth (mm/cycle)
10 -3
10 -4
10 -5
10 -6
10 -7
1
10
10 2
Stress Intensity Range (MPa√m)
ALLOY 2090 Peakaged, L—T, f=5 Hz
*—1% NaCl, −0.760 V (SCE)
□—1% NaCl + 0.05M Li2CO3 −0.760 V (SCE)
×—1% NACl, −1.16 V (SCE), △— Moist Air

Figure 3

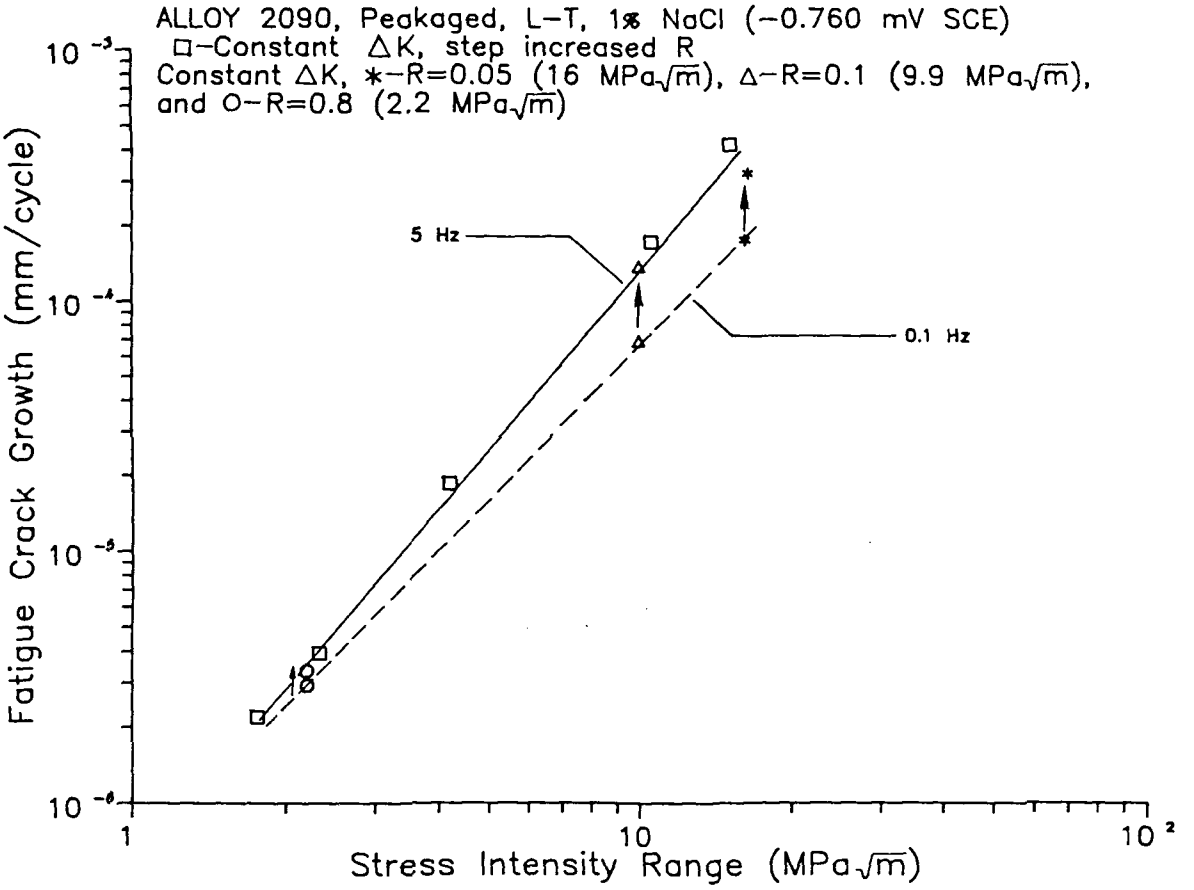
ALLOY 2090, Peakaged, L-T, 1% NaCl (-0.760 mV SCE)
□-Constant ΔK, step increased R
Constant ΔK, *-R=0.05 (16 MPa√m), Δ-R=0.1 (9.9 MPa√m),
and O-R=0.8 (2.2 MPa√m)
5 Hz
0.1 Hz
Fatigue Crack Growth (mm/cycle)
10 -3
10 -4
10 -5
10 -6
1
10
10 2
Stress Intensity Range (MPa√m)

Figure 4

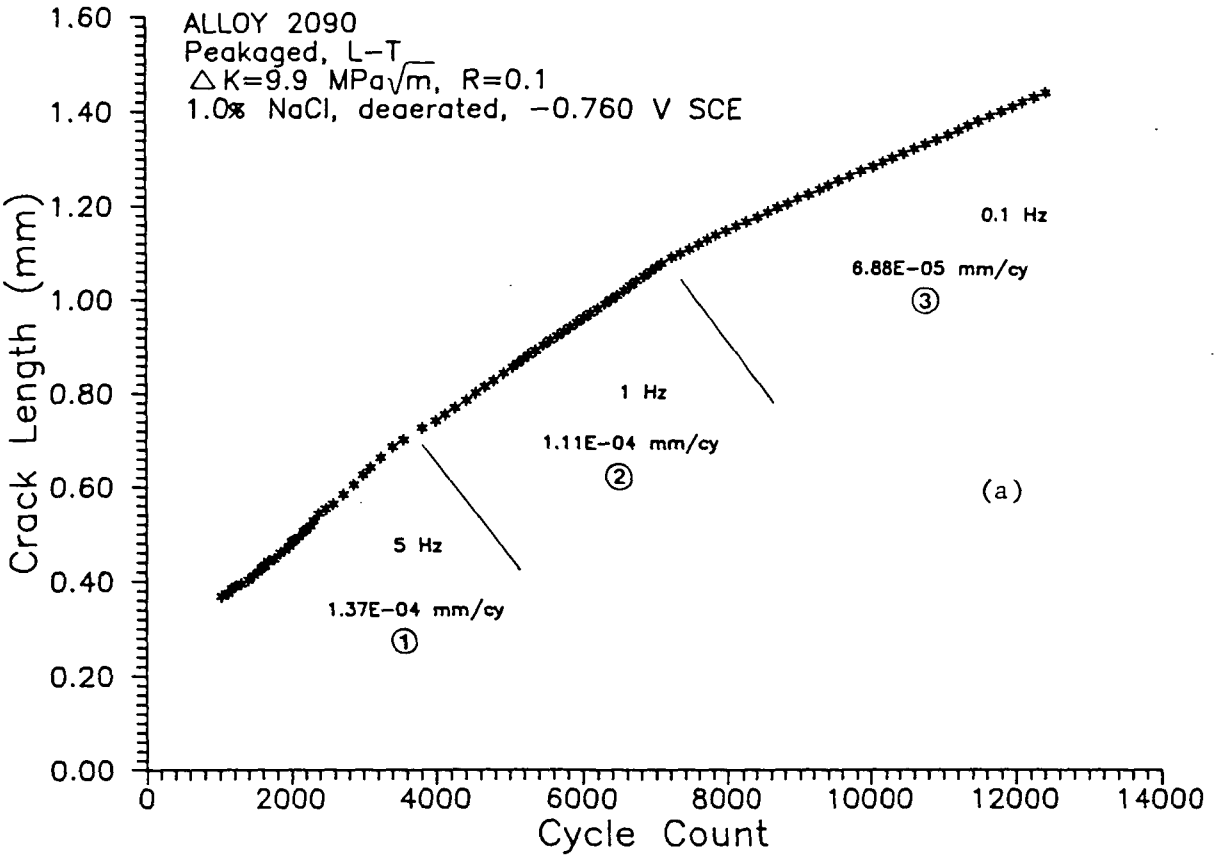
ALLOY 2090
Peakaged, L-T
ΔK=9.9 MPa√m, R=0.1
1.0% NaCl, deaerated, -0.760 V SCE
Crack Length (mm)
Cycle Count
0.1 Hz
6.88E-05 mm/cy
③
1 Hz
1.11E-04 mm/cy
②
5 Hz
1.37E-04 mm/cy
①
(a)

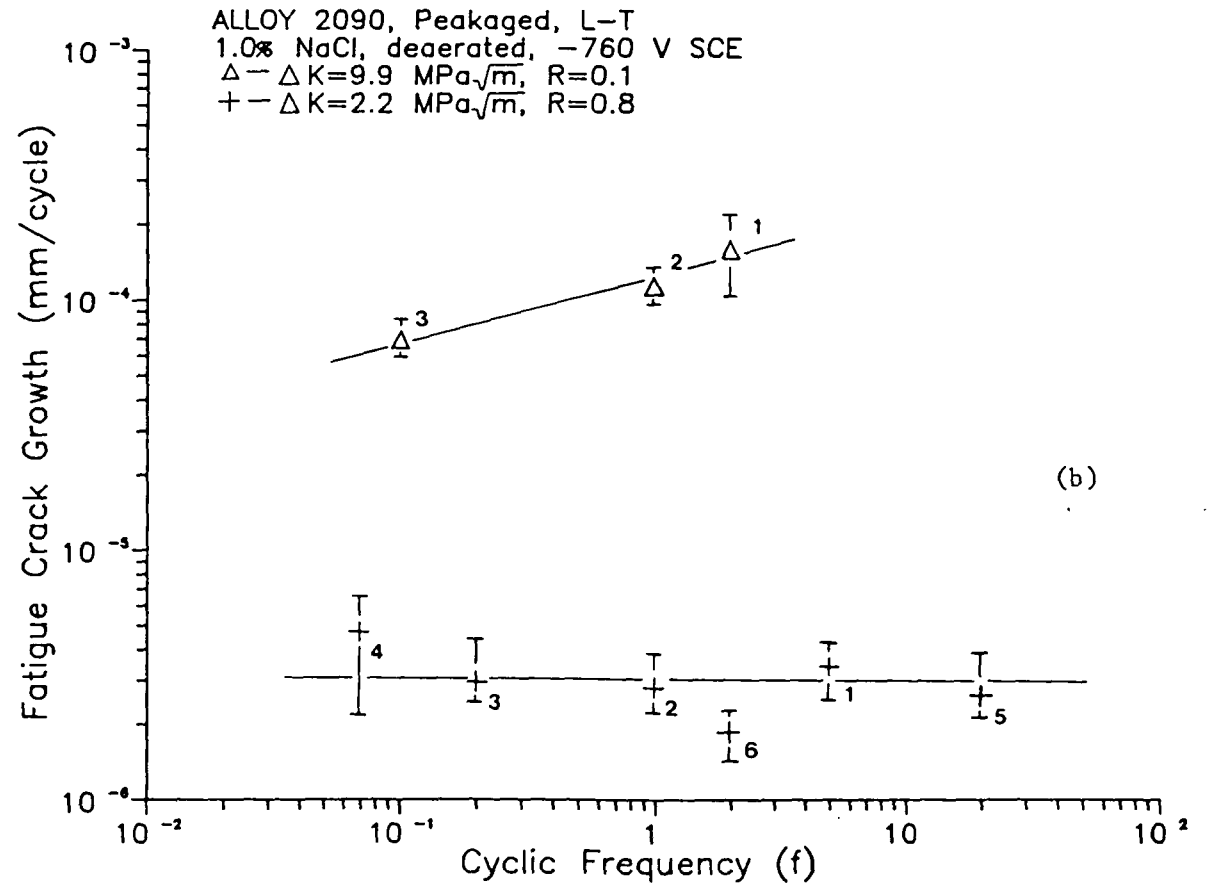
ALLOY 2090, Peakaged, L-T
1.0% NaCl, deaerated, -760 V SCE
Δ — ΔK=9.9 MPa√m, R=0.1
+ — ΔK=2.2 MPa√m, R=0.8
Fatigue Crack Growth (mm/cycle)
Cyclic Frequency (f)
(b)

Figure 5

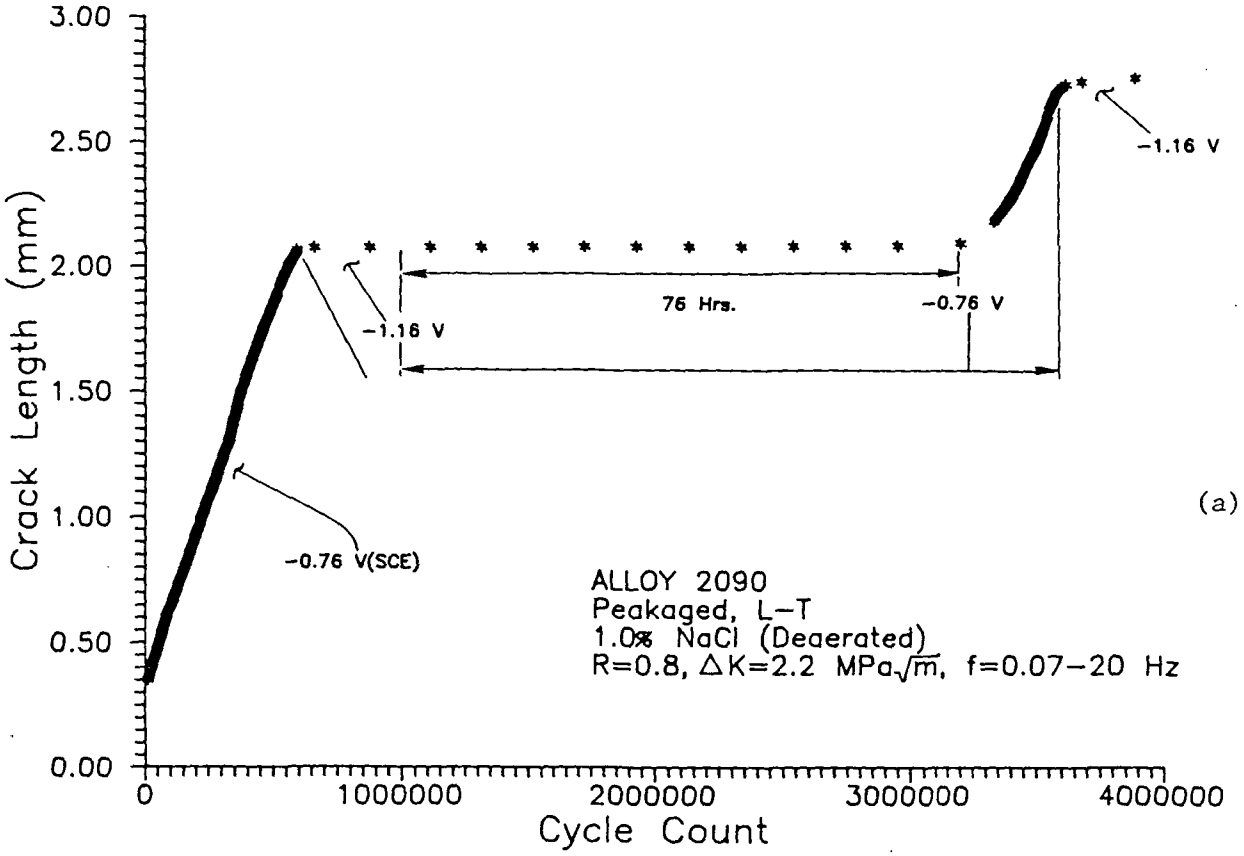
3.00
2.50
2.00
1.50
1.00
0.50
0.00
Crack Length (mm)
0
1000000
2000000
3000000
4000000
Cycle Count
-1.16 V
76 Hrs.
-0.76 V
-1.16 V
-0.76 V(SCE)
(a)
ALLOY 2090
Peakaged, L-T
1.0% NaCl (Deaerated)
R=0.8, ΔK=2.2 MPa√m, f=0.07-20 Hz

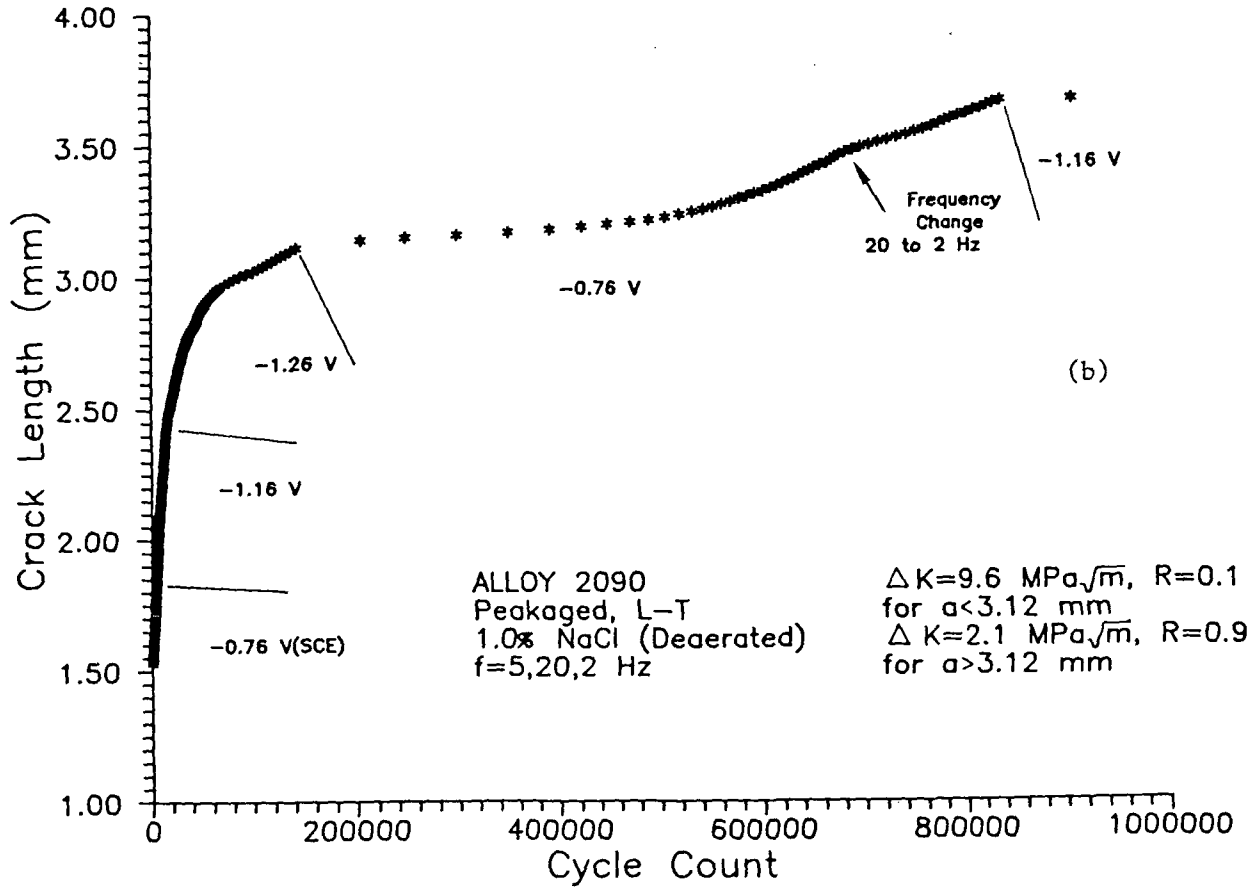
4.00
3.50
3.00
2.50
2.00
1.50
1.00
Crack Length (mm)
0
200000
400000
600000
800000
1000000
Cycle Count
-1.16 V
Frequency
Change
20 to 2 Hz
-0.76 V
-1.26 V
(b)
-1.16 V
-0.76 V(SCE)
ALLOY 2090
Peakaged, L-T
1.0% NaCl (Deaerated)
f=5,20,2 Hz
ΔK=9.6 MPa√m, R=0.1
for a<3.12 mm
Δ K=2.1 MPa√m, R=0.9
for a>3.12 mm

Figure 6

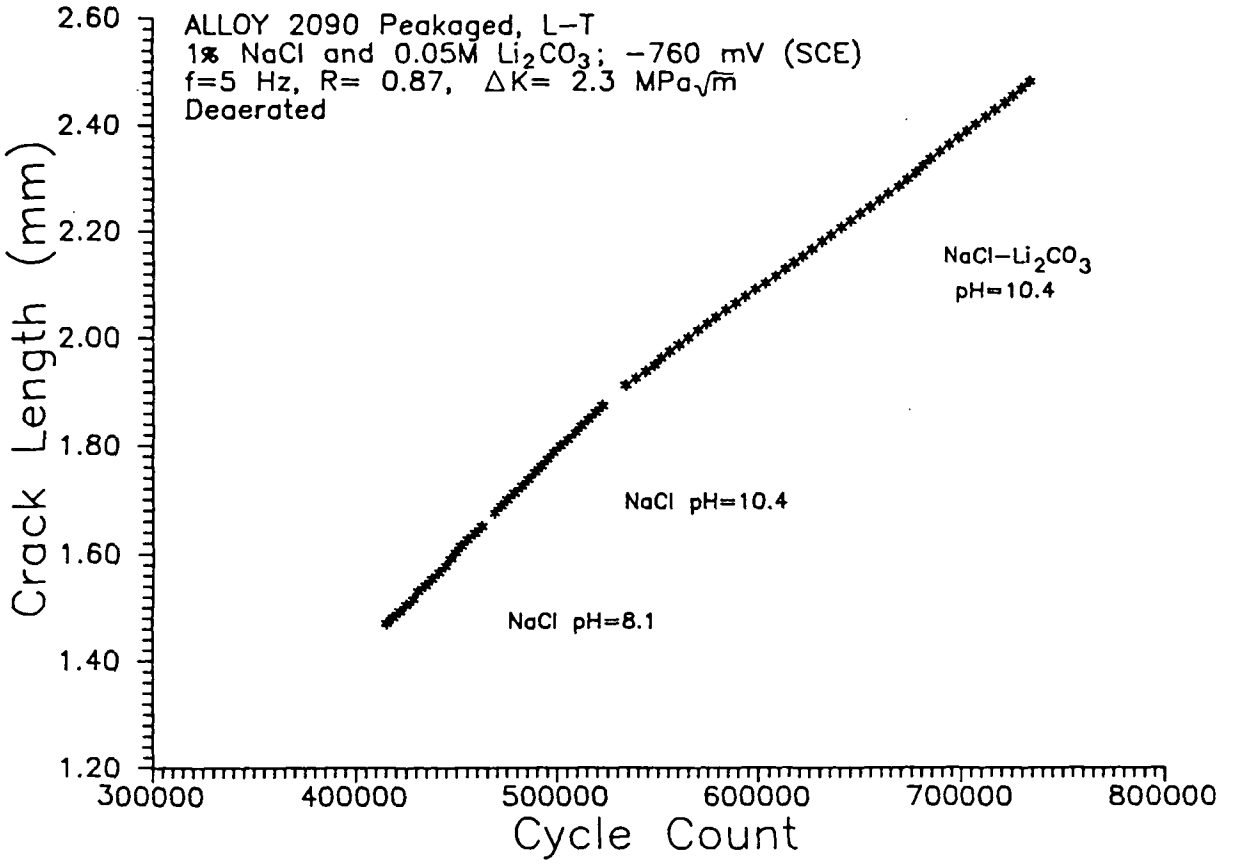
ALLOY 2090 Peakaged, L-T
1% NaCl and 0.05M Li_2CO_3; -760 mV (SCE)
f=5 Hz, R= 0.87, ΔK= 2.3 MPa$\sqrt{m}$
Deaerated
Crack Length (mm)
2.60
2.40
2.20
2.00
1.80
1.60
1.40
1.20
300000
400000
500000
600000
700000
800000
Cycle Count
NaCl-Li_2CO_3
pH=10.4
NaCl pH=10.4
NaCl pH=8.1

Figure 7

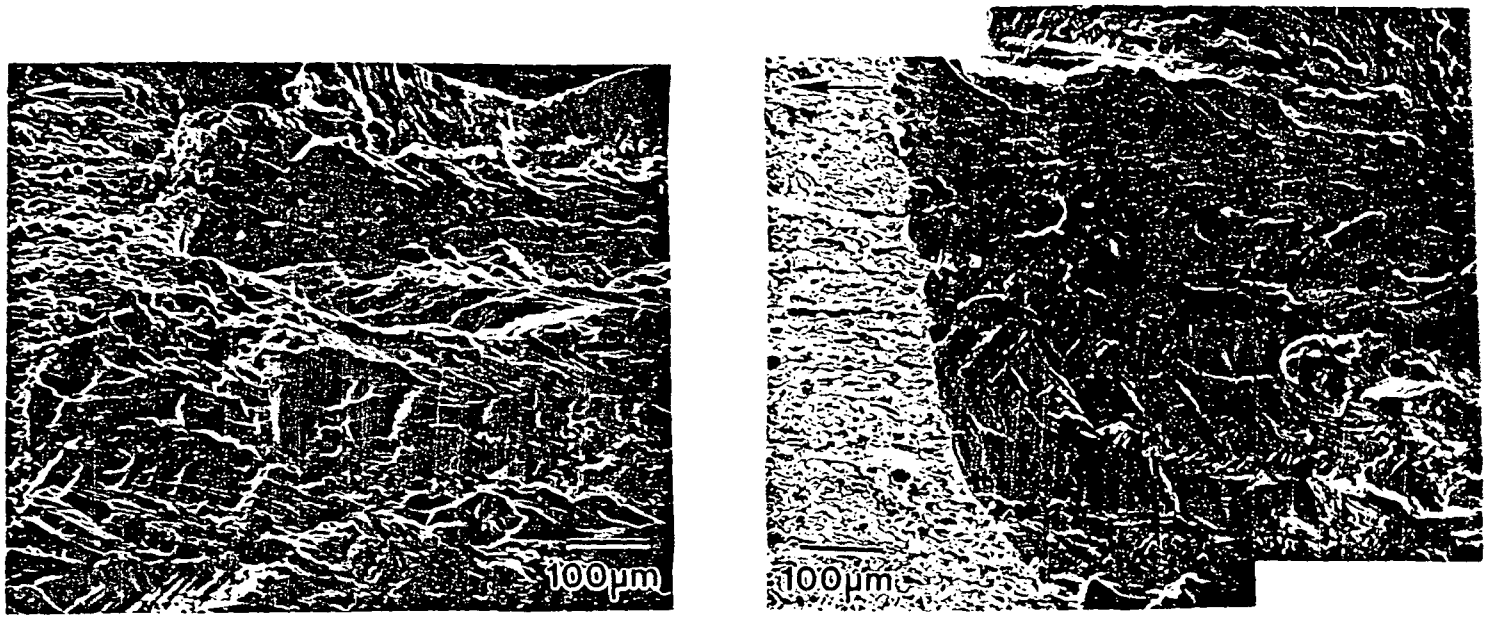

(a) (b)

Figure 8

Extended Abstract for ICF-7; Houston, Texas (1989)
"Fatigue and Fracture of Advanced Aerospace Materials"

(Session Organizer: T. W. Crooker)

INTRINSIC FATIGUE CRACK PROPAGATION IN ALUMINUM-LITHIUM ALLOYS: THE EFFECT OF GASEOUS ENVIRONMENTS

ROBERT S. PIASCIK AND RICHARD P. GANGLOFF

Department of Materials Science
University of Virginia
Charlottesville, VA 22901

Advanced aluminum-lithium based alloys exhibit outstanding fatigue crack propagation resistance, but attributable to the extrinsic effects of crack surface closure contact and crack tip deflection. Extrinsic crack growth resistance is likely to be geometry, orientation and loading history dependent; thus complicating defect tolerant predictions. It is critical to understand the intrinsic fatigue response of such materials, and particularly environmental and microstructural influences on crack tip damage mechanisms.

Intrinsic fatigue crack propagation is effectively studied by in situ, direct current, electrical potential monitoring of single, short, but through-thickness, edge cracks sized between 0.3 and 5 mm. Computer control enables constant stress intensity range and constant K_{max} load shedding at high mean stress levels near threshold. Results obtained to date complement studies of microstructurally small cracks.

The intrinsic growth kinetics of such short cracks in peak aged Alloy 2090, exposed to moist air, are rapid at stress intensity ranges between 1 and 2 $MPa \cdot m^{1/2}$. The near threshold behavior of 2 to 5 mm edge cracks in freely rotating specimens agrees with data for standardized compact tension specimens subjected to high mean stress loading programs; the apparent threshold is near 2 $MPa \cdot m^{1/2}$. If rotation is restricted by either short crack length or by mechanical constraint, crack growth continues to a ΔK level of about 1 $MPa \cdot m^{1/2}$; similar to the behavior of microstructurally small cracks. These results for benign environments are interpreted based on crack closure and bending related, Mode II displacements.

Equal intrinsic fatigue behavior is observed for two orientations of short cracks in anisotropic, unrecrystallized Alloy 2090, peak aged. This result is significant because such cracks sample either single or multiple grains along the propagating front. The later case is given by an LT orientation where the 2.5 mm wide edge cracks grow normal to and intersect

about 50 thin, elongated grains. In the LS orientation, the short cracks grow entirely within one or two grains and often encounter high angle boundaries. Electrical potential monitoring at constant stress intensity range gives no indication of grain by grain changes in growth rate for the LS orientation, despite significant crack deflections. No evidence is obtained to confirm reports of uniquely high growth rates of small cracks within single grains in Alloy 2090.

Gaseous environmental effects on intrinsic fatigue crack growth are significant for Alloy 2090. For high ΔK-low R loading, crack growth rates decrease according to the environment order: purified water vapor, moist air, helium and oxygen. For low ΔK-high R, the fastest intrinsic crack growth rates are observed for helium, with slower rates measured for water vapor, moist air and oxygen. These data are unique in that crack growth in oxygen is substantially reduced and growth in helium is unexpectedly rapid. The environmental effects are most pronounced near threshold and are not obviously closure dominated. Similar results were obtained for Alloy 7075-T651. While these environments were established in an ultra-high vacuum chamber, the complicating effects of trace impurities cannot, at present, be eliminated; and the contributions of oxide debris, hydrogen and surface film-dislocation interactions are not yet understood. Experiments are in progress to probe these issues.

This research is supported by the NASA-Langley Research Center, grant NAG-1-745, with D.L. Dicus as monitor.

APPENDIX II. TRAVEL AND CONFERENCE PARTICIPATION NOVEMBER, 1987 TO JUNE 1988

Travel

G.E. Stoner, R.P. Gangloff, R.S. Piascik and R.G. Buchheit, Jr.: Alcoa Technical Center; Pittsburgh, PA, February, 1988; Student presentations on environmental effects research.

R.P. Gangloff: NASA meeting on National Aerospace Plane-Hydrogen Environment Effects; Phoenix, AZ, June, 1988; H.G. Nelson, organizer; Presented talk on "Fracture Mechanics and Environmental Fracture of Advanced Materials".

Local

R.P. Gangloff, "Advanced Metallic Materials for Light Aerospace Structures" Virginia Academy of Science, Charlottesville, VA, May, 1988.

R.G. Buchheit, Jr. and G.E. Stoner, Abstracts follow.

EXTENDED ABSTRACTS

1/15/88 Presentation at The Alcoa Technical Center, Pittsburg, PA.

4/27/88 Presentation to the Industrial Associates of the Light Metals Center, Charlottesville, VA.

"Measurements and Mechanisms of Localized Aqueous Corrosion in Aluminum-Lithium Alloys"

Based on a review of literature, microreference Ag|AgCl electrodes have been constructed and tested. Microreference electrode tips have been made as small as 5 micrometers (inner bore diameter). Electrodes constructed show excellent reference potential stability and have been used to measure potential variations as small as 0.6 mV on an actively corroding metal surface. Microreference electrodes have been used to measure the variation in potential in the vicinity of corrosion pits on peak aged 2090 (Al-2.7Cu-2.2Li-0.12Zr) during potentiodynamic polarization scans.

Measurements of the change in pH versus time have been performed for artificial crevices and immersed machine shavings in solutionized and peak aged 2090. Preliminary results suggest that pH vs. time behavior is dependent on alloy heat treatment. Results obtained for 2090 are compared with results obtained in similar tests performed on alloys 2024 and 7075.

Scanning electron microscopy, energy dispersive spectroscopy and X-ray mapping have been used to examine pit morphology and variations in the concentrations of metallic elements like copper, iron and magnesium in pitted regions.

4/15/88 Electrochemical Seminar Series at the University of Virginia.

"An Ongoing Investigation of the Stress Corrosion Cracking and Localized Corrosion Behavior on an Al-Li-Cu Alloy" (presentation with Jim Moran).

The localized aqueous corrosion and stress corrosion cracking behavior of alloy 2090 (Al-Li-Cu) are presently being studied. Progress to date includes a microstructural characterization of the alloy, anodic polarization experiments, and constant immersion and constant extension rate (CERT) SCC tests. In addition, localized pH and localized potential experiments have been performed using both conventional and micro-electrodes. A brief review of pertinent microstructural features of Al-Li alloys (2090, in particular), along with a summary of the corrosion work to date will also be presented.

The polarization and SCC experiments were performed in various NaCl based environments. Additions to the environment included carbonate and sulfate anions, with Li, Na and K cations. In addition to the quantitative information obtained from these experiments, the SCC fracture surfaces and the polarization corrosion surfaces were examined. The results to date suggest that SCC and polarization behavior can be significantly changed by the addition of these various species.

the pH and potential of the solution contained within artificial crevices formed in 2090 and 2024 alloys has been measured <u>in situ</u>. The effect of alloy heat treatment, alloy composition, degree of solution agitation and aeration on the crevice solution behavior has been monitored as a function of time. The effect of coupling an external cathode to the crevice

has also been studied.

Potential variations in the solution near actively corroding pits on aluminum alloy surfaces have been measured with specially constructed microreference electrodes. Potential variations as small as 0.6 mV have been detected. The pitting of polished alloy specimens has been observed <u>in situ</u> using an optical microscope equipped with long working distance objective lenses.

5/26/88 Meeting of the Virginia Academy of Science, Charlottesville, VA

"Characterization of Occluded Aqueous Environments in Al-Li-Cu Alloy 2090"

Changes in potential and pH occurring in simulated crevices machined in alloy 2090 have been monitored as a function of bulk environment condition and time. In this talk, the methods used for simulating crevices and making measurements of potential and pH in occluded environments will be described. The chemistry developed in crevices formed in 2090 will be compared to that developed in conventional aluminum alloys like 2024 and 7075. The corrosion mechanisms thought to cause the observed potential and pH changes will also be discussed.

DISTRIBUTION LIST

Copy No.	
1 - 3	Mr. Dennis Dicus M/S 188A, Metallic Materials Branch National Aeronautics and Space Administration Langley Research Center Hampton, VA 23665
4	Mr. W. Barry Lisagor M/S 188A, Metallic Materials Branch National Aeronautics and Space Administration Langley Research Center Hampton, VA 23665
5	National Aeronautics and Space Administration Langley Research Center Hampton, VA 23665 Attention: Mr. J. F. Royall, Jr. Grants Officer, MS 126
6	Thomas H. Courtney, Chairman, MS
7 - 18	Richard P. Gangloff, MS
19 - 20	Glenn E. Stoner, MS
21 - 22	Robert E. Swanson, Assistant Professor Department of Materials Engineering Virginia Polytechnic and State University Blacksburg, VA 24061
23	SEAS Publications Files
24 - 25*	NASA Scientific and Technical Information Facility P.O. Box 8757 Baltimore/Washington International Airport Baltimore, MD 21240

*Reproducible copy

1656:ald:DW212R

UNIVERSITY OF VIRGINIA
School of Engineering and Applied Science

The University of Virginia's School of Engineering and Applied Science has an undergraduate enrollment of approximately 1,500 students with a graduate enrollment of approximately 560. There are 150 faculty members, a majority of whom conduct research in addition to teaching.

Research is a vital part of the educational program and interests parallel academic specialties. These range from the classical engineering disciplines of Chemical, Civil, Electrical, and Mechanical and Aerospace to newer, more specialized fields of Biomedical Engineering, Systems Engineering, Materials Science, Nuclear Engineering and Engineering Physics, Applied Mathematics and Computer Science. Within these disciplines there are well equipped laboratories for conducting highly specialized research. All departments offer the doctorate; Biomedical and Materials Science grant only graduate degrees. In addition, courses in the humanities are offered within the School.

The University of Virginia (which includes approximately 2,000 faculty and a total of full-time student enrollment of about 16,400), also offers professional degrees under the schools of Architecture, Law, Medicine, Nursing, Commerce, Business Administration, and Education. In addition, the College of Arts and Sciences houses departments of Mathematics, Physics, Chemistry and others relevant to the engineering research program. The School of Engineering and Applied Science is an integral part of this University community which provides opportunities for interdisciplinary work in pursuit of the basic goals of education, research, and public service.